Transport critical current density measurements on high and low temperature superconductors in magnetic fields up to 15 tesla

Christopher Michael Friend

Transport Critical Current Density Measurements on High and Low Temperature Superconductors in Magnetic Fields up to 15 Tesla

by

Christopher Michael Friend
Hatfield College, Durham

A thesis submitted in partial fulfilment of the requirements for the degree of Doctor of Philosophy

Department of Physics, University of Durham

1994

Abstract

A probe for measuring the transport critical current density ($J_c(B,T)$) of superconductors has been constructed, extending the magnetic field and temperature range of previous probes. It can measure critical currents up to 500A, from 2K up to 150K, inside the bore of a 17T Tesla magnet. The temperature is held constant during measurement to: $\pm$50mK at 4.2K and below; $\pm$70mK at 20K; $\pm$100mK at 80K and $\pm$200mK at 150K.

The $J_c(B,T)$ of a Nb(46.5wt%)Ti multifilamentary wire has been measured in transverse and longitudinal fields. The longitudinal orientation has both a higher J_c and upper critical field. It is found that the orientation, field and temperature dependence of $J_c(B,T)$ is described by a single functional form. In particular, the orientation dependence determined only by the upper critical field, the anisotropy of which is due to variations in the microstructure or flux cutting events.

A $Bi_2Sr_2Ca_2Cu_3O_x$ tape has been measured in three different orientations. An anomaly in J_c is observed, only below 10K, at a field $B_j(T)$ for each orientation. Above 1T the data are best described by the function $J_c(B,T)=\alpha_j(T)\exp\{-B/\beta(T)\}$. There is a crossover to a stronger field and temperature dependence of J_c at temperatures above 55K. Close to the irreversibility line there is a markedly different field dependence of J_c depending on whether the field is perpendicular or parallel to the tape surface. A new description has been put forward to explain the data. It is suggested that the intergrain material of the tape is a low T_c BSCCO phase, possibly the 2201 or 2011 phase, of which $B_j(T)$ is the upper critical field. Above 10K, in fields less than 1T, J_c is determined by coupling across S-N-S Josephson junctions at the grain boundaries. Above 1T, current mainly flows between grains by connections which allow it to remain in the crystal ab-planes. $J_c(B,T)$ is then determined by intrinsic properties and follows the exponential functional form. This form is determined by the average field component parallel to the c-axis. It is proposed that collective pinning theory offers the best framework for describing J_c, in which case the crossover could be due to a pinning phase transition.

The $J_c(B,T)$ of some $Bi_2Sr_2Ca_1Cu_2O_x$ multifilamentary wires is explained using the same description of S-N-S coupling and ab-plane connections as for the 2223-tape. However, whereas the tape was highly aligned throughout, each wire filament has aligned grains in the region of the BSCCO-Ag interface but an untextured core. It is in the aligned regions of each filament that most of the ab-plane connections exist. Increasing the number of filaments therefore improves the wire performance in high fields, though phase purity and density are still important. The 19 and 37 filament wires are promising for high field applications below 20K.

The results on the BiSrCaCuO tape and wires demonstrate that, in this material, $J_c(B,T)$ can be improved with better texturing and connectivity between grains. To advance the theory a better understanding of the average pinning potentials in BSCCO is required.

I hereby declare that the work contained within this thesis is my own original work and nothing that is a result of collaboration, unless otherwise stated. No part of this work has been submitted for a degree or other qualification at this or any other University.

C.M. Friend, August 1994.

Acknowledgements

My thanks go to the following:

The Science and Engineering Research Council which provided the financial support for this work; Professors A.D. Martin and D. Bloor who allowed me the use of the Physics Department facilities; my supervisor Dr Damian Hampshire for his help and advice; Dr T. Beales, BICC Pyrotenax Ltd, for supplying the BSCCO-2223 tape; Dr J. Tenbrink, Vacuumschmelze GmbH, for supplying the BSCCO-2212 wires; Dr Luc Le Lay for his help in the lab, in particular the computing and vigorous testing of the $J_c(B,T)$ probe's mechanical strength; the student workshop, Phil Armstrong, Michael Greener, Peter Luke and George Teasdale without whose skill the $J_c(B,T)$ probe would not exist; Chris Mullaney for building the 500A power supply and his patient advice; the Audio-Visual group, Mike Lee, Vicki Greener and Pauline Russell whose help with the drawings is much appreciated.

I also acknowledge those who kept me sane by driving me mad:

Doctors Chris Gregory, John Hudson and Steve Westwood (aka Shaggy, Spam and Trog), housemates and Solid State Rebels; Luc Le Lay for listening to my rantings and his french wardrobe; Paul Foley for drilling that hole; Wayne Dobby who allowed me to escape from 2H students in his refuge; Harry Ramsbottom, Rob Luscombe, Salamat Ali, Hamidi Hamid and Dong-Ning Zheng who comprise the RIS group and make it the hip hop happy group it is. Special mention is made of Harry's curtain salesman impression; Small Paul Barker, Caroline Moore, Desmond Phillips, Pete Ratcliffe and Malcolm Weaver (a miscellaneous collection of buddies); Jon 'Trowsers' Tait who makes up for being a chemist with his bar talk and morris dancing; my parents and grandad for their vital support; Laura for reasons that cannot be put in words; Jimi and Ravi for special help in times of stress; and anyone I've missed and who once bought me a pint.

'Every intellectual has a very special responsibility ... he owes it to his fellow men (or to 'society') to represent the results of his study as simply, clearly and modestly as he can. The worst thing he can do - the cardinal sin - is to try to set himself up as a great prophet vis-a-vis his fellow men and to impress them with puzzling philosophies. Anyone who cannot speak clearly should say nothing and continue to work until he can do so'

- Karl Popper (in his essay: 'Against big words')

'The real and immense study to be undertaken is the manifold picture of nature'

- Paul Cézanne (in a letter to Emile Bernard, 1904)

Table of Contents

List of variables

The following is a list of all the variables used in the thesis with a brief description of their meaning:

A	normalisation constant
a_0	flux line lattice spacing
α_p	bulk pinning force parameter
α_j	pair breaking current parameter
B	magnetic induction
B_1	the field at which the critical current density of the BSCCO-2223 tape first starts to drop
B_{2D}	crossover field from 3D to 2D pinning or field at which layers become decoupled
B_{3D}	crossover field from 2D to 3D collective pinning
B_c	thermodynamic critical field
B_{c1}	lower critical field
B_{c2}	upper critical field
B_{c2}°	the effective upper critical field - as measured in chapter 5
B_{cp}	crossover field from single flux line pinning to collective pinning
B_d	field at which the critical current density of the BSCCO-2223 tape starts to decrease quicker than the exponential field dependence
B_{exp}	the field at which the critical current density of the BSCCO-2223 tape begins to decrease exponentially with field.
B_{irr}	irreversibility field
B_j	the field value at which the anomaly in the critical current density of the BSCCO-2223 tape was observed below 10K
b	reduced magnetic field
ß	pair breaking current parameter (field term)

C_s superconducting specific heat

$C_{11,12}$ compression moduli of the FLL

C_{44} tilt modulus of the FLL

C_{66} shear modulus of the FLL

c_L Lindemann criterion

Γ anisotropy factor

γ electronic specific heat coefficient

γ_P mean-square random pinning force in 2D collective pinning

γ_{P0} value of γ_P at which the pinning force overcomes the interlayer coupling

d superconducting layer thickness

Δ BCS energy gap

δ exponent of B_{irr} temperature dependence

E electric field strength

E_0 flux creep electric field parameter

E_F Fermi energy

e electronic charge

ϵ_i the stresses in the FLL

F_P bulk volume pinning force

F_{Pmax} maximum bulk volume pinning force

f_P pinning force of an individual centre

G the characteristic strength of the pinning potential in 3D collective pinning

G_∞ the value of the parameter G corresponding to strong short range disorder

List of Variables

η	pinning force efficiency factor
$\hbar$	Planck's constant/2π
θ	angle of magnetic field with respect to some axis
κ_{GL}	Ginzburg-Landau parameter
J	macroscopic current density
J_C	critical current density
J_0	collective flux creep current parameter
J_{c0}	depairing current density
j_s	local superconducting current
k	wave vector (k_F - Fermi wave vector)
k_B	Boltzmann constant
L_c	longitudinal correlation length of a flux bundle
l_e	electron mean free path
Λ	2D film current screening length
λ_L	London penetration depth
$\lambda_{ab,c}$	anisotropic penetration depths (in ab-plane and parallel to the c-axis)
M	atomic mass
m_e	electron mass
$m_{ab,c}$	anisotropic effective masses of the cooper pairs

μ_0 permeability of a vacuum

μ exponent of U(J) dependence from flux creep theory

ξ_0 BCS coherence length

ξ_p Pippard coherence length

ξ_{GL} Ginzburg-Landau coherence length

$\xi_{ab,c}$ anisotropic coherence lengths

N(E) density of electron states

n_p density of pinning centres

n exponent of upper critical field in pinning force scaling function

n_s number density of cooper pairs

R_C transverse correlation length of a flux bundle

R_j characteristic length of interlayer Josephson coupling strength

ρ resistivity

ρ_C the flux flow resistivity at $J=J_C$

S entropy

σ_i the strains of the FLL

T temperature

T_{3D} temperature at which crossover from 2D to 3D collective pinning occurs

T_C critical temperature

T_α observed line marking a crossover to a stronger temperature dependence of the critical current density for the BSCCO-2223 tape

T_d decoupling temperature of pancake vortices (no pinning)

T_m lattice melting temperature

T_p depinning temperature

List of Variables

T_v	thermal decoupling temperature in zero field
t	reduced temperature, T/T_c
t	time
U	activation energy for flux creep
U_0	activation energy at zero temperature
U_P	pinning energy
U_{tilt}	lattice tilt energy
U_{shear}	lattice shear energy
u	thermally induced flux line displacement
V	electron-phonon coupling constant
V_c	volume of a correlated flux bundle for collective pinning
v_s	velocity of cooper pair
υ	flux creep jump rate
υ_0	characteristic frequency for flux jumping
v_F	Fermi velocity
ϕ	phase coherence or angle of the magnetic field to some axis
ω_D	Debye frequency

1. Introduction

Superconductors are important technological materials, already in use in vital applications such as medical body scanners. For other uses such as: high speed switches; generators; magnetic energy storage; ore separation; power cables and levitation; their potential has yet to be realised. One reason for this is that conventional superconducting materials have critical temperatures below 40K and require liquid helium as a coolant. Liquid helium is expensive and its associated refrigeration equipment is bulky and heavy.

With the dramatic discovery of the high temperature superconductors (HTSC's) in the late 1980's, with critical temperatures above that of liquid nitrogen (77K), it seemed that all the old problems would soon be overcome. Liquid nitrogen is relatively cheap and its refrigeration system can be made light and transportable. With these new materials however, new problems arrived which have produced many new theories of superconductivity. From the practical point of view, HTSC's are brittle. They cannot easily be made into mechanically strong wire which is the preferred form for most applications. In addition they are granular and have a highly anisotropic crystal structure leading to anisotropic superconducting and transport properties. The most important parameter is the critical current density (J_c). High values of J_c are needed for many applications. It has been found that intrinsically, HTSC's can sustain very high values of J_c but the effective transport J_c is always much smaller.

To be able to fabricate significantly better materials the mechanisms which limit J_c in the HTSC's have to be understood. Data across as wide a range of the magnetic field and temperature phase space of a superconductor is required so that the theories which have been proposed to explain these mechanisms can be considered. This thesis describes the design and operation of a probe which can measure high values of J_c in magnetic fields up to 17T and at temperatures from 2K up to 150K. This probe has been used to measure three different materials with the aim of gaining insight into the complex mechanisms limiting J_c in each of them.

Chapter two presents the fundamental theories of superconductivity and chapter three describes in detail the flux line lattice of type II superconductors. The ideas covered in chapter three are used to discuss the experimental results of J_c measurements in later chapters. Chapter four describes the design and operation of the J_c probe and discusses possible measurement errors. The next three chapters present and analyse the results of J_c measurments on three different types of superconducting materials: a NbTi multifilamentary wire; a $Bi_2Sr_2Ca_2Cu_3O_x$ silver-clad tape and three different $Bi_2Sr_2Ca_1Cu_2O_x$ silver sheathed multifilamentary wires. Finally, chapter eight summarises the main conclusions and suggests some further work.

2. Superconductivity

This chapter introduces the superconducting state and presents the fundamental theories that have been formulated to explain it. It begins in section 2.1 with a brief historical introduction to the subject and then section 2.2 describes the two properties which characterise a superconducting material. Section 2.3 discusses the microscopic theory of superconductivity by Bardeen, Cooper and Schrieffer and details its main predictions which have all been experimentally confirmed for low temperature superconductors. Amendments to the BCS theory and other new theories used to describe the recently discovered high temperature superconductors are not discussed here. The complimentary phenomenological theories of London-London and Ginzburg-Landau (GL) are presented in section 2.4. The London model introduces the ideas of a penetration depth and through a modification by Pippard, a coherence length. The GL theory uses the notion of an order parameter and Landau's theory of 2nd order transitions. Using only one free parameter it predicts the variation of the critical fields and currents near T_c. The GL theory also leads onto the flux line lattice in type II superconductors - the subject of the next chapter. The next two sections discuss Josephson junctions and the application of the GL theory to an anisotropic material respectively. Finally, section 2.7 lists a few of the many different materials which have been found to be superconducting and gives the values of the fundamental parameters for some of them.

2.1. An introduction to superconductivity

At the turn of the century Heike Kammerlingh Onnes succeeded in liquifying Helium. Temperatures below 10K could now be accessed and Onnes set about investigating how the resistance of metals changed as absolute zero was approached. In 1911 he made a remarkable new discovery[1]. With his co-worker von Holst he found that just below 4.2K the resistance of Mercury (the purest metal then available) dropped discontinuously and within a few hundredths of a Kelvin to zero. Here was a new state of matter which Onnes named as the *superconductive state*[2]. Many other materials were soon found to be superconducting below some critical temperature, T_c.

It was to be another 50 years before a theory of superconductivity emerged and led to useful applications for these types of materials. A sudden drop in resistance, on its own, does not necessarily determine if a material is a superconductor. It must also be shown to expel a magnetic field. Section 2.2 briefly addresses these two intrinsic properties. The following sections in this chapter then present the general theories of superconductivity, finishing with a table of fundamental constants.

2.2. Zero resistivity and the Meissner-Ochsenfeld effect

Persistent currents with no measurable decay have been shown to flow in a superconductor for over two and a half years[3]. This corresponds to a resistivity which is less than 18 orders of magnitude smaller than that of copper at room temperature. A microscopic description of how this zero resistivity (or infinite conductivity) comes about is given in section 2.3.

When a superconductor is cooled down from the normal state to below T_c in a small magnetic field, the flux inside it is expelled. This is known as the Meissner-Ochsenfeld effect[4]. It is not as a result of having an infinite conductivity but is another intrinsic property of a superconductor. Taking Maxwell's equation,

$$\nabla\times\mathbb{E} = \nabla\times\{\rho\mathbb{J}\} = -\partial\mathbb{B}/\partial t,$$

zero resistivity would imply $\partial\mathbb{B}/\partial t = 0$. The Meissner effect however, always occurs whether the sample was cooled in a magnetic field or the field was applied after cooling below T_c. Hence the superconducting state is a thermodynamic equilibrium state and exhibits perfect diamagnetism.

There are two types of superconductors which can be distinguished by their magnetic behaviour. Consider a superconducting sample cooled in zero field. On applying a magnetic field a Type I superconductor excludes the flux up to the *thermodynamic critical field* B_c. Above B_c, the sample becomes a normal conductor. For a Type II superconductor the flux is excluded only up to the *lower critical field* B_{c1}, at which point it penetrates in the form of quantised flux lines. The superconductivity is only destroyed in a field greater than the *upper critical field*, B_{c2}.

2.3. The microscopic theory (BCS)

2.3.1. The electron-phonon interaction

In 1957 L. Cooper showed that if there is a net attractive interaction between two electrons they bind *whatever the strength of the interaction*[5]. If the electrons have equal and opposite momentum the total energy of the system is reduced and the normal ground state model is no longer valid. How an attractive interaction arises can be explained by the following heuristic argument. As an electron moves through the lattice it attracts the positive ions forming a path of polarization. Another electron going along the same path will have a lower energy as the lattice is already polarized. The time it takes for the lattice to respond to the electron's passage depends on its natural frequency. Therefore this attractive interaction between the electrons would be weaker for heavier ions. If this interaction is stronger than the Coulomb repulsion then we have a correlated electron pair, called a *Cooper pair*. The distance over which this pair is correlated is the BCS coherence length ξ_0. Looking at it a different way, the electrons can be described as interacting by the exchange of a virtual phonon. Because the pair has a total momentum of zero it cannot be influenced, say by an electric field, without being destroyed (broken apart). The Cooper pair does not interact with the lattice unless it is subjected to an energy greater than its binding energy. This leads to zero resistance in the superconducting material.

The next section presents the main predictions of the BCS theory and the experiments with which they were verified.

2.3.2. The important predictions of the BCS theory

Bardeen, Cooper and Schrieffer formulated their theory as follows[6]. Pairs of electrons with opposite momentum and spin (or wave vectors $k\uparrow$ and $-k\downarrow$) are

considered. The coherence length of the pairs is given by

$$\xi_0 = 0.18\frac{\hbar v_F}{k_B T_C} \tag{2.1}$$

where v_F is the Fermi velocity. With a net attractive interaction the pairs will condense into the ground state, expressed in terms of the states ($\mathbb{k}\uparrow$, $-\mathbb{k}\downarrow$). In the normal phase all the states are filled up to the Fermi wave vector $\mathbb{k}_F$. The energy gap between a paired state and two single electron states is denoted by 2Δ. The BCS theory gives the energy gap at zero temperature as

$$2\Delta(T=0) = 3.52 k_B T_C \tag{2.2}$$

and near T_C,

$$\frac{\Delta(T)}{\Delta(0)} = 1.74\left(1 - \frac{T}{T_C}\right)^{1/2} \tag{2.3}$$

To break up a pair an excitation of energy more than 2Δ is needed. Therefore, above T=0 both Cooper pairs and single electrons exist. The energy gap can be obtained from infrared or ultrasound absorption and tunnelling experiments with good agreement.

The temperature dependence of the thermodynamic critical field is predicted to be

$$B_C(T) = B_C(0)(1-t^2) \tag{2.4}$$

where t is the reduced temperature, T/T_C. The change in entropy per unit volume between the normal and superconducting state is $\Delta S = -(B_C/\mu_0)\partial B_C/\partial T$ and is proportional to the heat of transition. As $B_C \to 0$ when $T \to T_C$ we have a second order phase transition.

Another successful prediction by BCS was the temperature dependence of the specific heat, given as $T \to 0$ by

$$C_s \propto \gamma \exp\left(\frac{\Delta(0)}{k_B T}\right) \tag{2.5}$$

where γ is the electronic specific heat coefficient.

Finally, the theory provided an expression for T_C,

$$T_C = 1.13\frac{\hbar\omega_D}{k_B}\exp\left(\frac{1}{N(E_F)V}\right) \qquad (2.6)$$

where ω_D is the Debye frequency, $N(E_F)$ is the density of electron states at the Fermi energy and V is an electron-phonon coupling constant. If it is assumed that V is constant then $\omega_D \propto 1/\sqrt{M}$ and $T_C \propto M^{-1/2}$ - the Isotope effect.

2.4. The phenomenological theory

2.4.1. The London model

In the theory given by F. London and H. London[7] it is assumed that the supercurrent is always determined by the local magnetic field. Using a two fluid model (where only a fraction, n_s, of the total density of electrons, n, are superconducting) the supercurrent is $j_s = n_s e v_s$ and $m_e(dv_s/dt) = eE$ which leads to

$$\frac{\partial j_s}{\partial t} = \frac{n_s e^2}{m_e}E \qquad (2.7)$$

(here, m_e is the electron mass, v_s is the velocity of the superconducting electrons and E is the electric field strength). Combining Eq.(2.7) with the Maxwell equation $\nabla\times E = -\partial B/\partial t$ and integrating they obtained

$$\nabla\times j_s = \frac{n_s e^2}{m_e}B \qquad (2.8)$$

Eq.(2.7) and Eq.(2.8) are the two London equations. The first one describes a conductor with R=0 and the second one describes the Meissner-Ochsenfeld effect. By applying the Maxwell equation $\nabla\times B = \mu_0 j_s$ to Eq.(2.8) and solving for a simple one-dimensional case, it can be shown that the parameter λ_L, called the *London Penetration Depth*, describes the range over which the field extends inside the superconductor and

is given by

$$\lambda_L = \left(\frac{m_e}{\mu_0 n_s e^2} \right)^{1/2} \tag{2.9}$$

This model assumes a small spatial variation of j_s so only holds for $\lambda_L \gg \xi_0$ which is the case for type II superconductors. To describe type I materials ($\lambda_L \ll \xi_0$) it needs a modification to Eq.(2.8) by A.B. Pippard[8]. He introduced the *Pippard coherence length* which characterises the distance over which the local field determines the current at one point and is related to the coherence of the cooper pair by

$$\frac{1}{\xi_p} = \frac{1}{\xi_0} + \frac{1}{l_e} \tag{2.10}$$

where l_e is the mean free path of an electron.

The London model does not allow for variations in n_s (with field, current etc.). This leads us to the more general Ginzburg-Landau Theory.

2.4.2. The Ginzburg-Landau theory

Ginzburg and Landau introduced an order parameter[9], the wave function $\psi(r) = |\Psi(r)|e^{i\phi}$ (ϕ is the phase) which characterises the degree of superconductivity at some point in a material. It is defined to be zero in a normal region and unity in a fully superconducting region at T=0. The superfluid density is obtained as

$$n_s(r) = |\psi(r)|^2 \tag{2.11}$$

They assumed the transition was of 2nd order, then the superconducting free energy in a magnetic field is

$$F_s = F_n + \alpha|\psi|^2 + \frac{1}{2}\beta|\psi|^4 + \frac{1}{2\mu_0}|B_e - B_i|^2 + \frac{1}{2m_e}|(-i\hbar\nabla - 2e\mathbf{A})\psi|^2 \tag{2.12}$$

The first three terms come from Landau's own theory of 2nd order transitions[10]. F_n is the free energy in the normal state and α, β are suitable coefficients. Close to T_c, a good approximation is made by neglecting terms in higher powers of $|\psi|$. The fourth term gives the energy to change the magnetic field from its external value, B_e to the internal field, B_i. The last term is the energy associated with the local variation in the supercurrent and Cooper pair density ($\mathbb{A}$ is the vector potential). By integrating Eq.(2.12) over the whole volume and minimising with respect to ψ and $\mathbb{A}$ we obtain the two coupled Ginzburg-Landau (GL) equations :

$$\alpha\psi + \beta|\psi|^2 + \frac{1}{2m_e}(i\hbar\nabla - 2e\mathbb{A})^2\psi = 0 , \qquad (2.13)$$

$$j_s = \frac{e}{m_e}\psi(-i\hbar\nabla - 2e\mathbb{A}) \qquad (2.14)$$

The GL coherence length ξ_{GL} varies with T near T_c as

$$\xi_{GL} \propto (1-t)^{-1/2} \qquad (2.15)$$

The magnetic penetration depth varies with T in the same way near T_c and the GL theory can be described in terms of just one parameter - the *Ginzburg-Landau parameter,*

$$\kappa_{GL} = \frac{\lambda_L}{\xi_{GL}} \qquad (2.16)$$

By applying the appropriate boundary condition, Abrikosov[11] solved equations (2.13 and 2.14) for a type II superconductor in fields $B_{c1} < B < B_{c2}$ (the mixed state). He showed that the flux penetrates as tubes of flux, each containing one flux quantum

$$\phi_0 = \frac{h}{2e} = 2.07\times10^{-15}\ Wb . \qquad (2.17)$$

Each flux line (or flux vortex) is surrounded by a supercurrent ring of spatial extent λ_L. The flux lines penetrate in the form of a regular lattice, normally in a hexagonal (or triangular) configuration (see Figure 2.1).

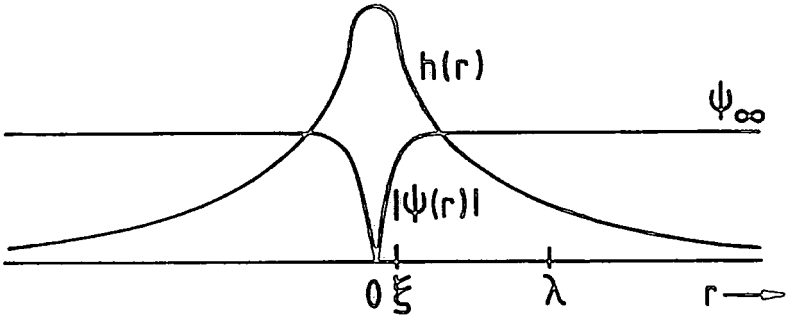

(a)

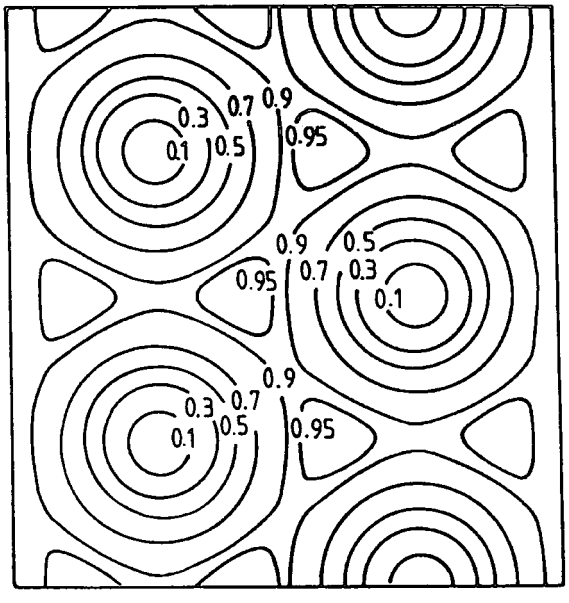

(b)

Figure 2.1: (a) the structure of a vortex with $\kappa_{GL} >> 1$; (b) the spatial variation of the order parameter in a type II superconductor showing the hexagonal/triangular lattice.

The two critical fields can then be derived as:

$$B_{C2} = \frac{\phi_0}{2\pi\xi^2} = \sqrt{2}\kappa_{GL}B_C \; ; \tag{2.18}$$

$$B_{C1} \approx \frac{B_C}{\sqrt{2}\kappa_{GL}} \ln\kappa_{GL} \; . \tag{2.19}$$

If the applied field is parallel to the surface of a sample (at a superconductor-insulator boundary) then superconductivity first nucleates in a sheath at a field higher than B_{C2}, given by

$$B_{C3} = 1.695 B_{C2} \tag{2.20}$$

From equation 2.18, it can be seen that the condition for a material to be a type II superconductor is that $\kappa_{GL} > 1/\sqrt{2}$.

Finally, the highest critical current density that a superconductor can carry before being driven normal, called the *depairing current density*, is predicted to be

$$J_{C0} = \left(\frac{4}{3\sqrt{6}}\right)\frac{B_C(T)}{\mu_0\lambda(T)} \propto (1 - t)^{3/2} \tag{2.21}$$

using the temperature dependence of B_c and λ from G-L theory.

2.5. Josephson junctions

Josephson[12] predicted that Cooper pairs could tunnel through a thin insulating layer. In practice the layer can also be normal or weakly superconducting. This tunnelling allows the Josephson junction to sustain a current with zero voltage across it up to a critical current which is less than that of the bulk superconducting material. The junction critical current is a pair breaking current and can be related to the energy gap $\Delta(T)$[13].

The electrical transport properties of superconductor-normal metal-superconductor (SNS) junctions have been investigated by Clarke[14] and Hsiang and Finnemore[15] and analyzed using the theory of the proximity effect by de Gennes and Werthamer[16]. In the dirty limit, Clarke found that the critical current density of his SNS junctions varied with T near T_c as

$$J_c \propto (1-T/T_c)^2 \tag{2.22}$$

Hsiang and Finnemore investigated the magnetic field dependence of J_c for SNS junctions in the clean limit. They found that the critical current decreased exponentially with field such that

$$J_c = \alpha_f(T) e^{-B/\beta(T)} \tag{2.23}$$

and described their results phenomenologically using a pair breaking mechanism.

2.6. Anisotropy

The GL theory can be applied to anisotropic materials by replacing the Cooper pair mass by an effective-mass tensor which has elements m_i, where $i=1,2,3$ corresponding to the a,b,c crystal axes. They are normalized so that $m_1m_2m_3=1$ and the penetration depths and coherence lengths can be written as

$$\begin{aligned} \lambda_i &= \lambda.(m_i)^{1/2}, \quad and \quad \lambda = (\lambda_a\lambda_b\lambda_c)^{1/3} \\ \xi_i &= \xi/(m_i)^{1/2}, \quad and \quad \xi = (\xi_a\xi_b\xi_c)^{1/3} \end{aligned} \tag{2.24}$$

and the upper critical fields then become

$$\begin{aligned} B^a_{C2} &= \phi_0/(2\pi\xi_b\xi_c), \quad B^b_{C2} = \phi_0/(2\pi\xi_a\xi_c) \\ and \quad B^c_{C2} &= \phi_0/(2\pi\xi_a\xi_b) \end{aligned} \tag{2.25}$$

Lawrence and Doniach[17] (LD) formulated a useful phenomenological theory for

layered superconductors. Consider the superconducting layers to be parallel to the ab-plane and to have a spacing s. For $\xi_c > s$, the layers are described by a 2D GL Theory and the gradient along c is replaced by a finite difference. The anisotropy can then be defined as

$$\Gamma = \frac{m_c}{m_{ab}} = \left(\frac{\xi_{ab}}{\xi_c}\right)^2 = \left(\frac{\lambda_c}{\lambda_{ab}}\right)^2 , \qquad (2.26)$$

For $\xi_c \gg s$, anisotropic G-L theory must be used. When ξ_c approaches half the layer spacing the superconducting planes become decoupled and the LD formalism is no longer appropriate. From equation 2.15 and 2.24 the temperature at which this transition, from a three-dimensional LD model at high temperatures to a 2D problem at lower temperatures is calculated as

$$T_{3D\text{-}2D} = T_C\left[1 - \frac{1}{\Gamma}\left(\frac{2\xi_{ab}}{s}\right)^2\right] . \qquad (2.27)$$

The theory of weakly coupled layers is covered in chapter 3.

2.7. Types of superconducting materials

There are hundreds of different superconducting materials, here I list only a few: most elements; the commercially important alloys NbTi and Nb_3Sn; the high temperature ceramic copper oxides, BiSrCaCuO and YBaCuO; buckyballs (doped C_{60}) and organic superconductors such as BEDT-TTF. New materials are being discovered all the time, such as recently, the quaternary intermetallics[18]. Tables 2.1 and 2.2 list some values of the important parameters for materials relevant to this work.

Material	T_c (K)	κ_{GL}	$\xi(0)$ (Å)	$\lambda(0)$ (Å)	$B_{c2}(0)$ (T)	$B_{c1}(0)$ (T)
Pb	7.2	0.6	510	320	B_c=0.08	
NbTi	9.8	1.5	400	600	17	0.06

Table 2.1. The important parameters for two low-temperature superconductors. The data for Pb is from the CRC Handbook[19] and the data on NbTi is from Collings[20].

Parameters	$Bi_2Sr_2Ca_2Cu_3O_x$ (s=18Å)		$YBa_2Ca_3O_{7-x}$ (s=11.6Å)	
	‖ab-plane	‖c-axis	‖ab-plane	‖c-axis
T_c, (K)	110		92	
κ_{GL}	150		90	
$\xi(0)$, (Å)	29	0.9	16	3
$\lambda(0)$, (Å)	1500	46000	1400	7000
$B_{c2}(0)$, (T)	1200	40	670	120
$B_{c1}(0)$, (mT)	2	0.2	85	25
Γ	960		25	
$T_{3D\to 2D}$, (K)	109		64	

Table 2.2. The important parameters for two high-temperature superconductors, s is the spacing between the Cu-O_2 planes in each compound and $T_{3D\to 2D}$ is calculated using the tabulated values from equation 2.27. The data on YBCO is from Burns[21] and the data on BSCCO is from Matsubara et al.[22].

References for Chapter 2

1. Onnes H.K., Comm. Leiden, 120b (1911).
2. Onnes H.K., Comm. Leiden, Suppl. Nr 34 (1913).
3. Quinn D.J. and Ittner W.B., J. Appl. Phys. 33, 748 (1962).
4. Meissner W. and Ochsenfeld R., Naturwissenschaften 21, 787 (1933).
5. Cooper L.N., Phys. Rev. 104 1189 (1956).
6. Bardeen J., Cooper L.N. and Schrieffer J.R., Phys. Rev. 108(5), 1175 (1957).
7. London F. and London H., Proc, Roy. Soc. (London) A149, 71 (1935)
8. Pippard A.B., Proc. Roy. Soc. (London) A216, 547 (1953).
9. Ginzburg V.L. and Landau L.D., Zh. Exsperim. i Teor. Fiz. 20, 1064 (1950).
10. Landau L.D. and Lifshitz E.M., *Course of Theoretical Physics* 5, 430, Pergamon Press (1959).
11. Abrikosov A.A., Sov. Phys. JETP 5, 1174 (1957), [Translation of Zh. Eksp. Teor. Fiz. 32, 1442 (1957)].
12. Josephson B.D., Phys. Lett. 1, 251 (1962).
13. Ambegaokar V. and Baratoff A., Phys. Rev. Lett. 11, 104 (1963).
14. Clarke J., Proc. R. Soc. London, Ser A 308, 447 (1969).
15. Hsiang T.Y. and Finnemore D.K., Phys. Rev. B., 22, 154 (1980).
16. de Gennes P.G., *Superconductivity of Metals and Alloys* (Benjamin, New York 1966);
    Werthamer N.R., Phys. Rev. 132, 2440 (1963).
17. Lawrence W.E. and Doniach S., *Proc. 12th Internatl. Conf. of Low Temperature Physics LT12* (ed Kanda E., Academic Press of Japan: Kyoto) 361 (1971).
18. Cava R.J., Takagi H., Batlogg B., Zandbergen H.W., Krajewski J.J., Peck Jr W.F., van Dover R.B., Felder R.J., Siegrist T., Mizuhashi K., Lee J.O., Eisaki H., Carter S.A. and Uchida S., Nature 367, 146 (1994).
19. *CRC Handbook of Chemistry and Physics, 69th Edition*, Ed. Weast R.C. (CRC Press Inc, Florida 1988).

20. Collings E.W., *Applied Superconductivity, Metallurgy and Physics of Titanium Alloys* (Plenum Press, N.Y. 1986).

21. Burns G., *High-Temperature Superconductivity, An Introduction* (Academic Press 1992).

22. Matsubara I., Tanigawa H., Ogura T., Yamashita H. and Kinoshita M., Phys. Rev. B. 45(13), 7414 (1992).

3. The Flux Line Lattice

This chapter covers the theory of the flux line lattice (FLL) predicted by Abrikosov in 1957 (see section 2.4.2). Sections 3.2 and 3.3 discuss how the flux lines can be pinned (singly and collectively) leading to a critical current density. The FLL can then be described in terms of three elastic constants. Early measurements on low temperature superconductors showed scaling of the pinning force and several theories were developed to explain this. More recently, measurements on layered structures and/or materials with a high T_c have shown a violation of the scaling laws (for example section 3.4). New theories incorporating strong thermal fluctuations and possible different phases of the FLL have been developed and are explained in sections 3.5 - 3.8. Section 3.9 notes the particular complexities of the high temperature ceramic oxide superconductors with their crystal anisotropy and granularity. First though, in section 3.1 some experimental evidence for the existence of the FLL is presented.

3.1. Evidence for the flux line lattice

The FLL has been observed in many different materials through magnetic decoration experiments. Figure 3.1 is a bitter pattern by M. Leghissa et al[1] of a $Bi_2Sr_2Ca_1Cu_2O_x$ (BSCCO-2212) single crystal before and after irradiation by heavy ions. In the unirradiated picture the hexagonal lattice can be clearly seen. After radiation the lattice is severely distorted due to the introduction of a large number of defects or pinning centres. Only recently, using Lorentz microscopy has imaging of a dynamic lattice been obtained in low magnetic fields[2]. Resolving the vortices in high fields is still a problem.

A complete mathematical description of the FLL is a complex and very difficult problem. After 34 years there is still a lot of progress to be made in this area. The following sections present some of the basic ideas on the subject.

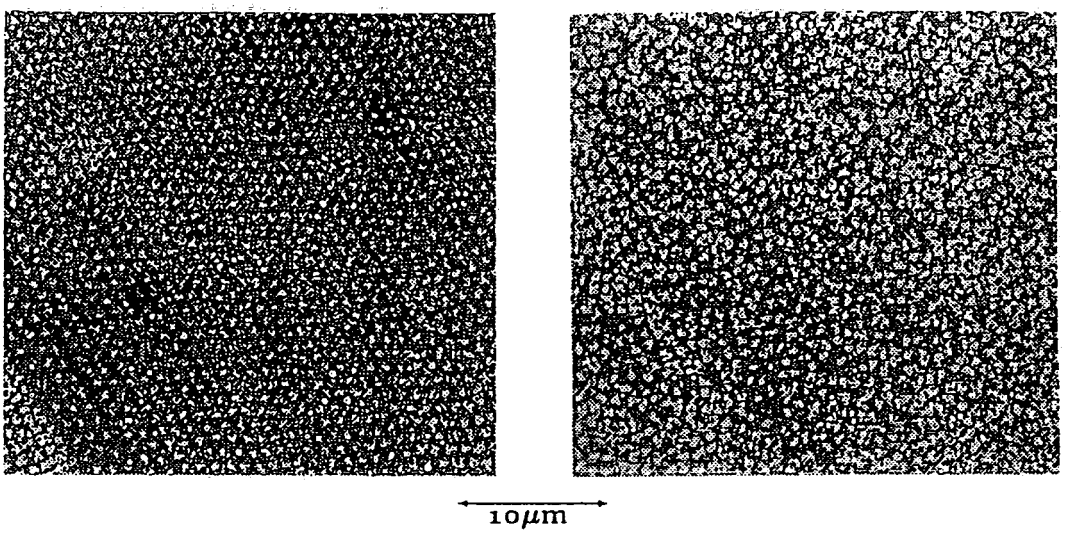

Figure 3.1: A bitter pattern of a BSCCO-2212 crystal before (left) and after (right) irradiation by heavy ions. Picture courtesy of Leghissa et al.[1].

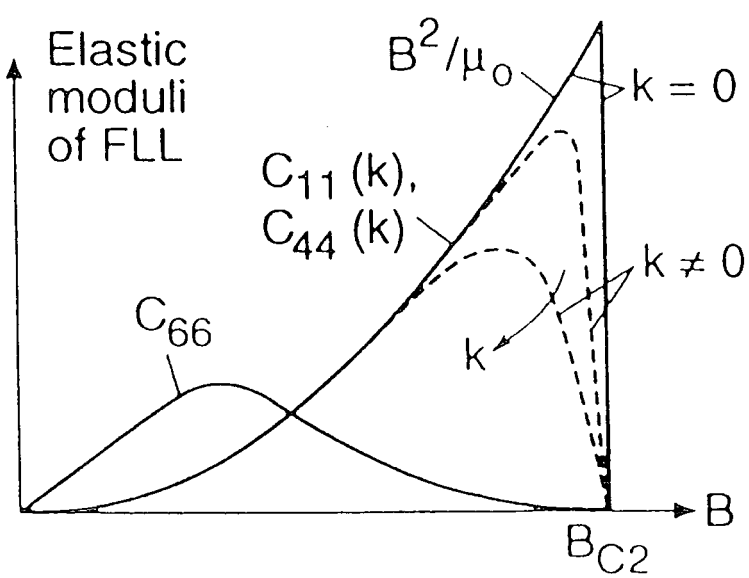

Figure 3.2: The variation of the elastic moduli with distortion wavevector k, as calculated by Brandt[7].

3.2. The driving force on flux lines

Inhomogeneities in a material such as precipitates, grain boundaries and atomic lattice defects locally depress the free energy of the flux line. These pinning centres cause the FLL to become non-periodic and form a gradient in the local B-field. This leads to regions where flux is either trapped or excluded and the magnetisation curve becomes irreversible. In the presence of a transport current density $\mathbb{J}$, the flux lines are subjected to a Lorentz force $\mathbb{J} \times \mathbb{B}$. This force is supported by the pinning centres up to a critical value of the current density such that

$$\vec{J}_C \times \vec{B} = \vec{F}_P \tag{3.1}$$

where F_p is the pinning force per unit volume of the material and J_c is the *critical current density*. There are several phenomenological theories that attempt to describe the dependence of J_c on the pinning force. The most important ones are covered in section 3.3.

As the current density is increased above J_c there will be flux flow and dissipation within the material, so J_c determines the useful working limit for most superconducting applications.

3.3. The bulk pinning force

3.3.1. Types of pinning

For single flux lines in a material with a large value of κ_{GL}, the two main pinning interactions are:

i. Core interaction. The order parameter drops to zero at the centre of a flux line. This normal vortex core can gain energy by passing through a region where the order parameter is reduced or already zero. This type of pinning occurs with normal (or weakly superconducting) inclusions of the size of or

larger than the core radius ξ_0.

ii. Magnetic interaction. Material inhomogeneities alter the distribution of the local magnetic fields and currents. This creates changes in the line energy and leads to magnetic pinning. The pinning centres can be large normal inclusions or voids or boundaries between superconductors with different κ_{GL}. The range of interaction is approximately the penetration depth.

For materials with large κ_{GL} the core interaction is often dominant. A realistic model must include vortex-vortex interactions through the elasticity of the lattice. Theories of collective pinning are covered in section 3.3.4. Pinning interactions are covered in more detail by Campbell and Evetts[3] and Huebener[4].

3.3.2. The elastic constants

A useful approach to describing distortions in a non-periodic lattice is by introducing effective elastic constants of the FLL. The Voigts notation for anisotropic crystals is used, relating the stresses σ_i to the strains ϵ_i by

$$\sigma_i = C_{ij}\epsilon_i \qquad (3.2)$$
$$i = 1,2,3,4,5,6 \rightarrow xx, yy, zz, yz, xz, xy$$

For a hexagonal lattice with the flux lines parallel to z and assuming the superconductor is isotropic this gives

$$\begin{pmatrix}\sigma_{xx}\\ \sigma_{yy}\\ \sigma_{yz}\\ \sigma_{xz}\\ \sigma_{xy}\end{pmatrix} = \begin{pmatrix}C_{11} & C_{12} & 0 & 0 & 0\\ C_{12} & C_{11} & 0 & 0 & 0\\ 0 & 0 & C_{44} & 0 & 0\\ 0 & 0 & 0 & C_{44} & 0\\ 0 & 0 & 0 & 0 & C_{66}\end{pmatrix}.\begin{pmatrix}\epsilon_{xx}\\ \epsilon_{yy}\\ \epsilon_{yz}\\ \epsilon_{xz}\\ \epsilon_{xy}\end{pmatrix} \qquad (3.3)$$

$$2C_{66} = C_{11} - C_{12}$$

C_{11} and C_{12} are the compression moduli and C_{44} is the tilt modulus. The shear modulus

(in xy-plane) is unique to the FLL. Hence only three independent constants need to be found (C_{11}, C_{44} and C_{66}) to describe the lattice distortions.

For an applied magnetic field in the z-direction Labusch[5] calculated these constants to be:

$$C_{11} + C_{12} = 2B^2 \frac{dH}{dB} \quad ; \tag{3.4}$$

$$C_{44} = \underline{B}.\underline{H} \quad ; \tag{3.5}$$

and for large κ_{GL} near B_{C2},

$$C_{66} \approx 0.1(B_{C2}^2/\mu_0\kappa_{GL}^2)(1-b)^2 \quad . \tag{3.6}$$

For materials with high κ_{GL} the shear modulus is very small compared to the compression and tilt moduli and goes to zero as the upper critical field is approached.

Further work by Brandt[6] has shown that Labusch's equations are only valid if the wavevector of the lattice distortions, k, is zero. He goes on to derive expressions for C_{11} and C_{44} dependent on k for high and low fields. The shear modulus is only weakly dependent on k. Figure 3.2 from Brandt[7] demonstrates the effect of non-locality on the elastic moduli.

3.3.3. Summation of pinning forces

The elementary pinning force, f_p, can be calculated for the various types of pinning centres[8] but computing the bulk pinning force density, F_p, is a more difficult problem. Assuming there is only one type of pinning interaction, F_p can be given by

$$F_P = \eta n_P f_P \tag{3.7}$$

where n_p is the number density of the randomly distributed pinning centres and η is an efficiency depending on how the FLL is treated. If it is rigid it would not be able to

find a position of minimum energy and therefore not be pinned. Dew-Hughes[8] assumed it to be plastic, leading to the maximum possible pinning force. Considering the lattice to be elastic falls between these two extremes but involves the calculation of an effective elastic modulus C_ϕ (in terms of C_{44} and C_{66}). Equation 3.8 summarises the possible cases.

$$\begin{aligned} &\textit{rigid lattice}, && \eta = 0, && F_P = 0 \ ; \\ &\textit{elastic lattice}, && \eta = f_P/C_\phi, && F_P = n_P f_P^2/C_\phi \ ; \\ &\textit{plastic lattice}, && \eta = 1, && F_P = n_P f_P \ . \end{aligned} \tag{3.8}$$

3.3.4. Collective pinning

The important theory of collective pinning was formulated by Larkin and Ovchinnikov[9]. They investigated the deformation of the flux line lattice from a random array of pinning centres. In a volume V_c there is a short range order and the lattice is periodic. At long distances however, this order is lost. When a current flows, each of the correlated volumes, V_c, are displaced over a distance less than ξ_{GL} under the action of the Lorentz force. The transverse and longitudinal lengths of the region within which short range order exists are R_c and L_c respectively such that $V_c = R_c^2 L_c$. Larkin and Ovchinnikov found these lengths to vary as follows :

$$R_C \propto \frac{C_{66}^{3/2} C_{44}^{1/2} a_0^2}{n_P f_P^2} \ ; \quad L_C \propto \frac{C_{66} C_{44} a_0^2}{n_P f_P^2} \ ; \qquad V_C \propto \frac{C_{44}^2 C_{66}^4 a_0^6}{n_P^3 f_P^6} \tag{3.9}$$

where a_0 is the spacing of the FLL, n_P is the density of pinning centres and f_P is the pinning force of an individual centre.

They then calculated the critical current density as

$$J_C \propto \frac{n_P^2 f_P^4}{B a_0^3 C_{44} C_{66}^2} \qquad (3.10)$$

with B as the magnetic field.

If R_c and L_c are larger than the lattice spacing, a_0, then there will be collective pinning of the flux lines in a volume V_c. The field range over which collective pinning can occur varies according to the values of n_p and f_p and the dimensionality. Generally, for very weak fields (where a_0 is large) and close to B_{c2} (where the lattice softens and C_{66} approaches zero) the pinning is of a single flux-line nature. Collective pinning then occurs in the intermediate fields.

3.3.5. The vortex glass state

The *vortex glass* was introduced by M.P.A. Fisher[10] in 1989 and developed in 1991 by D.S. Fisher et al.[11]. In a vortex glass there is no long range order of the lattice but there is long range phase coherence in the order parameter. Fisher et al.[11] considered the fact that along the length of a flux line the pinning strength varies. The vortex glass forms metastable states which have very high energy barriers between them, leading to zero flux flow resistivity. Above a temperature T_g the vortex glass is destroyed by thermal fluctuations and it is suggested that it becomes a vortex liquid. In pure 2D systems a vortex glass is unstable.

The theories of collective pinning and vortex glass essentially consider the same physics but using different length scales.

3.3.6. Scaling

Fietz and Webb[12] demonstrated that for most materials the pinning force density followed a scaling law of the form

$$F_p(B,T) = \alpha_p(T) B_{C2}^n(T) b^m (1-b)^k \qquad (3.11)$$

such that plotting F_P/F_{Pmax} ($F_{Pmax} \propto \alpha_p(T)B^n_{C2}$) vs the reduced field b causes the pinning curve for all temperatures to lie on the same curve.

A couple of important models have been developed to explain the observed pinning curves (the parameters n,m and k vary with materials and their mechanical history). Kramer[13] assumed that below F_{Pmax} flux motion occurred from the unpinning of line pins but above it the FLL shears about a few strongly pinned lines. He predicted that n=2.5, m=0.5 and k=2. This model fitted some data well but could not account for the variety of different curves measured. Dew-Hughes[8] considered the geometry of possible pinning centres and whether the interaction was a core or magnetic one. He obtained a series of pinning curves which could explain most of the observed ones. In his analysis however he assumed the FLL was plastic, neglecting any elasticity effects.

Scaling in low temperature superconductors is not always observed[14] but this could be due to the method of measurement of B_{C2}. It is still not clear if there is scaling in the high-temperature superconductors, partly because accurate determination of B_{C2} is difficult and the value of the irreversibility field (used instead as the scaling field) depends somewhat on the type of measurement used to determine it. If there is large thermally activated depinning (as is the case for HTSCs) it is suggested that, except for special cases, scaling should not occur[3,15].

3.4. The irreversibility line

Early magnetic measurements on the newly discovered HTSC crystals[16] showed that at certain fields and temperatures, below B_{C2} and T_C respectively, the magnetisation

became reversible. This line in the B-T phase diagram is known as the *irreversibility line*, $B_{irr}(T)$. At this line the critical current drops to zero and the flux lines are no longer pinned. Hence although it is still in the superconducting phase, at fields between B_{irr} and B_{c2} the HTSC materials are technologically useless. After B_{irr} was discovered in HTSC's it was also found to exist in conventional superconductors such as NbTi[17,18,19] but occurred very close to B_{c2}.

With the HTSCs, the more anisotropic compounds have a lower $B_{irr}(T)$[19] and as with other properties, B_{irr} is also anisotropic with respect to crystal direction (it is higher when B is parallel to the ab-plane). Slightly different values of B_{irr} for the same sample are obtained from different measurements (e.g. resistive, susceptibility, vibrating reed). This is probably due to the different time scales involved in each experiment[20]. For the HTSCs, the irreversibility line can be altered by doping[21], changing the oxygen content[22] and neutron irradiation[23] (producing cascades of defects). For ultra-fine multifilamentary NbTi wire the filament size greatly affects $B_{irr}(T)$[18].

The mechanism that is behind the irreversibility line is controversial. It is thought to be caused either by thermal depinning of the flux lines or a *melting* of the flux line lattice. It could be a different mechanism in different materials. Thermally activated depinning of flux lines is covered briefly in section 3.7.3. Melting, where the FLL loses all order, is discussed in section 3.6.2. Possible thermal fluctuation induced depinning of collectively pinned flux lines is covered in section 3.7.4. Today, the low values of the irreversibility line in the high temperature superconductors are the main causes in limiting their potential for applications.

3.5. Flux lines in layered structures

In a layered structure the anisotropic Ginzburg-Landau theory cannot describe the vortex structure if the coherence length perpendicular to the superconducting planes is smaller than the inter-planar spacing. Using the Lawrence-Doniach model as a basis, Clem[24] has described the structure of a flux line passing through a stack of weakly coupled layers. His calculations hold for the limit where the Josephson coupling

(but not the magnetic coupling) between the layers is zero.

If the magnetic field is parallel to the layers, from the L-D model the supercurrent distribution of one vortex is as shown in figure 3.3a. The supercurrent decays with a scale length λ_c in the ab-plane (or x-y plane) and λ_{ab} along the c-axis (or z-axis). When the field is along the c-direction the supercurrent flows in ellipses confined in the ab-plane and there is no current in the c-direction. The field lines of one such *pancake vortex*, modified by the screening currents of adjacent layers is shown in figure 3.3b from Clem[24]. The spatial extent of a pancake is determined by the length λ_c. A flux line can then be constructed by stacking several pancake vortices together. Figure 3.3c is such a stack at an angle to the c-axis. The individual pancakes are coupled via Josephson vortices (or strings) whose cores are parallel to the planes and are similar to that in figure 3.3a.

3.6. Flux line lattice melting

3.6.1. Pancake decoupling

In a layered material where the flux lines are composed of pancake vortices, thermal agitation of the flux lines can overcome the magnetic interaction between the layers and decouple the superconducting layers. Clem[24] calculated an expression for the decoupling temperature of the pancakes as

$$T_d(B) \approx \left(\frac{\phi_0^2}{4\pi\mu_0 k_B \Lambda}\right)\left(1 + \frac{B}{B_1}\right)^{-1} \qquad (3.12)$$

$$\Lambda = \frac{2\lambda_{ab}^2}{s}, \qquad B_1 = \frac{\sqrt{3}\phi_0}{8\pi^2\lambda_{ab}^2}$$

where Λ is the 2D film current screening length. T_d was obtained by neglecting pinning effects. It is strongly suppressed in high fields. Above this temperature the pancakes are thermally decoupled in the c-direction but form a 2D lattice in each layer. The FLL must then be treated as quasi-2D.

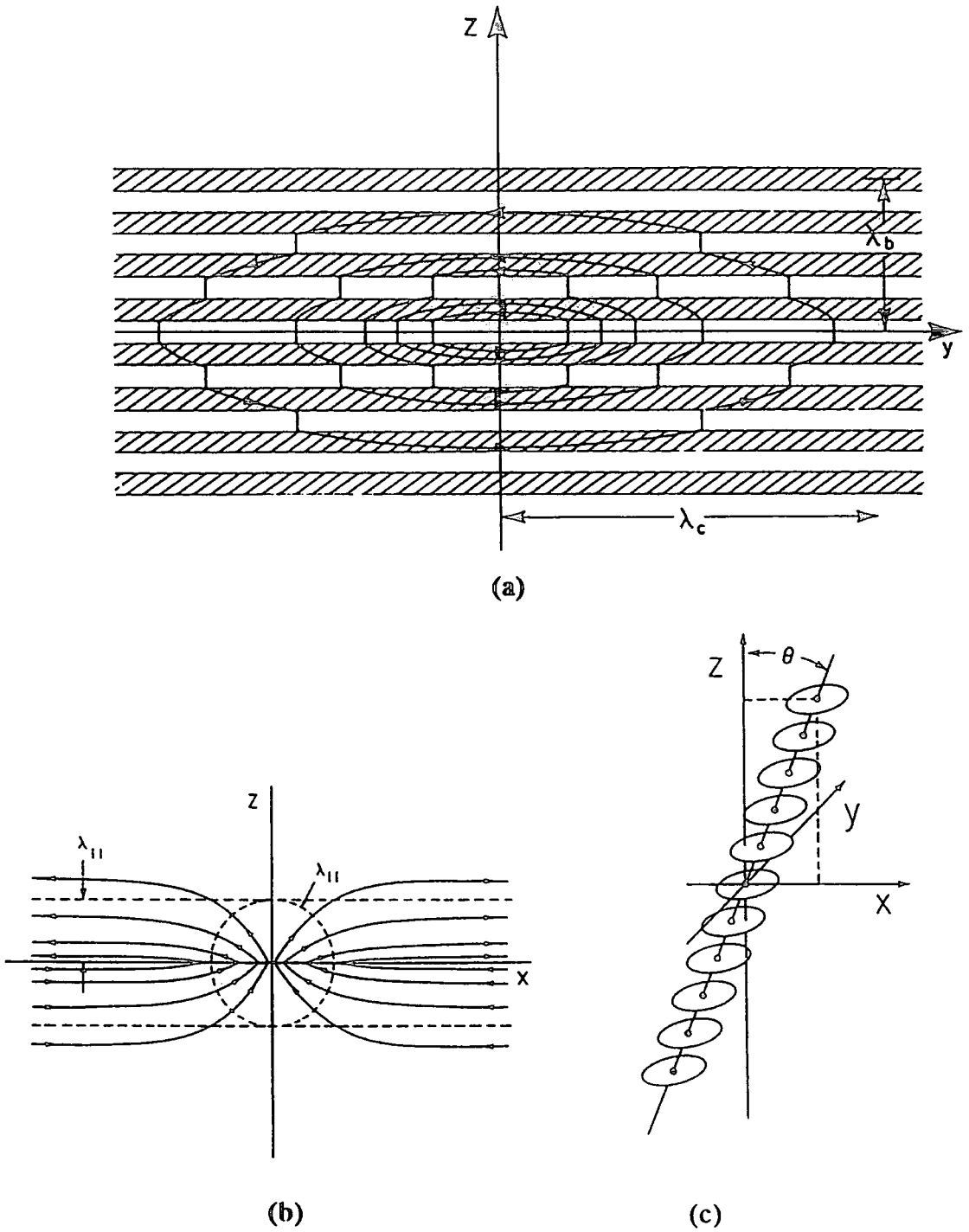

Figure 3.3: Flux lines in layered superconductors: (a) the supercurrent distribution of a single vortex parallel lying parallel to the x-axis in an insulating layer (white); (b) the magnetic field lines of a single pancake vortex, modified by screening currents (λ_1 is the penetration depth in the superconducting layer) and (c) a flux line composed of a stack of pancakes, tilted at an angle θ to the plane of the layers.

3.6.2. Lindemann melting

The idea of a vortex glass to vortex liquid transition was first put forward by M.P.A. Fisher[10]. In the vortex liquid state there is no short range order at all and the lattice consists of mobile fluctuating vortices. The vortex glass melting can be estimated using the Lindemann criterion which says that the lattice will melt when $<u^2>^{1/2}=c_L a_0$ where a_0 is the lattice spacing and c_L is approximately 0.1. Several authors have derived such a melting temperature[10,20,25]. Brandt[20] derives

$$B_{irr}(T_m) = B_{C2}(0)(1 - t^2)(1 - t^4)t^{*2}/t^2 ,$$
$$t = T_m/T_C , \qquad t^* = \frac{0.82 c_L^2 \phi_0^2}{\mu_0 k_B T_C \lambda_C(0) \kappa_{GL}} \tag{3.13}$$

where T_m is the melting temperature. Near T_C, $B_{irr} \propto (1-t)^2$. Brandt points out that the idea of melting from a lattice softening is not clearly justified. It would be reasonable to assume that a soft lattice is pinned much *more* easily with the density of pins that exist in HTSC's. Also these melting theories do not account for the correct 3D vortex-vortex interaction and possible flux line cutting. Values for T_m, predicted using $c_L=0.1$, are generally too low.

3.7. Thermal effects on the flux line lattice

3.7.1. Effect of thermal fluctuations on the critical current and dimensionality

In incorporating thermal fluctuations into the theory of collective pinning for HTSC's it is generally assumed that the pinning is due to some small scale weak disorder and that there is weak Josephson or magnetic coupling between the layers. Only the case where B is parallel to the c-axis is covered. Such pinning could be due to oxygen defects and will vary on a scale of the coherence length. Thermal fluctuations will then start to reduce the critical current as the mean squared displacement of a flux line, $<u^2>$, becomes larger than the square of the coherence length, or $<u^2> \geq \xi^2$.

a) 3D collective pinning

Feigel'man and Vinokur[26] have discussed the case for a 3D flux lattice for three pinning regimes :

i. Single flux line pinning occurs below a temperature T_v and for small magnetic fields. In this regime J_c should be independent of field.

ii. In medium fields there is pinning of small bundles and the critical current is

$$J_C = \frac{3\sqrt{3}}{32\pi} J_{C0} \frac{B}{B_{C2}} \left(1 + \frac{T}{T_P}\right)^{\frac{1}{2}} \exp\left[-\pi\sqrt{2}\left(\frac{B}{B_{C2}}\right)\frac{G_m}{G}\left(1 + \frac{T}{T_P}\right)^3\right] \qquad (3.14)$$

J_{C0} is the depairing current and the temperature T_P is when $\langle u^2 \rangle = \xi^2$ and is given by

$$k_B T_P = \frac{\phi_0^{3/2} B^{1/2}}{\pi \mu_0 \kappa^2} \qquad (3.15)$$

At low fields $T_P \rightarrow T_V$. It can be seen that the argument of the exponential is almost field independent. The factor G is the characteristic strength of the random pinning potential and G_m is the value of G corresponding to strong short scale disorder.

iii. In large magnetic fields there is collective pinning of large bundles and the critical current becomes

$$J_C \approx \frac{10 J_{C0}}{\kappa^2}\left(\frac{G}{G_m}\right)^2\left(\frac{B_{C2}}{B}\right)^3\left(1 + \frac{T_P}{T}\right)^{11/2} \qquad (3.16)$$

which has a stronger field dependence.

The crossover fields from one regime to the other depend on the parameter G/G_m.

b) Magnetically coupled layers

Collective pinning in the limit of magnetically coupled layers has been investigated by Koshelev and Kes[27]. They calculated the tilt modulus C_{44} and found that it depends only on the c-axis component of the lattice distortion wavevector, k_c. As the lattice spacing, a_0, falls below the layer spacing, s, C_{44} decreases sharply. They predict that the following pinning regimes are possible, depending on the relative magnitudes of the energies U_P (the pinning energy), U_{tilt} (the lattice tilt energy) and U_{shear} (the lattice shear energy):

i. independently pinned flux lines when $U_{tilt} > U_P > U_{shear}$;
ii. independently pinned pancake vortices when $U_P > U_{tilt}$ and U_{shear};
iii. collective pinning of the 2D pancakes when $U_{shear} > U_P > U_{tilt}$;
iv. a 3D collectively pinned state when U_{tilt} and $U_{shear} > U_P$.

Not all the regimes would necessarily be present in a material. They further defined the lattice disorder using the mean square random force, $\gamma_P = (U_P/r_P)^2$ where r_P is the range of the pinning force. At the crossover from regime i to ii, $\gamma_P = \gamma_{P0}$, i.e. γ_{P0} is the value of γ_P at which the interaction with the pinning potential becomes stronger than the interlayer pancake coupling. The fields at which dimensional crossovers occur and the value of J_c in each regime is determined sensitively by the parameter γ_P/γ_{P0} and the maximum critical current at small fields, J_{c0}.

Koshelev and Kes predict that the 2D to 3D crossover (going from regime iii to iv) is a first order phase transition but that J_c has the same field dependence in both regimes (unless at very high fields). Approximate values of γ_P/γ_{P0} suggest that in BSCCO compounds the transition from independently pinned flux lines to 2D pancake lattices could occur in the region of 1-5T at 4.2K.

c) Josephson coupled layers

Feigel'man et al.[28] and Vinokur et al.[29] have developed the theory of 3D

collective pinning of section 3.7.1a to take account of the possible 2D nature of the lattice in layered compounds. Depending on the material anisotropy, Γ and the relative lattice energies, some or all of the regimes listed in 3.7.1b for magnetic coupling are possible. The amount of anisotropy is important because for $\lambda > a_0$ the non-local tilt modulus C_{44} is reduced by a factor Γ[25]. The relevant scale lengths are R_c, the transverse pinning correlation length and R_j, the characteristic length of the interlayer coupling. Fluctuations of the FLL are of 2D nature when $R_j > a_0$, the lattice spacing. This is true for fields above

$$B_{2D} = \frac{\phi_0}{s^2\Gamma} \tag{3.17}$$

Below the field B_{2D} there is 3D single flux line pinning of the lattice. Above this field the lattice consists of 2D vortex pancakes which are pinned independently until $R_c > a_0$ which occurs at a temperature T_v and a field

$$B_{CP} \approx \alpha^{1/2} B_{C2} \tag{3.18}$$

where α is a dimensionless parameter (characterising the pinning strength) which is much less than one. At zero field $k_B T_v = U_p$. In this regime the critical current varies (if it is assumed to be less than the depairing current) as

$$J_C \propto \frac{U_p}{s\phi_0\xi_{ab}} \tag{3.19}$$

For 2D collective pinning J_c is given by

$$\begin{aligned} T < T_P , \quad J_C = J_{C1} &\propto J_{C0}\left(\frac{\xi_{ab}}{R_C}\right)^2 \\ T > T_P , \quad J_C &\propto B^{3/2} \end{aligned} \tag{3.20}$$

where T_p is the temperature at which the thermal fluctuations of the lattice become important.

The pinning is of 2D nature until $R_C \geq R_J$ which occurs at a field and temperature

$$B_{3D} = B_{C2}\left(\frac{\alpha\Gamma^{1/2}s}{\xi_{ab}}\right)^{2/3}$$
$$T_{3D}(B) \propto \frac{B^{1/2}}{\ln B} \qquad (3.21)$$

Note that for 2D collective pinning above T_P, J_C is predicted to increase with increasing field.

3.7.2. Flux creep

If the thermal fluctuations in a superconductor are of the same order of magnitude as the pinning energies there will be some hopping of the flux lines out of their potential wells. Because of vortex-vortex interactions there could be bundles of flux jumping. In the presence of a transport current this thermally activated flux creep acts to reduce the flux-density gradient. This flux motion is found to decay logarithmically with time. The basic theory of flux creep was formulated by Anderson and Kim[30]. Assuming that the jump rate is given by

$$\nu = \nu_0 e^{-U/k_BT} \qquad (3.22)$$

where υ_0 is a characteristic attempt frequency and U(B,T) is the activation energy, the electric field due to thermally activated flux creep can be shown[31] to be

$$E(J) = 2\rho_C J_C e^{-U/k_BT}\sinh(JU/J_C k_B T) \qquad (3.23)$$

with ρ_C as the resistivity at $J=J_C$.

In conventional superconductors flux creep is only observed close to J_C when the resistivity (equal to E/J) varies exponentially :

$$\rho \propto e^{J/J_0} \qquad (3.24)$$

where $J_0=J_C k_B T/U$ (this relationship can be obtained from equation 3.23 as an

approximation when $U \gg k_B T$). In HTSC materials however, because of the small coherence length and hence small pinning energy, flux creep is observed at much smaller temperatures and currents. This case is sometimes referred to as *thermally activated flux flow (TAFF)* and from equation 3.23 for $J < J_0$ it can be shown that the resistivity is current independent, giving rise to ohmic behaviour. The Anderson-Kim model predicts a finite resistivity at all temperatures above zero Kelvin.

Using the theory of collective pinning for layered structures[28,29], in the regime of 2D pinning the flux creep can be of 2D or 3D nature. Above T_p the activation energy for flux creep is expected to follow the law $U(J) \propto J^{-\mu}$ which leads to

$$E/E_0 = \exp\left\{-\frac{U_0}{\mu k_B T}\left[\left(\frac{J_0}{J}\right)^{\mu} - 1\right]\right\} \qquad (3.25)$$

which can be compared to equation 3.23.

A similar flux creep behaviour to equation 3.25 is also expected for a vortex glass[11].

3.7.3. Thermally activated depinning

Considering the irreversibility line as a thermally activated depinning line (when $k_B T$ becomes of the order of U_p), Yeshurun and Malozemoff[16] estimated the pinning potential and predicted that $B_{irr}(T)$ should vary as

$$B_{irr} \propto (1 - t)^{\delta} \qquad (3.26)$$

The experimental results for YBaCuO fit this relationship well with $\delta = 1.5$. Matsushita et al.[32] developed this further using local values of the elastic moduli to include the effects of different pinning mechanisms. The temperature dependence is the same as that taken for the variation of B_{c2} with an exponent $\delta = 2n/(3-2m)$ where the parameters n and m are the exponents from the pinning force scaling relation - equation 3.11. Matsushita[33] found that B_{irr} for a bulk $Bi_2Sr_2Ca_2Cu_3O_x$ sample varied as $(1-t^2)^{\delta}$ with $\delta = 4.5$.

3.7.4. Fluctuation induced melting of a collectively pinned lattice

Feigel'man et al.[28] have used collective pinning theory to calculate a melting temperature. They argue that thermal fluctuation of the flux lines, $<u^2>$, increases the effective range of the pinning force and results in smoothing out the pinning potential. The collective pinning force then goes to zero at

$$k_B T_m = \left(\frac{c_L^2}{\pi \Gamma^{1/2} \mu_0}\right)\left(\frac{\phi_0^{5/2}}{B^{1/2} \lambda_L^2(0)}\right) \qquad (3.27)$$

This is sometimes described as a melting of the lattice though it could also be effectively described as thermal depinning.

In a purely 2D system (e.g. thin films) the lattice does melt, at the predicted Berezinkiĭ-Kosterlitz-Thouless transition[34]:

$$k_B T_{BKT} = \frac{\phi_0^2 d}{64\pi^2 \lambda_L^2 \mu_0} \qquad (3.28)$$

where d is the film thickness. The melting in this case is mediated by dislocations. Feigel'man et al.[28] predict that in the context of 2D collective pinning in HTSC materials this transition takes place at AT_{BKT} where A is a constant less than unity.

3.8. Angular dependence of the critical current density

3.8.1. The Lorentz force free orientation

If the applied field is at an angle, θ to the current direction then J_c is determined by using the perpendicular field component, $B\sin\theta$ in the critical state equation, 3.1. As θ approaches zero however, this substitution is no longer valid. If B is parallel to J then the Lorentz force is zero and there should be no need to pin the flux lines. A wire (or a slab but a wire is considered for the following discussion) in a longitudinal field does have a higher J_c than when the field is perpendicular[35] but the mechanism

limiting the current density is not clear. As the flux lines are parallel to the field at the surface of the wire they must enter as helices. To generate a voltage along the wire there must be some collapsing of azimuthal flux to the centre. To prevent the continuous build up of flux at the centre of the wire several authors have introduced the concept of flux cutting (Timms and Walmsley[36], Campbell and Evetts[3] and Clem[37]). This is where two flux lines cut across each other and then reconnect after crossing such that their lengths are reduced. A combination of such cutting events would produce a net movement of azimuthal flux to the centre as required. It is possible however that the flux configuration is more complex and the simple helix collapses into a combination of different helices causing a varying potential along the length of the wire[38].

The current theoretical description of force free configurations is poor and does not adequately explain all the observed measurements.

It should be noted that if an applied field is macroscopically parallel to the transport current it is not necessarily parallel to the field microscopically. For granular and/or anisotropic materials the current will be at varying angles to the field along it's percolative path.

3.8.2. Weakly coupled layered structures

The collective pinning theory covered so far for layered structures only considers the case when the magnetic field is parallel to the c-axis (perpendicular to the superconducting planes). From the Lawrence-Doniach model[39] the order parameter between the superconducting planes is depressed. In a field parallel to the planes the flux lines are more likely to lie in the insulating layers (to minimise the free energy). This only holds if the coupling is weak and there is 2D pinning. Tachiki and Takahashi[40] and Kes et al.[41] have discussed this *intrinsic pinning*. They conclude that when the field is at an angle θ to the c-axis only the component parallel to c causes dissipation in the material. Scaling of the critical current with $B\sin\theta$ in

BSCCO-2223 films has been observed by Yamasaki et al.[42] and Schmitt et al.[43].

3.9. High temperature superconducting materials

The recently discovered family of high temperature cuprate superconductors have significantly different properties than conventional superconductors. Their structures and hence their superconducting properties are highly anisotropic. They have a layered crystal structure with planes of Cu-O separated from each other by planes of other oxides or rare earths. A schematic representation of some materials is presented in figure 3.4. It is not yet clear whether the very high values of T_c and critical fields can be described by the BCS theory. The charge carriers are paired[44] but the pairing mechanism is controversial. If it is phonon-mediated a modification to the BCS theory is required. It is clear however that the charge transfer is mostly confined to the Cu-O planes which are parallel to the a and b directions in the crystal. The coherence lengths in the c-direction are typically smaller than the separation between the Cu-O planes so the lattice must be considered in terms of the pinning theories for weakly coupled layers.

Because of the high temperatures, thermal effects are much more important over a wider range of the B-T phase diagram of the superconductor than for conventional materials. This may account for the *irreversibility line* existing well below the critical temperature for the HTSC's. The low values of $B_{irr}(T)$ are a major obstacle in applications of these materials at the economically favourable temperature of liquid nitrogen.

Finally, the high temperature materials are granular with the grain boundaries consisting of normal or weakly superconducting material. Because the coherence lengths are so small these *weak links* between grains can act as Josephson junctions, depressing transport critical currents and causing them to take complicated percolative paths. The intragranular critical currents, calculated by magnetic techniques, can be a factor of a hundred higher than the intergranular critical currents, measured from transport measurements. Dimos et al.[45] demonstrated that in YBaCuO crystals high angle

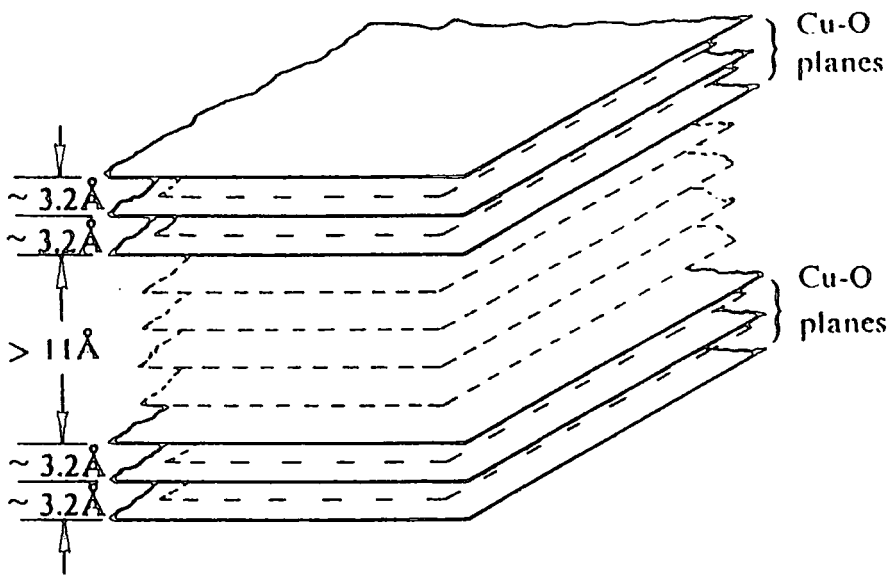

Figure 3.4: A representation of the structure of a layered HTSC superconductors with three Cu-O planes per superconducting layer ($Bi_2Sr_2Ca_2Cu_3O_x$ or $Tl_2Sr_2Ca_2Cu_3O_x$). The insulating layers inbetween are composed e.g., of the Bi/Sr and Ca ions. The c-axis is perpendicular to the layers. Diagram courtesy of Burns[46].

grain boundaries acted as weak links whilst the low angle grain boundaries were strongly coupled. Malozemoff[47], Bulaevskii et al.[48] and Daemen et al.[49] have used the *brick-wall model* to describe the percolative path of the current in BiSrCaCuO tapes where the crystal grains are to some degree orientated with a common c-axis. This model assumes that the transport current crosses from one grain to another via the ab-plane grain boundaries only, i.e. at the boundary the current flows parallel to the c-axis. By considering a distribution of these boundaries acting as Josephson junctions, the field and temperature dependence of the measured transport critical current density can be predicted. An alternative model is the *railway-switch model*[50] by Hensel et al. They suggest that the current passes between grains via small-angle c-axis grain boundaries. This allows the current flow to always be in the ab-plane. The measured J_c is then determined by the intrinsic anisotropy of BSCCO.

The combination of granularity and the layered crystal structure makes the FLL particularly difficult to describe and explain in the high temperature superconductors. Using collective pinning theory some of the pinning regimes we may expect to see in an HTSC are illustrated in figure 3.5. Typical values for the superconducting parameters of $YBa_2Cu_3O_{7-\delta}$ and $Bi_2Sr_2Ca_2Cu_3O_x$ were given in table 2.2.

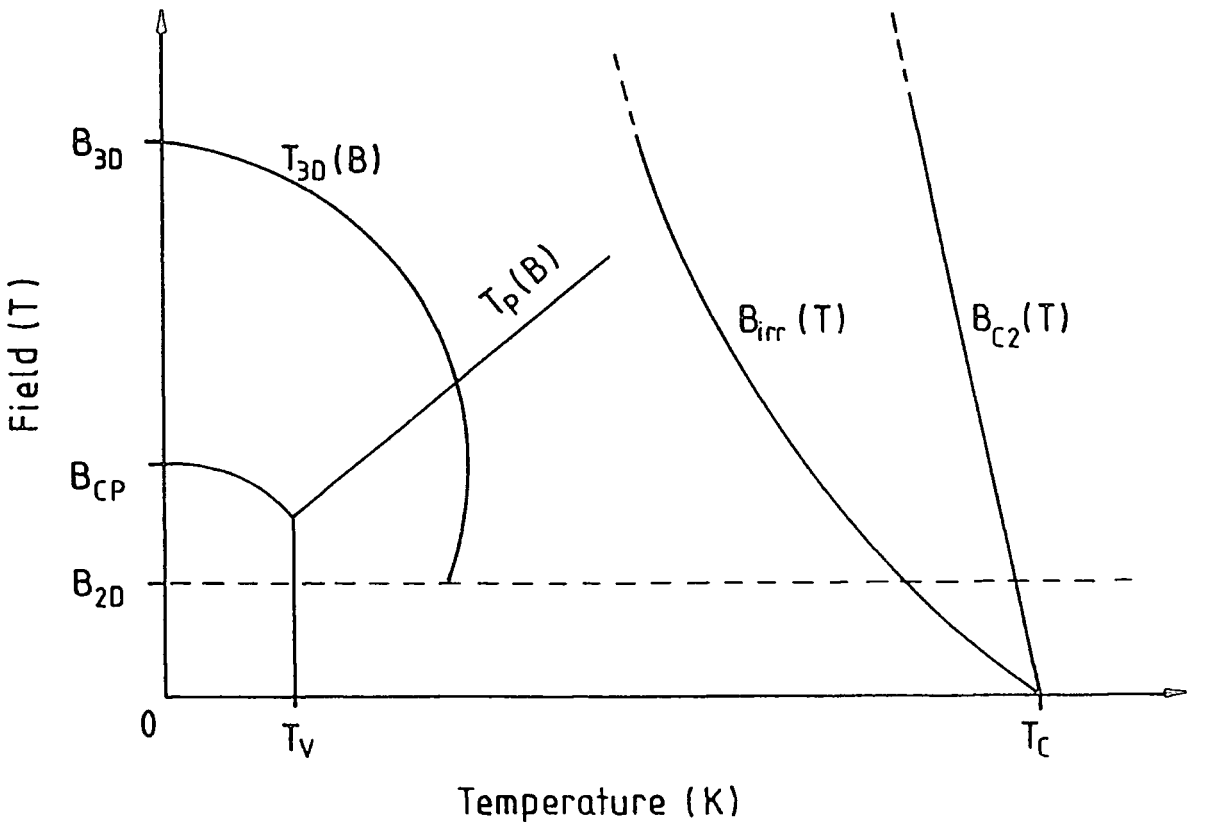

Figure 3.5: A possible B-T phase diagram for collective pinning in a layered superconductor. Above the field B_{2D} the flux lines are composed as pancakes which are pinned independently up to T_V and B_{CP}. T_P marks the point at which the thermal fluctuations become important and T_{3D} marks the crossover from 2D-3D like collective pinning. $B_{irr}(T)$ is the irreversibility line. See section 3.7.1c for more detail.

3.10. Summary on the flux line lattice

This chapter has covered some of the complexities of the flux line lattice in the presence of a transport current density. The basic idea that the Lorentz force on the flux lines by the current is supported by pinning centres, up to a critical threshold has been presented. The problem of this critical state then becomes the problem of determining the bulk volume pinning force of a material. Interactions between the individual flux lines must also be considered. They can be explained in terms of the flux line lattice elastic constants. These interactions and the random distribution of pinning centres leads to the idea of small correlated regions of the lattice and the theories of collective pinning and the vortex glass.

Generally, the volume pinning force is found to scale with temperature. This scaling breaks down if there are large thermal fluctuations of the lattice or if the superconductor has a weakly coupled layer structure. In the latter case the flux lines are thought to form pancake vortices in the superconducting layers connected by Josephson strings through the insulating layers. If the interlayer coupling strength is weak compared to the vortex-vortex interactions within a layer the superconductor has to be described in terms of a 2D lattice.

The theory of thermally activated flux creep and depinning has been discussed briefly. The possible melting of the lattice from a loss of all order and from a thermally induced smearing of the pinning potential was also covered. As of yet, it is not known whether the irreversibility line is a melting of the lattice or a thermal depinning line.

A description of the FLL in high temperature superconductors is made difficult by a combination of large critical temperatures, granularity and an anisotropic structure. A summary of the possible pinning regimes in the B-T phase diagram of a layered superconductor based on the collective pinning theory of Feigel'man et al.[28] and Vinokur et al.[29] is illustrated in figure 3.5. The shape of the crossover lines are only drawn approximately.

References for Chapter 3

1. Leghissa M.,Kreiselmeyer G., Kraus M., Holzapfel B., Vinnikov L. Ya., Schuster Th. and Saemann-Ischenko G., *EUCAS 1993 - Applied Superconductivity Vol. I*, Ed. Freyhardt H.C. (DGM, 1993) p.787-790.

2. Harada K., Matsuda T., Bonevich J.E., Igarashi M., Kondo S., Pozzi G., Kawabe U. and Tonomura A., Nature 360, 51 (1992).
Harada K., Matsuda T., Kasai H., Bonevich J.E., Yoshida T., Kawabe U. and Tonomura A., Phys. Rev. Lett. 71(20), 3371 (1993)

3. Campbell A.M. and Evetts J.E., Adv. in Phys. XXI (90), 199-428 (1972).

4. Huebener R.P., *Magnetic Flux Structures in Superconductors*, (Springer-Verlag, Berlin 1979).

5. Labusch R., Phys. Stat. Sol., 19 715 (1967);
Labusch R., Phys. Stat. Sol., 32 439 (1969).

6. Brandt E.H., J. Low Temp. Phys., 26 709 (1976);
Brandt E.H., J. Low Temp. Phys., 26 735 (1976);

7. Brandt E.H., *High-Temperature Superconductivity*, 437-445, Ed. Ashkenazi et al. (Plenum Press, N.Y. 1991).

8. Dew-Hughes D., Philos. Mag. 30, 293 (1974).

9. Larkin A.I. and Ovchinnikov Yu.N., J. Low Temp. Phys. 34, 409 (1979).

10. Fisher M.P.A., Phys. Rev. Lett. 62(12), 1415 (1989).

11. Fisher D.S., Fisher M.P.A. and Huse D.A., Phys. Rev. B. 43(1), 130 (1991).

12. Fietz W.A. and Webb W.W., Phys. Rev. 178(2), 657 (1969).

13. Kramer E.J., J. Appl. Phys. 44(3), 1360 (1973).

14. Collings E.W., *Applied Superconductivity, Metallurgy and Physics of Titanium Alloys Vol.2* (Plenum Press, N.Y. 1986).

15. Niel L., Cryogenics 32(11), 975 (1992).

16. Yeshurun Y. and Malozemoff A.P., Phys. Rev. Lett. 60, 2202 (1988).

17. Suenaga M., Ghosh A.K., Xu Y. and Welch D.O., Phys. Rev. Lett. 66, 1177 (1991); Suenaga M., Welch D.O. and Budhani R., Supercond. Sci. Technol. 5, S1 (1992).

18. Sulpice A., Jonnard P. and Giordanengo B., *Proc. EUCAS 1993 - Applied Superconductivity Vol 1*, ed. Freyhardt H.C. (DGM - 1993) p.697.

19. Zheng D-N., PhD Thesis, Christ's College, Cambridge (1994).

20. Brandt E.H., Intl. J. Mod. Phys. B 5(5), 751 (1991).

21. Zheng D.N., Campbell A.M., Johnson J.D., Cooper J.R., Blunt F.J., Porch A. and Freeman P.A., Phys. Rev. B. 49, 1417 (1994).

22. Czurda C. and Weber H.W., *EUCAS 1993-Applied Superconductivity Vol. I*, Ed. Freyhardt H.C. (DGM, 1993) p. 795-798.

23. Wisniewski A., Brandstätter G., Czurda C., Weber H.W., Morawski A. and Lada T., Physica C 220, 181 (1994).

24. Clem J.R., Phys. Rev. B. 43(10), 7837 (1991).

25. Houghton A., Pelcovits R.A. and Subdø A., Phys. Rev. B. 40, 6763 (1989).

26. Feigel'man M.V. and Vinokur V.M., Phys. Rev. B. 41(13), 8986 (1990).

27. Koshelev A.E. and Kes P.H., Phys. Rev. B. 48(9), 6539 (1993).

28. Feigel'man M.V., Geshkenbein V.B. and Larkin A.I., Physica C 167, 177 (1990).

29. Vinokur V.M., Kes P.H. and Koshelev A.E., Physica C 168, 29 (1990).

30. Anderson P.W. and Kim Y.B., Rev. Mod. Phys. 36, 39 (1964).

31. Tinkham M., *Introduction to Superconductivity*, (McGraw-Hill, New York 1975).

32. Matsushita T., Fujiyoshi T., Toko K. and Yamafuji K., Appl. Phys. Lett. 56(20), 2039 (1990).

33. Matsushita T., Otabe E.S. and Ni B., Supercond. Sci. & Technol. 5, S73 (1992).

34. Berezinskiĭ V.L., Zh. Eksp. Theor. Fiz. 59, 907 (1970) [Sov. Phys. JETP 32, 493 (1971)];
Kosterlitz J.M. and Thouless D.J., J. Phys. C. 6, 1181 (1973);
Hubermann B.A. and Doniach S., Phys. Rev. Lett. 44, 950 (1979).

35. Sekula S.T., Boom R.W. and Bergeron C.J., Appl. Phys. Lett. 2, 102 (1963).

36. Timms W.E. and Walmsley D.G., J. Phys. F: Metal Phys. 5, 287 (1975).

37. Clem J.R., Phys. Rev. B. 26(5), 2463 (1982).

38. Cave J.R., *Complex flux configurations in a type II superconductor*, Thesis, Clare Hall, Cambridge (1978).

39. Lawrence W.E. and Doniach S., *Proc. 12th Internatl. Conf. of Low Temperature Physics LT12* (ed. Kanda E., Academic Press of Japan: Kyoto) 361 (1971).

40. Tachiki M. and Takahashi S., Cryogenics 32(11), 923 (1992).

41. Kes P.H., Aarts J., Vinokur V.M. and van der Beek C.J., Phys. Rev. Lett. 64, 1063 (1990).

42. Yamasaki H., Endo K., Kosaka S., Umeda M., Misawa S., Yoshida S. and Kajimura K., IEEE Trans. Appl. Supercond. 3(1), 1536 (1993).

43. Schmitt P., Kummeth P., Schultz L. and Saemann-Ischenko G., Phys. Rev. lett. 67(2) 267 (1991).

44. Gough C.E., Colciough M.S., Forgan E.M., Jordan R.G., Keene M., Muirhead C.M., Rae A.I.M., Thomas N., Abell J.S. and Sutton S., Nature 326, 855 (1987).

45. Dimos D., Chaudhari P. and Mannhart J., Phys. Rev. B 41(7), 4038 (1990).

46. Burns G., *High-Temperature Superconductivity, An Introduction* (Academic Press 1992).

47. Malozemoff A.P., *High Temperature Superconducting Compounds II*, ed. Whang S.H. et al. (TMS Publications, Warrendale, PA, 1990) p.3.

48. Bulaevskii L.N., Clem J.R., Glazman L.I. and Malozemoff A.P., Phys Rev. B 45(5), 2545 (1992).

49. Daemen L.L., Bulaevskii L.N., Maley M.P. and Coulter J.Y., Phys. Rev. B 47(17), 11291 (1993).

50. Hensel B., Grivel J.C., Jeremie A., Perin A., Pollini A. and Flükiger R., Physica C 205, 329 (1993).

4. The Design and Operation of a Probe for the Measurement of the Critical Current Density of Superconductors

If high temperature superconductors (HTSC) are to be used successfully in applications such as high field magnets[1], power cables[2] and magnetic energy storage devices[3], we need to fabricate materials with high critical current densities ($J_c(B,T)$). In particular, these new superconductors open up the possibility of applications in the temperature range from 20K - 80K which is accessible with two-stage refrigerators[1]. At present, the most promising HTSC materials are $Bi_2Sr_2Ca_2Cu_3O_x$ silver-clad tapes[4]. However the bulk $J_c(B,T)$ is still well below its intrinsic maximum. A description of the mechanisms that limit the critical current in HTSC materials can best be obtained if we have data on $J_c(B,T)$ across as wide a range of the superconducting phase as possible and in particular, direct measurements of $B_{c2}(T)$.

This chapter describes the design and operation of a probe capable of measuring $J_c(B,T)$ of low temperature and high temperature superconductors across such a wide range of the superconducting phase. The probe (referred to as the $J_c(B,T)$ probe) and its accompanying system can accurately measure critical currents up to 500A in magnetic fields up to 17T and at temperatures of 2K up to 150 K.

4.1. The $J_c(B,T)$ probe

The $J_c(B,T)$ probe is based on the design of Hudson, Yin and Jones [5] and Hampshire and Jones[6] for helically wound low temperature superconductors. It extends the temperature range over which high critical currents can be measured in high fields up to 150K. Superconducting samples can be measured in cable, wire, tape and thin film form.

Several problems have been overcome including:

i. reducing the heating caused by the large sample currents present during the voltage-current measurement, which can make temperature control and noise

reduction difficult;

ii. incorporating the high field thermometry and temperature control into a restricted space which allows access to the small bore of high field magnets and

iii. ensuring low cryogen consumption during operation while maintaining a mechanically robust and durable design.

The probe that has been designed can be inserted into any high field magnet with a bore size greater than 20 mm. At Durham the measurement is computer controlled. Measurements are made throughout the temperature range 2 K - 150 K in the 40 mm bore of a 17 Tesla magnet system using a 500 A power supply built in-house.

In the next section, the general measurement and control system is described including standard voltage-current (V-I or equivalently E-J) traces from which $J_c(B,T)$ can be calculated. In section 4.1.2, the construction of the probe is described in detail, highlighting important mechanical and thermal design features and sample mounting procedures. Finally, in section 4.1.3, the thermometry and procedures employed to ensure accurate temperature control and measurement across the whole superconducting phase are outlined. This section includes discussion of the primary sources of error in the accuracy of the data generated. Section 4.2 describes the use of the probe to measure $B_{c2}(T)$ and section 4.4 finishes with some concluding remarks.

4.1.1. Principle of operation

The measurement consists of attaching current leads to the superconducting sample along with two voltage taps at a distance of 2-3 mm apart. The sample is then placed inside a high field magnet. The temperature of the sample and its environment is fixed at the first temperature required and a stable magnetic field applied. The voltage across the taps is monitored as the current through the sample is increased. Eventually a high enough current is supplied to generate a Lorentz force on the flux lines that is stronger than the pinning force, causing dissipative flux flow and an electric field along the sample. By convention, the critical current density is defined as that current which generates a particular electric field (1-2 μV cm^{-1} is typical) and can be determined from

the voltage-current trace. The critical current measurement is repeated at all the required fields at the first temperature. The sample is then heated to the next temperature required and the process repeated.

In figure 4.1, the external circuitry and equipment are presented. The sample current is ramped at variable speed by a Kepco voltage programmer and measured with a standard resistor in series. The sample voltage is measured using a Keithley 182 Nanovoltmeter. The heater and associated thermometry is controlled by a Lakeshore DRC 91A Temperature Controller. The system is controlled by interactive, real time graphical software written using ASYST (Keithley). All fields and temperatures for a sample orientation are required as input parameters at the start of the measurement run and no further user manipulation of the equipment is required. Communication is by the IEEE bus except for the magnet power supply, connected through the RS232 bus.

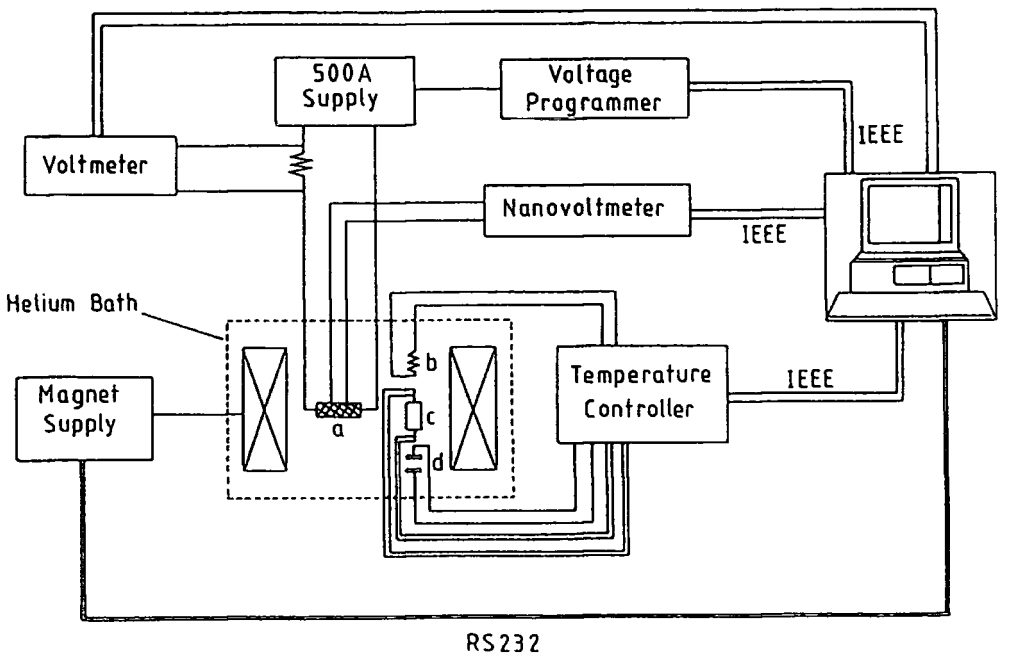

Figure 4.1: The measurement and control system for the $J_c(B,T)$ probe and 17T magnet system showing the communication protocols used for each instrument. a: the superconducting sample under measurement; b: 25 Watt heater; c: RhFe resistance thermometer; d: Capacitance thermometer.

In figures 4.2 and 4.3, typical E-J characteristics are shown for a $Bi_2Sr_2Ca_2Cu_3O_x$ silver-clad tape sample at 30 K and 70 K respectively for various fields. The traces exhibit flat baselines with a very low noise level (100 nV peak to peak), where the flux lines are pinned. Some of the characteristic features of HTSC materials can be observed: the resistive transitions are sharper at high fields primarily because of the magnetoresistance of the silver matrix that surrounds the $Bi_2Sr_2Ca_2Cu_3O_x$; applying a small field dramatically reduces the critical current; at 70 K, a field of 9 T is sufficient to reduce the lossless critical current density to zero.

4.1.2. Probe design

a) General design features

Figure 4.4 shows the general construction of the probe. The probe has been limited to a diameter of 20mm so that it can be used in conjunction with other high field inserts in the 40mm bore of our Oxford Instruments 17T magnet. The thermometry and copper block are located in a vacuum chamber bounded by the upper brass head, the pumping line and the demountable stainless steel lower can. The pumping line takes the instrumentation leads from two ten-pin connectors to the terminal strip. All instrumentation leads are twisted pairs and tied down to minimise electrical noise in high fields. The stainless steel upper sheath protects the pumping line and current leads. For temperatures above 4.2K the lower can, with a closed end, is mounted onto the stainless steel spacer with a Woods metal solder joint. Woods metal, with dilute orthoscorbic acid as the flux, is used because it has a low melting point of 70°C. For measurements from 2K to 4.2K, when the sample is directly immersed in the liquid, an open ended lower can is attached purely to protect the lower end of the probe. The pumping line, upper sheath and lower can are constructed using thin walled stainless steel to reduce heat losses and overall weight.

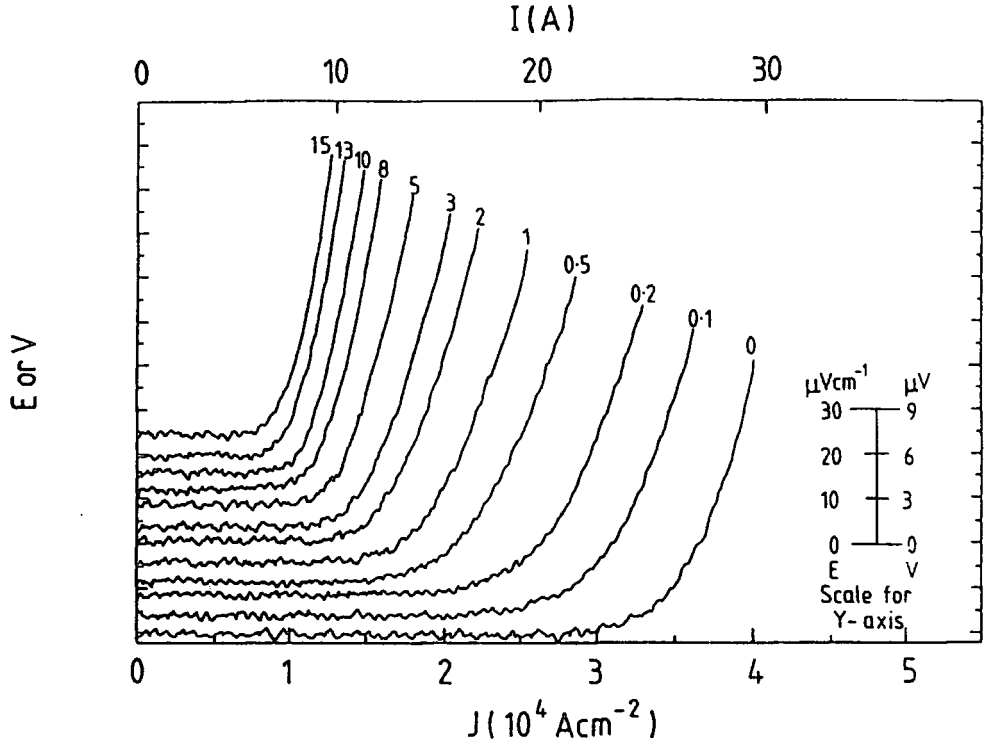

Figure 4.2: The E-J characteristics for a short section of a silver-clad $Bi_2Sr_2Ca_2Cu_3O_x$ tape at 30 K in magnetic fields up to 15 T.

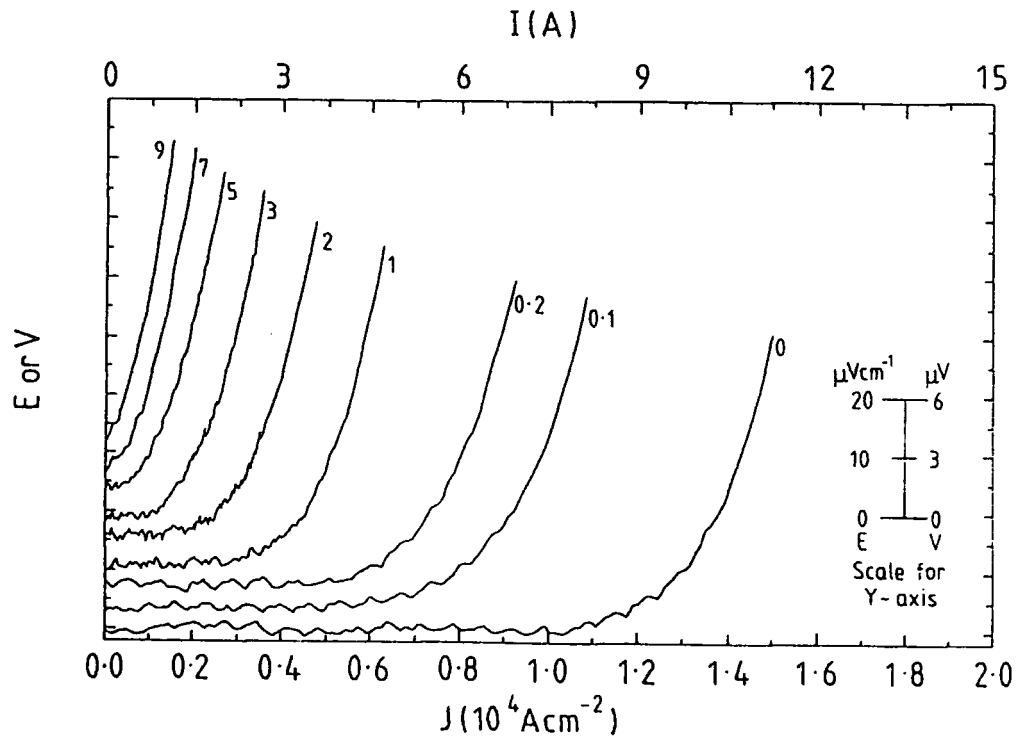

Figure 4.3: The E-J characteristics for the same $Bi_2Sr_2Ca_2Cu_3O_x$ sample as in figure 4.2 at 70 K in magnetic fields up to 9 T.

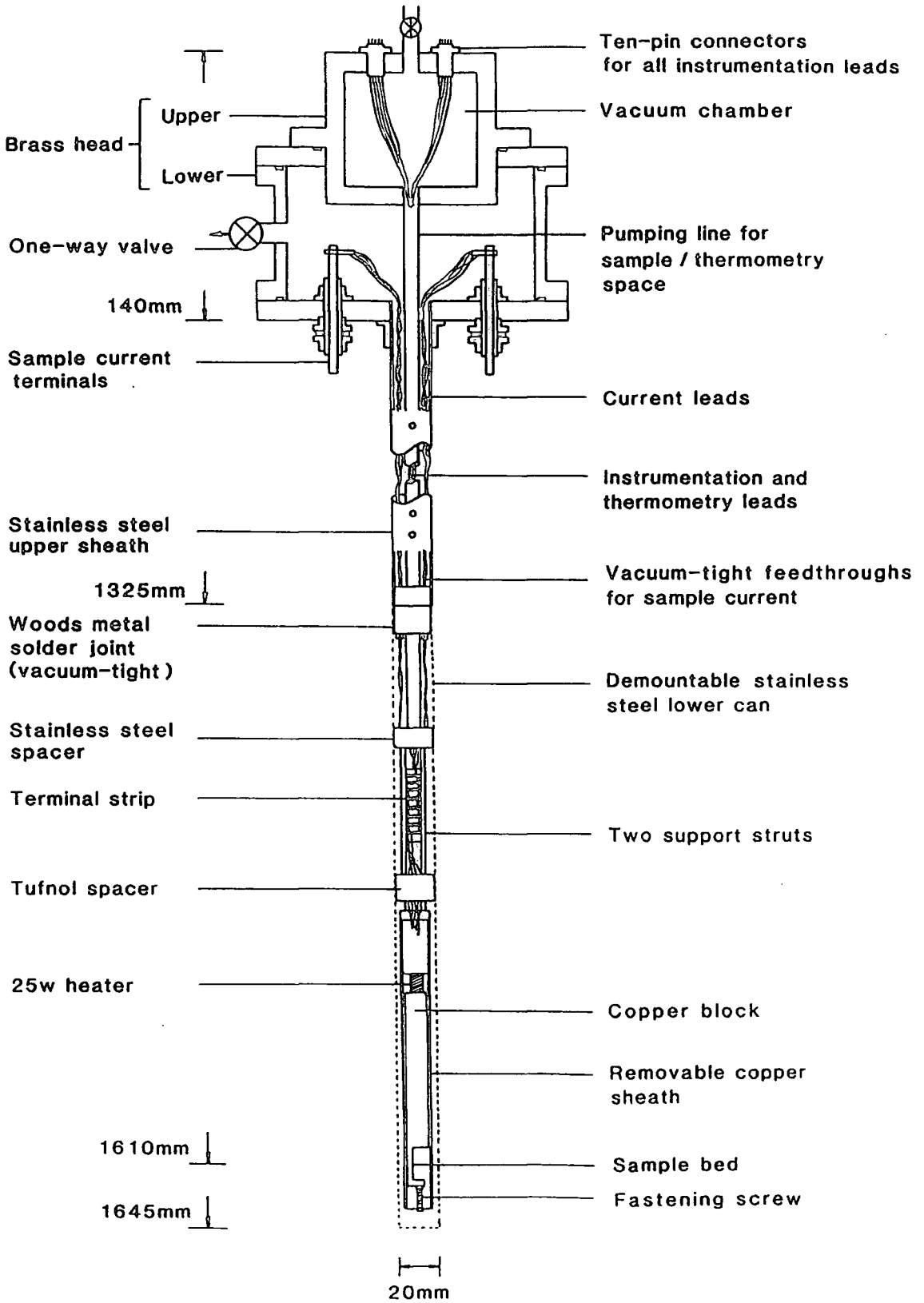

Figure 4.4: The construction of the Durham $J_c(B,T)$ probe (drawn to scale).

b) The high current leads

The current leads enter the lower section of the brass head via two vacuum-tight sample current terminals. At this point they each consist of 12 twisted copper wires of 0.7 mm diameter. Travelling down from the head, the number of wires in each lead is reduced until there is only a single twisted pair attached to the sample. The leads are electrically isolated from and strapped to the outside of the pumping line with mylar tape.

When the high sample currents flow, the Joule heating produces cold helium gas. Some of this gas flows past the current leads through several holes in the stainless steel upper sheath, placed below the line of the magnet cryostat baffles, and out through the one way valve in the lower brass head. This gas flow prevents the current leads from overheating and helps to minimise helium consumption.

To maintain the vacuum integrity of the sample and thermometry space the current leads enter the lower can by low temperature, vacuum-tight feedthroughs based on the design of Mathu and Mejer[7]. The performance of these feedthroughs is critical - with this probe they have survived in excess of 30 thermal cycles. Care must be taken when soldering the lower can into place not to heat the Stycast resin used in the feedthroughs above 100 $^{\circ}$C or it softens, creeps and has to be replaced.

Although we use a power supply which can supply sample currents up to 500A, we can only accurately measure such very high critical currents when the sample is directly immersed in liquid helium (i.e. between 2K and 4.2K). More generally, excessive Joule heating in the current leads can heat the sample and therefore limits the maximum critical current we can measure. This maximum critical current depends on the sample and the temperature. A more complete discussion of this limitation is provided in section 4.2

c) Thermal considerations

Figure 4.5 shows an enlarged view of the thermometry and copper block. The continuous copper block is fixed to the Tufnol spacer which in turn is suspended from the stainless steel spacer, attached to the bottom of the pumping line. The tufnol spacer helps to thermally isolate the copper block from the upper section of the probe. The copper block incorporates a 25W heater (made from a 1.5m wound length of constantan wire), two thermometers and a sample space of volume $12\times8\times20$ mm^3. The sample and thermometry leads are tied down in grooves running axially along the probe. The ceramic capacitance thermometer is mounted in a sealed pocket (filled with vacuum grease) directly under the sample space. Similarly, the RhFe resistance thermometer is mounted as close to the capacitance thermometer and sample as possible. The thermometry and current leads are thermally sunk to the copper block with vacuum grease. Finally, a removable copper sheath is placed over the copper block to reduce the temperature gradients along it.

d) Sample mounting

Low temperature wire samples are mounted in a hairpin shape. The bend section sits on the sample bed and the two straight lengths of the hair-pin are soldered in parallel with the copper current leads. The straight lengths are made as long as possible to increase the transfer length over which the current can flow from the copper current leads through the solder into the superconductor. This minimises Joule heating and helps to avoid causing a quench from localised heating.

High temperature superconductors are brittle and need special care in mounting. Short sections of silver-clad tapes or wires are mounted on a small piece of Tufnol board for mechanical protection. Separate short current leads are attached to the sample and the main current leads, such that if they are bent, no strain is transmitted to the sample. The direction of the sample current is arranged such that the macroscopic Lorentz force acts down onto the sample bed. For temperatures above 4.2 K, the sample is covered with vacuum grease to increase the thermal contact with the copper block. This

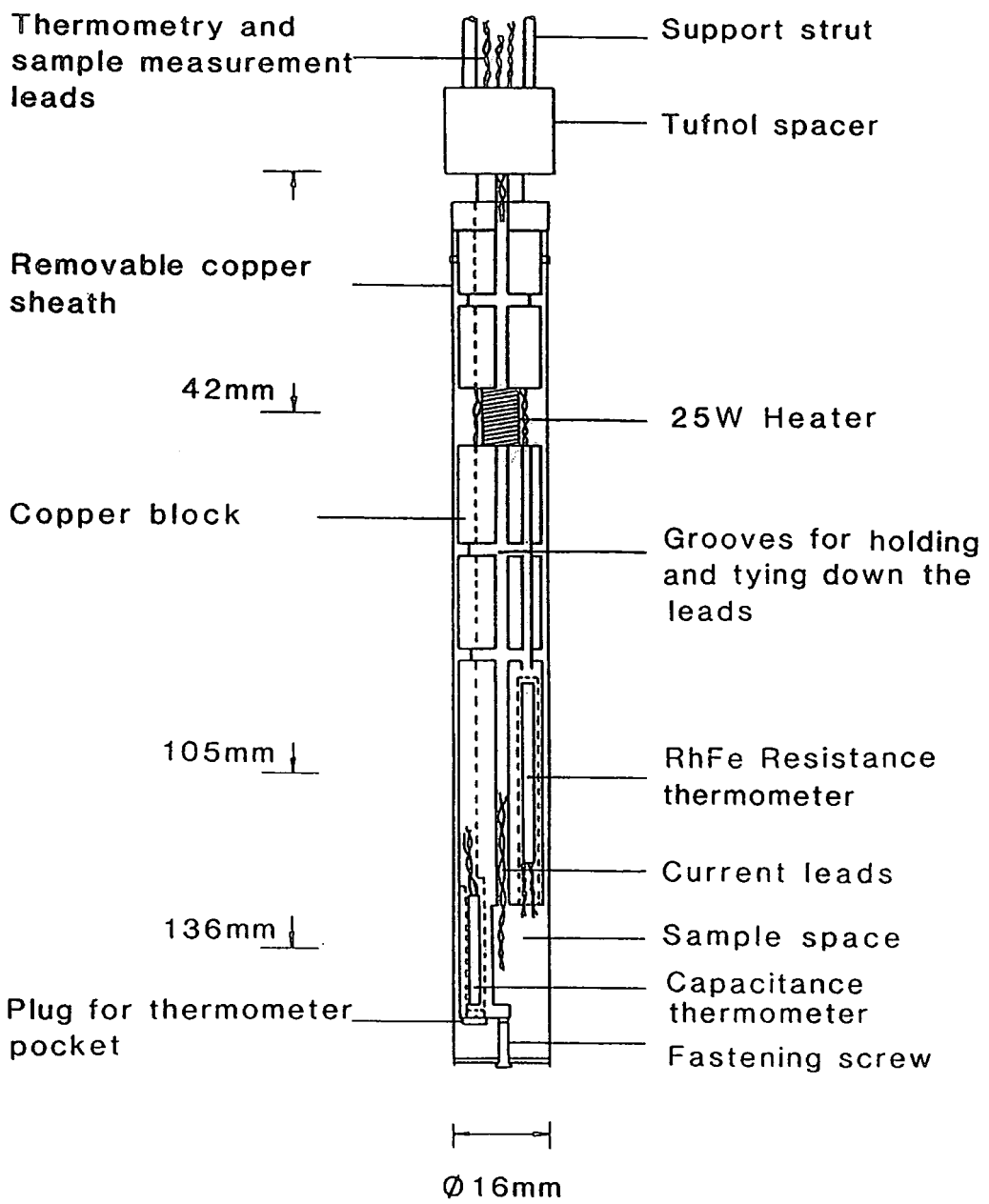

Figure 4.5: An enlarged view of the thermometry and copper block of the $J_c(B,T)$ probe (drawn to scale). The dashed lines represent hidden holes and recesses.

mounting procedure prevents the sample being damaged when its orientation is changed.

If the superconductor is not encapsulated in a normal metal matrix (e.g. a wire or tape) it can melt during the dissipative/resistive transition. We protect such samples by soldering a strip of copper wire in parallel with the superconductor which serves as an electrical shunt. For all superconductors, the current leads and voltage taps are attached with indium solder rather than lead-tin solder. This ensures that results at the lowest temperatures in low magnetic fields are not ambiguous because of the solder becoming superconducting.

4.1.3. Temperature control and measurement

a) Temperature control between 2 K - 4.2 K

In this regime the sample is in direct contact with the helium liquid which is pumped on with a 2-stage rotary pump. The pressure is controlled by a MKS Pressure controller and throttle valve to within $\pm$ 1 Torr. The temperature can then be obtained from standard helium vapour-pressure tables [8]. The accuracy of the pressure controller determines the error in this measurement, estimated to be $\pm$ 50 mK. No sample heating has been observed up to a current of 300 A.

b) Temperature control above 4.2 K

Above 4.2 K the lower can is soldered onto the stainless steel spacer and the vacuum chamber is evacuated to less than 7×10^{-2} mbar. The solder joint must be vacuum-tight. A small amount of He exchange gas is admitted in to the vacuum chamber and the probe is pre-cooled in liquid nitrogen. After placing the probe in the magnet cryostat the vacuum chamber is re-evacuated. Two thermometers are incorporated in the probe: one is a calibrated RhFe standard resistance thermometer for zero field measurements. This thermometer has a large magnetoresistance which renders it unsuitable for measurements in-field [9]; the second is a multi-layer ceramic capacitance thermometer which is field independent but not reproducible after thermal cycling. The

thermometers are used as follows; the superconductor is heated to the required temperature in zero field using the capacitance thermometer as a control thermometer whilst monitoring the actual temperature using the RhFe thermometer. The capacitance thermometer keeps the temperature fixed while ramping the magnetic field during measurements. The thermometer/heater feed-back control is regulated by the Lakeshore Temperature Controller.

If there is too much gas in the vacuum chamber, relatively high heater powers are needed to heat the sample which increases the temperature gradients along the copper block. On the other hand if the pressure is too low, the small heaters powers mean that temperature stability is harder to maintain and the vacuum chamber may cryopump. If, for example, measurements are required every 10 K, starting at 4.2 K, the vacuum chamber is pumped down to 7.10^{-2} mbar and the valve at the top of the upper brass head is then closed. As the temperature is increased, this valve is gradually opened until at 30 K - 40 K it is fully open. If measurements are only required at higher temperatures then the vacuum chamber is pumped on for about 30 minutes to obtain acceptable heater powers. Throughout all measurements, the heater power is continuously monitored.

Temperature control is most difficult from 5 K - 10 K both because of the small heat capacities of most materials and the large critical currents of superconductors at low temperatures. In addition the very small heater currents required to maintain the temperature makes it hard to compensate for Joule heating in the current leads. Eventually, at sufficiently high sample currents, the Joule heating will heat the sample up. This heating effectively determines the maximum $J_c(B,T)$ that can be measured. At 10K the samples measured in this paper start to heat at 25-30 A. At a temperature of 80K, currents up to 50 A have been supplied without the sample heating. Sample heating is indicated directly by an increase in the RhFe thermometer resistance or indirectly by a drifting E-field baseline in the E-J trace.

c) Estimation of accuracy (above 4.2 K)

The thermal gradient between sample and thermometer was minimised by placing the heater 150 mm from the sample (see figure 4.5). Decreasing this distance or adding a second heater increased the thermal gradient. These gradients were measured as a function of pressure and heater power using a second calibrated RhFe resistor placed on the sample bed where the sample normally lies. As an example, at 20 K the sample is 20 mK warmer than the RhFe thermometer (with an 80 mA heater current), whilst at 80 K the sample is 50 mK colder (200 mA heater current).

The temperature at the beginning and end of each set of fixed temperature measurements (of duration two hours on average) is recorded. It does not normally vary by more than 50 mK. Larger variations (up to 250 mK) can occur if there are any small leaks, incorrect PID parameters are used, the thermometry leads are not tied down or not enough time is allowed between measurements for the temperature to re-stabilise after sample heating.

Using the pumping procedure for measurements every 10K outlined in section 4.2, the critical current can be measured accurate to the equivalent of $\pm$ 70 mK at 20 K for currents up to 30 A and to $\pm$ 100 mK at 80 K for currents up to 50 A. At 150 K, temperature drifts are larger and the error rises to $\pm$ 200 mK.

4.2. Using the $J_c(B,T)$ probe to measure $B_{c2}(T)$

The $J_c(B,T)$ probe is also used to measure the effective $B_{c2}(T)$ of a sample resistively, with the following procedure:

i. the required temperature is fixed using the method outlined in section 4.2;
ii. a Lakeshore constant current source is connected to the sample current terminals in the lower brass head and a constant current between 1μA and 100mA is supplied to the sample and;

iii. the voltage (proportional to the resistivity) across the sample is measured by the Nanovoltmeter whilst the magnetic field is ramped from zero up to some value in steps of 1mT.

At B_{c2} a resistive transition is observed from zero to the normal state value.

4.3. Concluding remarks

Real progress in the fabrication of high temperature superconducting materials for applications will only be made if the factors limiting the transport $J_c(B,T)$ can be explained. To tackle these complex systems, data on the critical current density are needed across as wide a range of the superconducting phase as possible. The design and construction of a probe capable of such wide ranging measurements has been presented. The $J_c(B,T)$ of both high and low temperature materials can be measured in magnetic fields up to 17 T in the temperature range of 2-150 K. The system is designed to measure critical currents up to 500 A from 2K to 4.2K. Above 4.2K, Joule heating limits the maximum critical current that can be accurately measured. Critical currents can be measured accurately in high magnetic fields to the equivalent of $\pm$ 70 mK at 10 K and $\pm$ 100 mK at 80 K. At 4.2 K and below, the $J_c(B,T)$ values quoted are accurate to $\pm$ 50 mK.

The following chapters present and analyze comprehensive $J_c(B,T)$ data on high temperature and low temperature superconductors obtained using the probe described here.

References for Chapter 4

1. Ohkura K., Mukai H., Hikata T., Ueyama M., Kato T., Fujikami J. and Sato K., Jap. J. App. Phys. Part 2 Letters 32(11A), L1606 (1993).

2. Ashworth S.P., *Applied Superconductivity Vol. 2 - Proc. of the European Conference on Applied Superconductivity 93*, pg. 879, ed. Freyhardt H.C. (DGM Informationsgesellschaft, Germany, 1993).

3. Schoenung S.M., Meier W.R., Hull J.R., Fagaly R.L., Heiberger M., Stephens R.B., Leuer J.A. and Guzman R.A., IEEE Trans. App. Supercond. 3(1), 234 (1993).

4. Heine K., Tenbrink J. and Thöner M., App. Phys. Lett. 55(23), 2441 (1989); Sato K., Mukai T.H., Ueyama M., Shibuta N., Kato T., Masuda T., Nagata M., Iwata K. and Mitsui T., IEEE Trans. Mag. 27(2), 1231 (1991).

5. Hudson P.A., Yin F.C. and Jones H., IEEE Trans. Mag. MAG-19(3), 903 (1983).

6. Hampshire D.P. and Jones H., J. Phys. E: Sci. Instrum. 20, 516 (1987).

7. Mathu F. and Meijer H.C., Cryogenics 22, 428 (1982).

8. *CRC Handbook of Chemistry and Physics*, 69th edition, ed Weast R.C. (CRC Press: Florida 1988).

9. Rubin L.G., Brandt B.L. and Sample H.H., Adv. Cryogenic Engineering 31, 1221 (1986).

5. The Transverse and Longitudinal Critical Current Densities of a NbTi Multifilamentary Wire

A description of the flux line lattice in high temperature superconductors is made complex by the difficulty of distinguishing between intrinsic and sample dependent effects. In contrast, the fundamental parameters and microstructure of the low temperature superconductor NbTi are well known after 30 years of study. Even so, the flux line mechanics in these materials is still not completely understood. One particular area that requires further investigation is the Lorentz force free critical current density. The force free orientation with its higher J_c values could lead to possible commercial applications. Increased theoretical understanding of the low temperature superconductors can only enhance the chances of success in explaining the layered HTSC's.

This chapter details the measurement of the transverse and longitudinal critical current density and effective upper critical field of a commercial NbTi wire. Section 5.1 describes the type of wire measured and section 5.2 explains the experimental techniques used to measure $J_c(B,T)$ and $B^*_{c2}(T)$. The results are presented in section 5.3. In 5.4 the data is analyzed and the volume pinning force for the wire in both orientations is calculated. The findings are discussed in section 5.5 in terms of pinning mechanisms and force free theories and section 5.6 finishes with the main conclusions.

5.1. Measurements on a NbTi wire

The critical current density of a commercial Nb(46.5wt%)Ti multifilamentary wire was measured in a transverse magnetic field (with B perpendicular to the wire axis) and a longitudinal magnetic field (with B parallel to the wire axis). The NbTi wire, which is used in high field magnets, contained 61 filaments of diameter 28 μm. The overall diameter of the wire including the copper matrix was 0.4 mm. Additionally the effective upper critical field for both orientations was measured by a resistive method and from an extrapolation of the $J_c(B)$ curve to zero critical current density.

5.2. Experimental techniques

5.2.1. $J_c(B,T)$ measurements

The measurements were made from 2 K up to T_c in magnetic fields up to 15 T using the Durham $J_c(B,T)$ probe. The NbTi wire was mounted initially in a hairpin shape (see section 4.1.2d). The voltage taps were attached 2 mm apart on the section transverse to the field. The critical current was measured using a criterion of $1.5\mu V.cm^{-1}$. The temperature of the sample was measured to an accuracy of $\pm$ 50 mK at 4.2 K and below and $\pm$ 150 mK above 4.2K (section 4.1.3). The sample was then rotated so that the field was parallel to the current for the section containing the voltage taps and the measurements were repeated. Joule heating in the copper current leads and the resistive joints determined the maximum J_c which could be measured.

The critical current of a second sample, parallel to the field with three sets of voltage taps placed above, below and at the field centre was also measured. At 4.2K, when the centre section had been driven normal, the two end sections (at a lower field) were still superconducting. Hence J_c for the wire in the field centre was not determined by quenches originating in other parts of the wire. A small angular misorientation however, substantially reduced the size of J_c in this configuration.

5.2.2. $B_{c2}(T)$ measurements

The effective upper critical field, B^*_{c2}, of a third wire sample was measured resistively as described in section 4.2, from 4.2K - 9.5K. The configuration of the sample included sections parallel and orthogonal to the field, each with separate voltage taps. At each temperature the section being measured was placed into the magnetic field centre and the resistivity measured while the field was swept from zero to 15 T. The error in the sample alignment is estimated to be $\pm\ 2^\circ$.

5.3. Experimental results

5.3.1. E-J characteristics

Figure 5.1 shows the E-J characteristics of the wire at 2.5 K for both orientations. The relatively high noise on these traces originated from the sample current supply. For the transverse orientation there is the standard E-J characteristic with a flat base line at currents below the critical current and a sharp transition at high currents. For the longitudinal orientation similar transitions were observed at low fields. However, at all temperatures close to B°_{c2}, above the critical current, a low differential resistivity region occurred before the sharp transition.

5.3.2. $J_c(B,T)$ measurements

Figures 5.2 and 5.3 display $J_c(B,T)$ for the applied field longitudinal and transverse to the sample transport current respectively. Both figures exhibit broadly linear $J_c(B)$ characteristics across the whole temperature range. The $J_c(B)$ curves for the longitudinal orientation (when the macroscopic Lorentz force is zero) at each temperature are shifted to a higher field in relation to the curves for the transverse orientation. As discussed in section 4.1.3b, temperature control in a He gas atmosphere is most difficult close to 4.2 K. It can be seen from figures 5.2 and 5.3 that at 5K and above, the maximum J_c that could be measured without Joule heating is severely reduced compared to the measurements obtained using liquid thermometry.

5.3.3. Resistivity measurements

Figure 5.4 gives the normalised resistivity at 4.2 K for the NbTi wire in both orientations for a measuring current of 200 mA. Also included are data generated using a current of 300 μA from a sample which had its copper matrix etched off. The resistance of the etched sample just above $B^{\circ}_{c2}(T)$ was approximately 80mΩ for *both* orientations. Knowing the number and size of the filaments the resistivity can be estimated as approximately 1.5 $\mu\Omega$m. For the wire with the copper matrix the

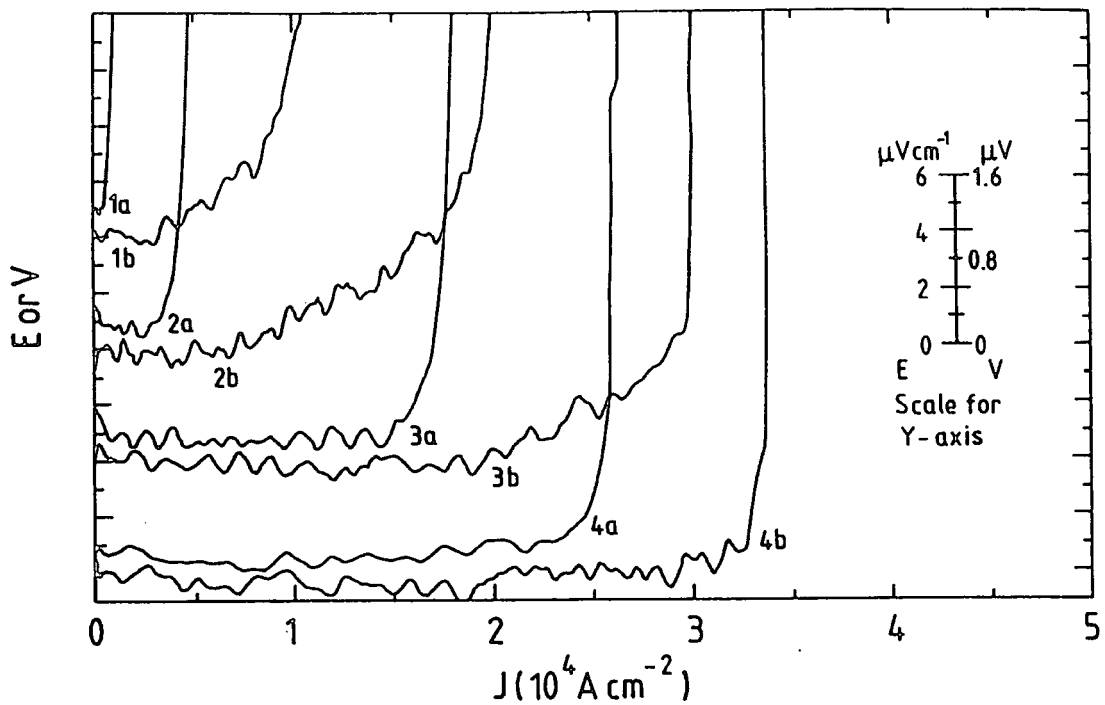

Figure 5.1: The E-J characteristics measured at 2.5K in fields of 1: 13T, 2: 12.5T, 3: 11.5T and 4: 11.0T where the label 'a' signifies B ⊥ I and 'b' signifies B ∥ I.

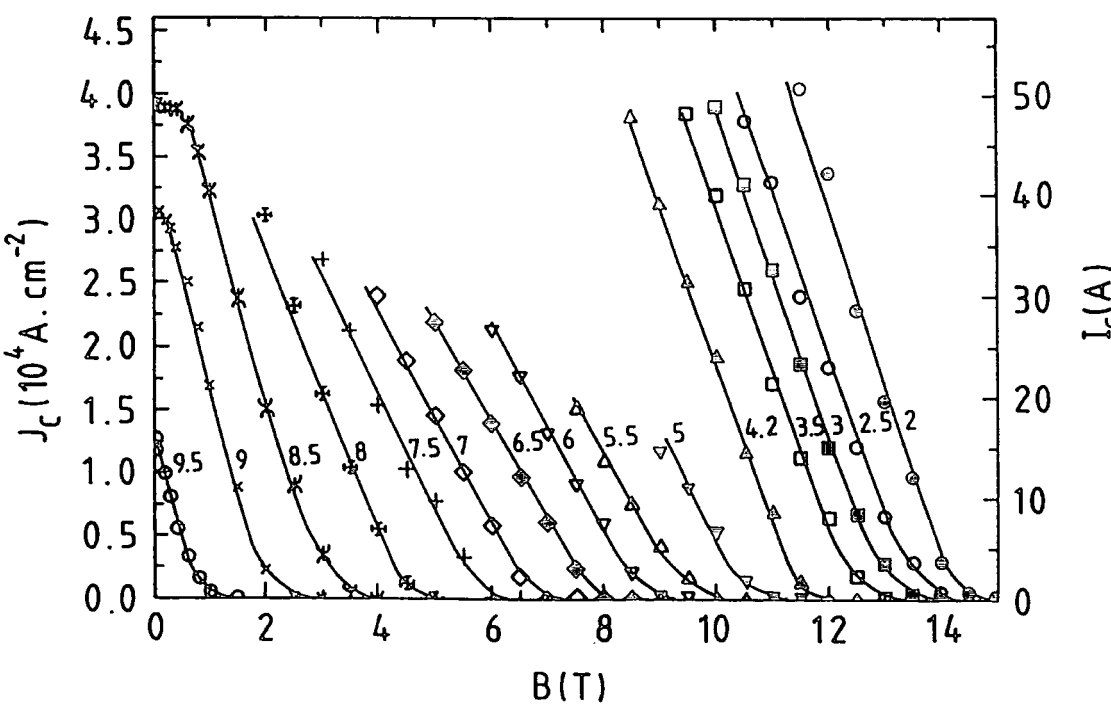

Figure 5.2: The critical current density as a function of field and temperature from 2K up to T_c in magnetic fields up to 15 Tesla. The applied field is parallel to the macroscopic current direction.

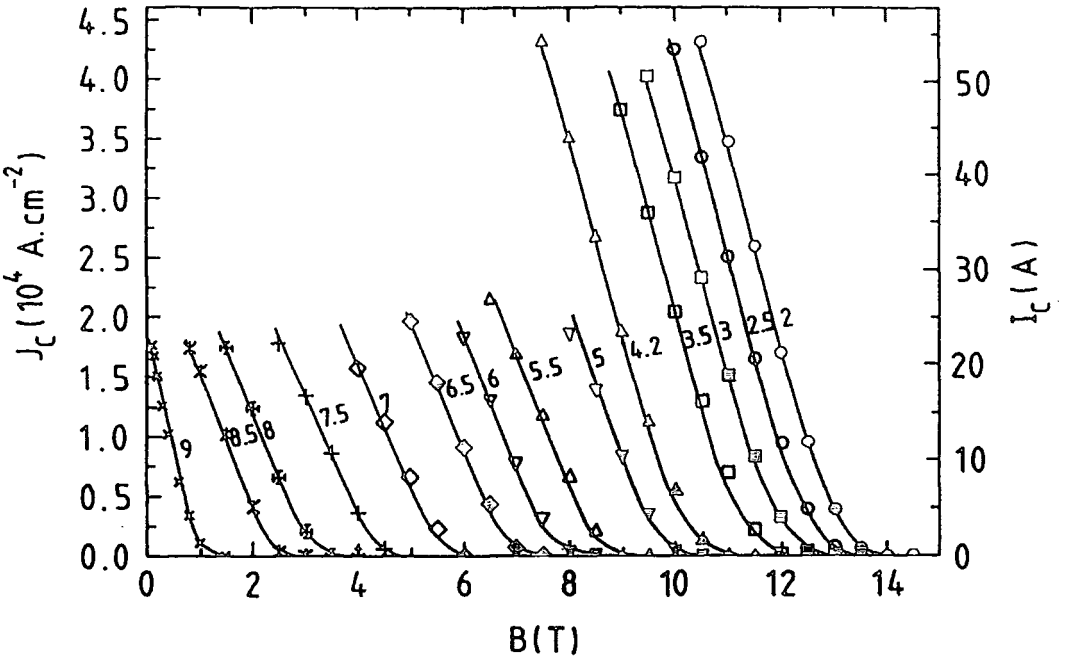

Figure 5.3: The critical current density as a function of field and temperature from 2K up to T_c in magnetic fields up to 15 Tesla. The applied field is transverse to the macroscopic current direction.

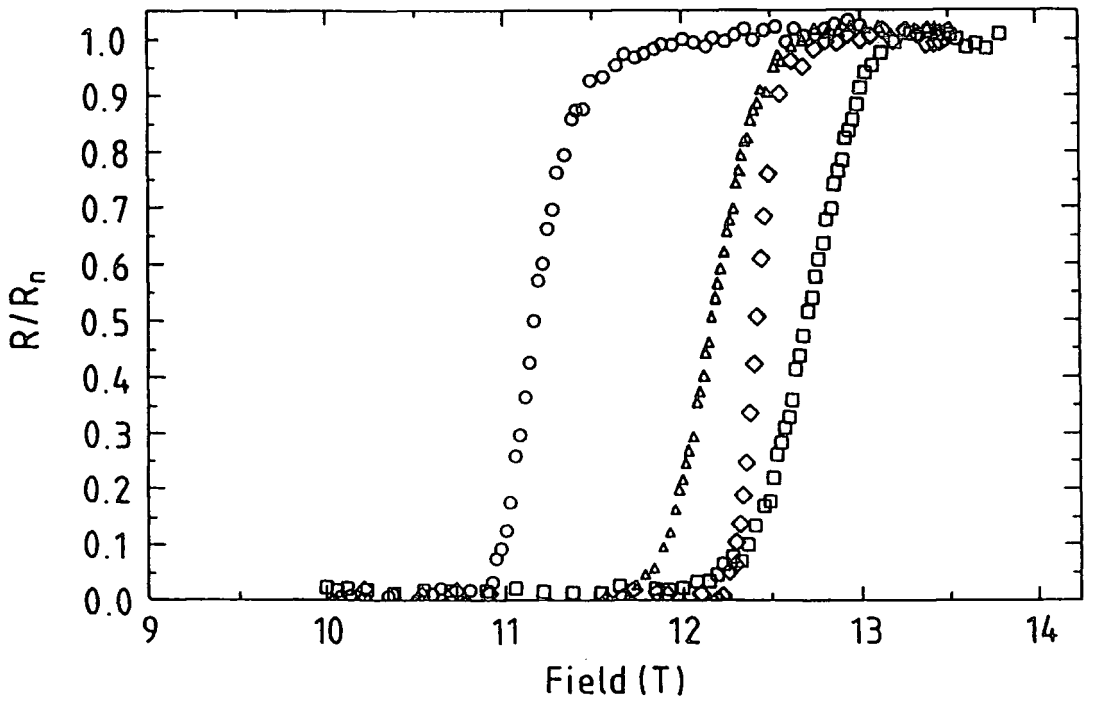

Figure 5.4: The normalised resistivity as a function of field at 4.2K (measuring current in brackets) : ○ Wire with matrix, B ⊥ I (200mA) ; ◇ Wire with matrix, B ∥ I (200mA) ; △ Wire with matrix etched off, B ⊥ I (300μA) ; □ Wire with matrix etched off, B ∥ I (300μA).

corresponding resistance was 24$\mu\Omega$ with the magnetic field perpendicular to the current and 17$\mu\Omega$ in the longitudinal orientation. At this point in the resistivity curve a large proportion of the current is flowing through the copper rather than the NbTi.

It should be noted that when the applied field is parallel to the current the effective upper critical field is higher than when the field is perpendicular to the wire, whether or not the matrix is removed.

5.4. Analysis of the experimental data

5.4.1. The upper critical field

The effective upper critical field has been calculated for the two configurations by two different methods. The first method was by extrapolation of the linear regime of the $J_c(B,T)$ data to $J_c = 0$, the second by defining B^*_{c2} as that field at which the resistivity drops to half its normal state value. Figure 5.5 presents these results. Clearly, B^*_{c2} is higher for the longitudinal configuration throughout the superconducting phase. The data from the resistive and extrapolation methods is similar near T_c but diverges below 7 K. Plotted in the inset to figure 5.5 is the ratio between the longitudinal and transverse critical fields. To within experimental accuracy the ratio is the same for both methods of determining B^*_{c2}.

5.4.2. The volume pinning force

The reduced pinning force near to T_c has been calculated and is plotted in figure 5.6 against $b = B/B^*_{c2}$ using the extrapolated values for B^*_{c2}, for the two orientations. A single curve can be drawn through most of the data consistent with Fietz-Webb scaling[1] (equation 3.11). The largest scatter results from the data obtained at the highest temperatures where the linear regime of the $J_c(B)$ curves are least well defined. The data for $b > 1$ originates from the small tail in each $J_c(B)$ curve close to $J_c=0$. A similar analysis using the resistively measured values for B^*_{c2} has been completed and it is found that the scaling is not as good. From figure 5.6 and the linear form of $J_c(B)$

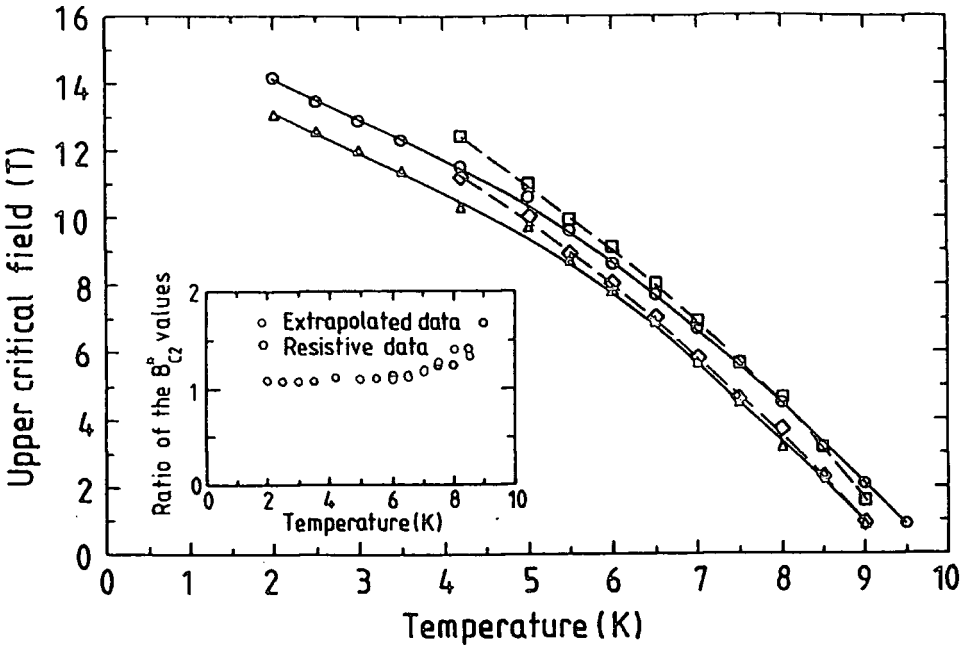

Figure 5.5: The Upper Critical Field ,B°_{c2} as a function of temperature. For curves ○ and △, B°_{c2} is calculated by extrapolating the linear part of the J_c versus B characteristic at each temperature. For curves □ and ◇, B°_{c2} is defined as the field at which the normal state resistivity of the wire drops by half. In each case, B is parallel and perpendicular to I respectively. The inset plots the ratio of the two upper critical fields.

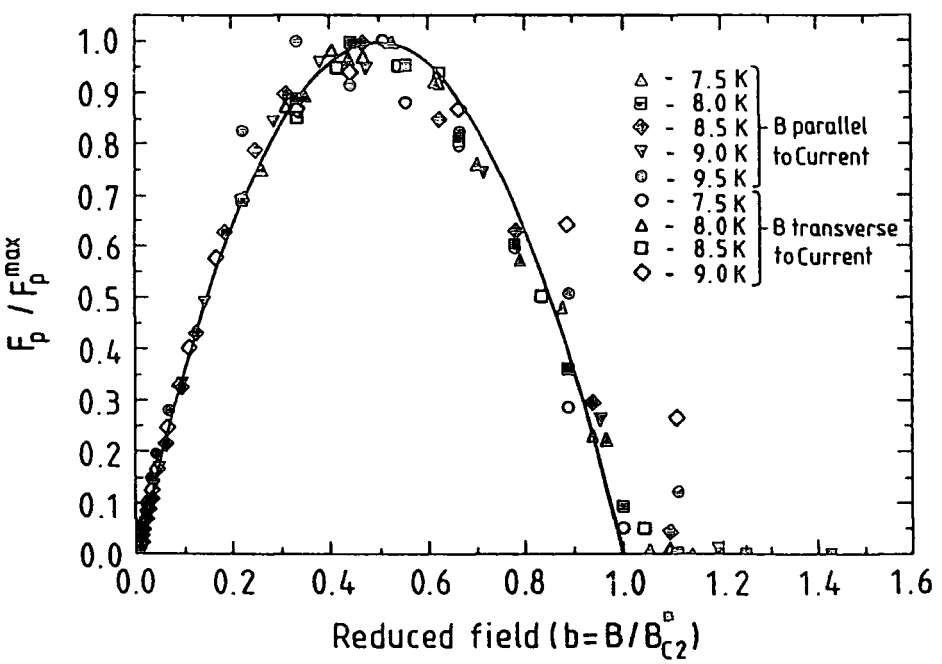

Figure 5.6: The Reduced Pinning Force versus Reduced Magnetic Field as a function of temperature. B parallel and transverse to I. $B^{\circ}_{c2}(T)$ is calculated by extrapolating the linear part of the J_c versus B characteristic at each temperature for each orientation.

in figures 5.2 and 5.3 it can be seen that pinning force for both orientations can be represented by the relation

$$F_p = \alpha_P B_{C2}^{n}(T) b(1-b) \qquad (5.1)$$

where α_P is a constant depending on the sample microstructure. The solid line in figure 5.6 represents the curve F_P/F_{Pmax} = b(1-b). The index n, which determines the temperature dependence can be calculated from a plot of $\log\{\partial J_C/\partial B\}$ vs $\log\{B^*_{C2}\}$. This is plotted in figure 5.7. Between 5 K and 9 K it seems likely that there has been some heating in the wire, slightly lowering the slope of J_C. Even though, the data can be well described by a single straight line with zero slope giving n=2 for both orientations. From the scatter in the data it is estimated that n=2± 0.25. The parameter α_P is then found to be $(1.4 \pm 0.3)\times 10^4$ A/cm^{2}T. This data shows that for both orientations J_C can be described by a single functional form and value for α_P - it is determined simply by the effective upper critical field.

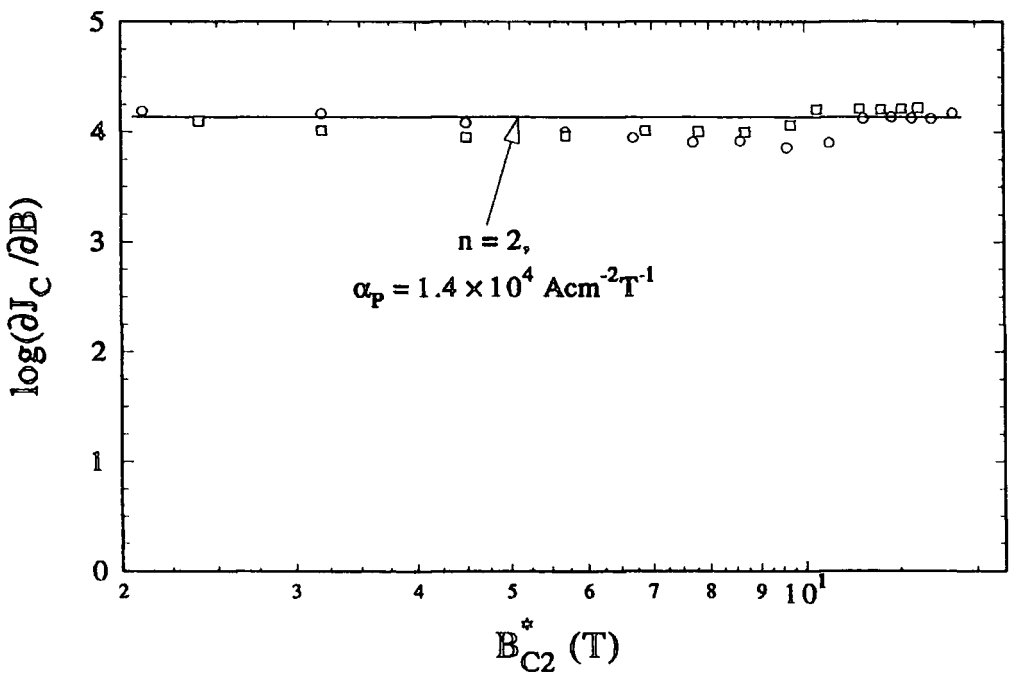

Figure 5.7: A plot of $\log\{\partial J_C/\partial B\}$ vs $\log\{B^*_{C2}\}$ to calculate n and α_P : ▣ for the magnetic field perpendicular to the current and ○ for the field parallel to the current.

5.5. Discussion

The change in the orientation dependence of E-J characteristics for a PbIn cylindrical sample has been investigated by Cave[2]. Consistent with the results presented here, his E-J data at an angular displacement of 1-2° show a similar structure to the B∥I traces in fig. 5.1. Equally at larger angles Cave's sample had the two regime E-J transition exhibited by the B⊥I traces in the figure.

It is generally agreed that $J_c(B,T)$ in NbTi is limited by a flux pinning mechanism such that at criticality, the Lorentz force is equal to the volume pinning force, i.e. $F_p = J_c \times B$. If the field is at an angle ϕ to the wire axis then the field term is simply replaced by its normal component $B\sin\phi$. However, the orientational difference of J_c in figures 5.2 and 5.3 cannot be explained by a simple scaling with angle. Furthermore we have found that the functional form of F_p is similar for the two orientations suggesting that a similar pinning mechanism operates in both orientations.

Close to, or at $\phi=0$ simple analyses[3] shows that the current and flux must enter as helices. This description leads to flux-line cutting theories[4,5], which are normally used to explain why the longitudinal J_c is larger than the value in a transverse field[6]. The data presented here show a relatively small difference (10%) in J_c for the two orientations. This may be explained if the NbTi filaments are twisted such that the angle between the field and the filaments when the field is along the wire axis is never zero. The structure of the E-J characteristic in the longitudinal orientation can be attributed to the increased difficulty of flux flow because of flux cutting events in the wire. However these theories are not sufficiently developed to provide a full quantitative description of the orientation dependence of $J_c(B,T)$ we have found in this work.

It has been found that from 2K to T_c the effective upper critical field is higher when measured parallel to the wire axis than when transverse. This is in contrast to the data of Karasik et al.[6] on NbTi monocore wires who found that B_{c2} was the same for both field orientations. The linearity of the curves in figures 5.2 and 5.3 and the resistive

measurements of figure 5.4, which show a difference in B_{c2}^{*} with or without the copper matrix, indicate that this orientational difference is a bulk effect and is not confined to a surface sheath. Commercial Nb46.5wt%Ti multifilamentary wire consists of long ribbons of α-Ti which lie along the drawing direction. This will lead to an anisotropy in the resistivity and the superconducting order parameter which may be the origin of the anisotropy in B_{c2}^{*}. Alternatively the larger B_{c2}^{*} in the longitudinal orientation could be due to an increased flux flow resistivity from flux line cutting events. The distance between each filament is of the order of 5 μm. By comparing this with the penetration depth of approximately 0.06 μm the possible effects of proximity coupling can be ignored.

Recent work on conventional superconductors has shown that as well as HTSC's they may also have an irreversibility line. A region of reversible flux flow close to and just below B_{c2} has been found by Suenaga et al.[7], Sulpice et al.[8] and Zheng[9] in multifilamentary NbTi and by Schmidt et al.[10] in Nb films. The existence of an irreversibility line cannot be corroborated from the resistivity traces of figure 5.4. Zheng[9] performed simultaneous dc magnetisation and resistivity measurements on a similar NbTi wire. The resistivity traces had the same characteristic as those in figure 5.4. The magnetisation data clearly showed the different fields B_{irr} and B_{c2}. The irreversibility field corresponded to the field at which zero resistivity is approached. The approximate onset of the resistive drop corresponded to the magnetically measured B_{c2}. No discontinuity in the resistivity was observed at B_{c2}, probably because of shorting through the copper matrix. For the data presented here the effective upper critical field is an average of the fields B_{irr} and B_{c2} and indicates that both the irreversibility line and the upper critical field are anisotropic.

5.6. Conclusions

From the measurements on a multifilamentary NbTi wire presented in this chapter the following points can be made:

i. a single functional form can be used to describe the orientation, temperature and magnetic field dependence of J_c,

$$F_p(B_{C2}) = 1.4\times10^{8}.B_{C2}^{2}(T)b(1-b) \qquad (5.2)$$

in S.I units and where $B_{c2}=B_{c2}^{\perp}$. In particular, the orientation dependence of J_c is primarily determined by the anisotropic effective upper critical field and not by the macroscopic Lorentz force operating;

ii. it is suggested that the anisotropy in B_{c2}^{*} is of microstructural origin or from an increased resistance to flux flow in the longitudinal orientation.

iii. The possible existence of an irreversibility line in NbTi has been discussed. If it exists for the wire considered here it would also be anisotropic with respect to the field direction.

iv. The measurements demonstrate that caution should be taken in defining the intrinsic critical fields of superconductors. Even with an isotropic crystal structure, changes in a material's microstructure can lead to anisotropy of its superconducting parameters.

These results highlight the difficulty of measuring the true upper critical field using transport techniques and the currently incomplete understanding of flux line dynamics - even in materials which have been studied for 25 years.

References for Chapter 5

1. Fietz W.A. and Webb W.W., Phys. Rev. 178(2), 657 (1969).

2. Cave J.R., PhD Thesis, Clare Hall, Cambridge (1978).

3. Timms W.E. and Walmsley D.G., J. Phys. F:Metal Phys. 5, 287 (1975).

4. Campbell A.M. and Evetts J.E., Adv. Phys. XXII, 199 (1972).

5. Clem J.R., Phys. Rev. B. 26(5), 2463 (1982).

6. Karasik V.R. and Vereshchagin V.G., Zh. Eksp. Teor. Fiz. 59, 36 (1970) [Sov. Phys. JETP 32, 20 (1971)].

7. Suenaga M., Ghosh A.K., Xu Y. and Welch D.O., Phys. Rev. Lett. 66, 1177 (1991); Suenaga M., Welch D.O. and Budhani R., Supercond. Sci. Technol. 5, S1 (1992).

8. Sulpice A., Jonnard P. and Giordanengo B., *Proc. EUCAS 1993 - Applied Superconductivity Vol 1*, ed. Freyhardt H.C. (DGM - 1993) p.697.

9. Zheng D-N., *An experimental study of flux pinning in high temperature superconductors*, PhD Thesis, Christ's College, Cambridge (1994).

6. The Critical Current Density of a $Bi_2Sr_2Ca_2Cu_3O_x$ Tape from 2K-110K

Since their discovery in the late 1980's, high temperature superconductors (HTSCs) have appeared to offer many possibilities in scientific and commercial applications. For superconducting power cables and high field magnets (operating at the more economic temperature of liquid nitrogen) the $Bi_2Sr_2Ca_2Cu_3O_x$ (BSCCO-2223) compound is the most promising. It has high intrinsic values of $J_c(B,T)$ and is relatively easy to fabricate in the form of metal sheathed tapes compared to other HTSCs . The crystal structure of BSCCO-2223 is highly anisotropic but the plate-like shape of the grains is such that rolling the tape naturally aligns them with their c-axis perpendicular to the plane of the tape.

The $J_c(B,T)$ of these BSCCO-2223 tapes however is much smaller than for thin films of the same material. In particular at high temperatures (e.g. 77K) and in high magnetic fields $J_c(B,T)$ is presently too low for useful applications. The reasons for the low measured values and strong field dependence of $J_c(B,T)$ in BSCCO-2223 tapes are still not clear. Factors to be considered are the strength of coupling between grains, the percolation path of the transport current, the types of pinning and the different possible phases of the flux line lattice. $J_c(B,T)$ data across as wide a range of temperatures and magnetic fields as possible are needed for comparison to any proposed theories.

This chapter details the measurement of $J_c(B,T)$ for a BSCCO-2223 tape supplied by T. Beales, BICC Cables Ltd. Data was obtained, for three different sample orientations in the temperature range between 2K and T_c in magnetic fields up to 15T and is initially presented in section 6.2. Such a complete data set of $J_c(B,T)$ for a BSCCO-2223 tape has not previously been presented in the literature. Section 6.3 is an analysis of the data, breaking it down into four sub-sections: the data below 10K; the data for fields less than 1T above 10K; the data for fields higher than 1T above 10K; the irreversibility line. Section 6.4 discusses the data in the same manner. Possible explanations of the data in terms of current theories will be given and the outstanding issues highlighted. Finally the main conclusions of the chapter are summarised in section 6.5.

6.1. The $Bi_2Sr_2Ca_2Cu_3O_x$ tape

The sample measured was a short section (approximately 10mm long) from a silver-clad tape of total length 50mm. The tape was made using the standard powder-in-tube method[1].

An optical micrograph of a cross-section of the measured sample is shown in figure 6.1. The cross-section is taken so that the direction of the macroscopic transport current was perpendicular to the plane of the paper. It can be seen that during rolling, on one side of the tape, the BSCCO-2223 material has broken through the silver sheath at several points. From this micrograph the cross-sectional area of the BSCCO-2223 was calculated to be 0.0466 mm^2.

6.2. The measurement

6.2.1. Technique

The sample was mounted in the $J_c(B,T)$ probe as described in section 4.2.2d with the voltage taps, attached to the opposite side to the one where the BSCCO-2223 could be seen through the sheath, at a distance of 2mm apart.

The E-J characteristics of the tape were measured from 4.2K up to T_c for three different orientations of the magnetic field with respect to the tape (in all cases the macroscopic transport current was parallel to the plane of the tape):

a) magnetic field perpendicular to the plane of the tape, called the **BPC** (B parallel to the c-axis) orientation;
b) magnetic field parallel to the plane of the tape but perpendicular to the transport current, called the **BPAB** (B parallel to the ab-plane) orientation and
c) magnetic field parallel to the plane of the tape and also to the transport current, called the **LFF** (lorentz force free) orientation.

The measurements were taken in increasing magnetic fields from 0 - 15T. Before and after each change of the sample orientation the critical current of the tape was measured in liquid nitrogen. This was to make sure that the sample had not been damaged during handling or from thermal cycling. No change in the critical current was observed.

The critical current density has been calculated from the E-J characteristics using a 2 $\mu V.cm^{-1}$ criterion.

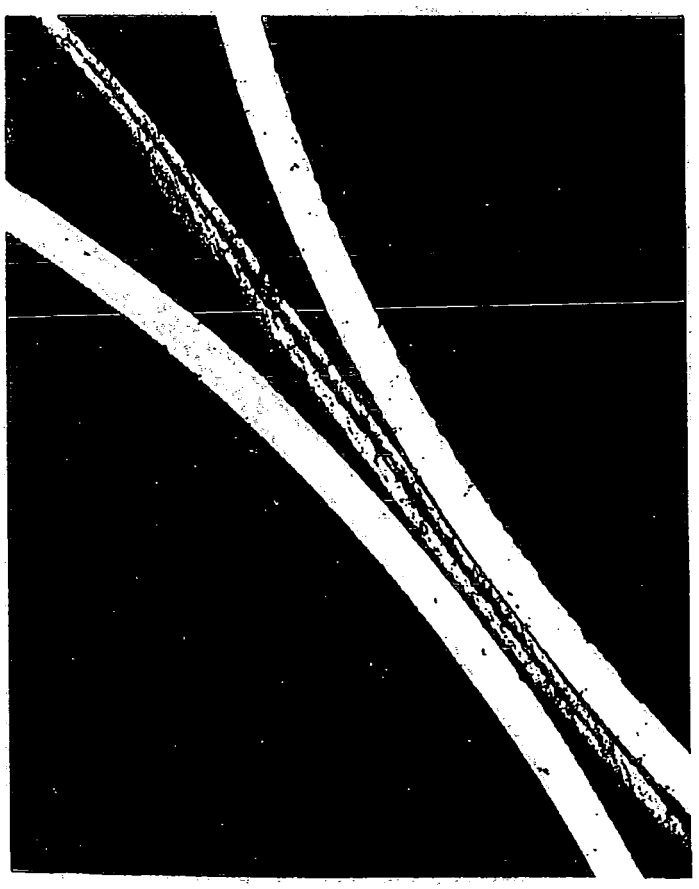

Figure 6.1: An optical micrograph of a cross-section of the $Bi_2Sr_2Ca_2Cu_3O_x$ silver-clad tape (scale is 1mm:5cm).

6.2.2. The data

The data is plotted for the three orientations on a log-log scale in figures 6.2 - 6.4. This format displays the data clearly over the complete magnetic field range. None of the lines at constant temperature cross over, indicating good temperature control during the measurement. In all three figures there is a dramatic anomaly in $J_c(B)$ at 4.2K at a field of 1.5T. At higher temperatures this anomaly disappears. The values of $J_c(B,T)$ at low temperatures and high fields (10^4 to 10^5 Acm^{-2}) are typical for such a tape. The critical current density was found to be zero in the self field at 110K. This temperature was taken as T_c.

More comprehensive measurements of J_c were taken at 2K-4.2K, in an increasing and decreasing field, for the same sample eight months after the data of figures 6.2 - 6.4 were taken. The results are shown in figures 6.5a,b,c for the three orientations on a log-linear scale. The magnitude of J_c is 10-20% smaller than for the initial set of readings, indicating a small degradation in the sample but the field and orientational dependence is the same.

6.3. Analysis of $J_c(B,T)$ for the tape

6.3.1. The data below 10K

As can be seen from figures 6.2 - 6.5, at 4.2 K for all three orientations, there is a rapid decrease in J_c up to a magnetic field which is to be called B_j. At temperatures of 10K and above, this anomaly has disappeared. Figure 6.6 compares J_c at 4.2K for the three orientations in an increasing field, from the data of figures 6.5a,b,c. The following observations can be made:

i. there is a large magnetic field hysteresis for all three orientations above and below B_j. On decreasing the field the J_c is typically measured to be 20% - 40% higher than in an increasing field;

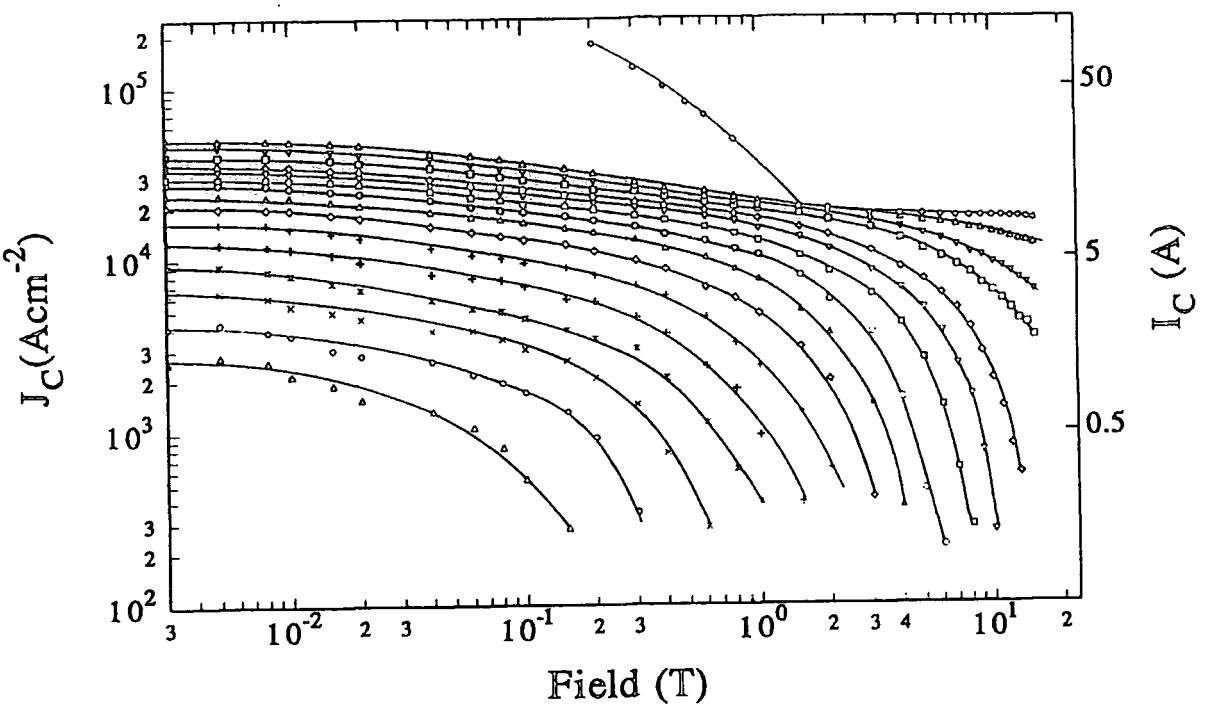

Figure 6.2: The critical current density of the tape for the BPC orientation on a log-log scale. The curves are measurements at constant temperatures of (from the top down): 4.2, 10, 20, 30, 40, 45, 50, 55, 60, 65, 70, 75, 80, 85, 90 and 95K respectively.

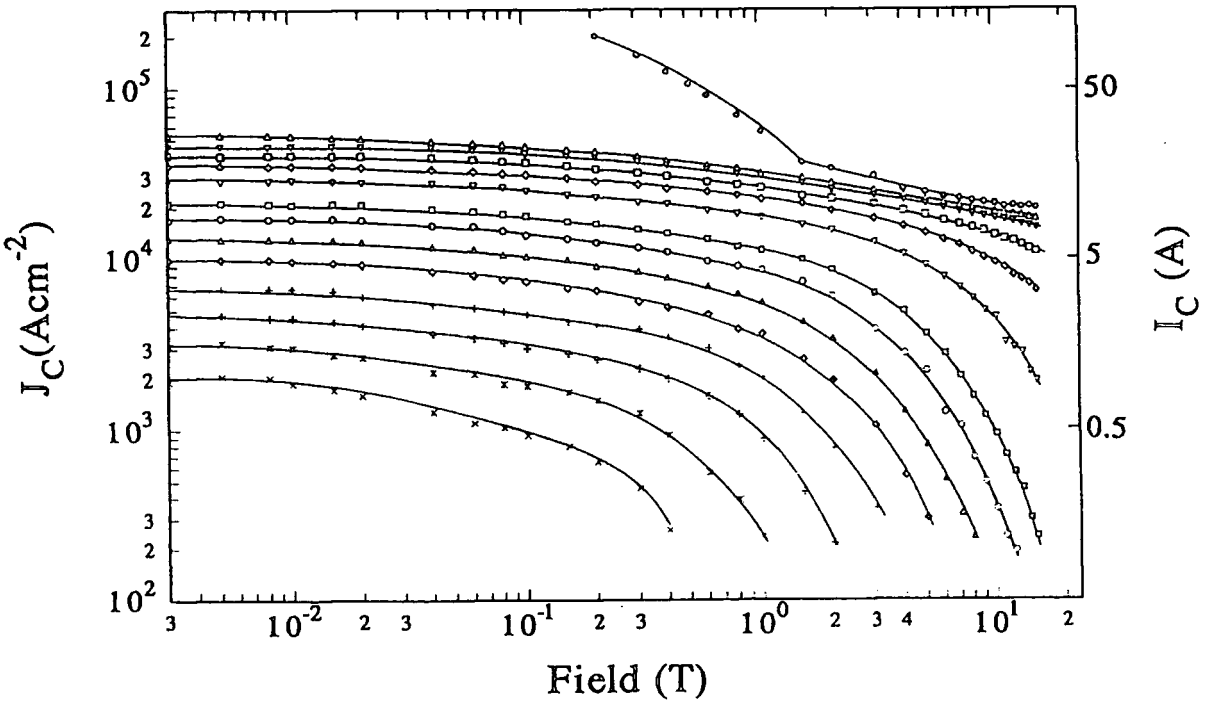

Figure 6.3: The critical current density of the tape for the BPAB orientation on a log-log scale. The curves are measurements at constant temperatures of (from the top down): 4.2, 10, 20, 30, 40, 50, 60, 65, 70, 75, 80, 85, 90 and 95K respectively.

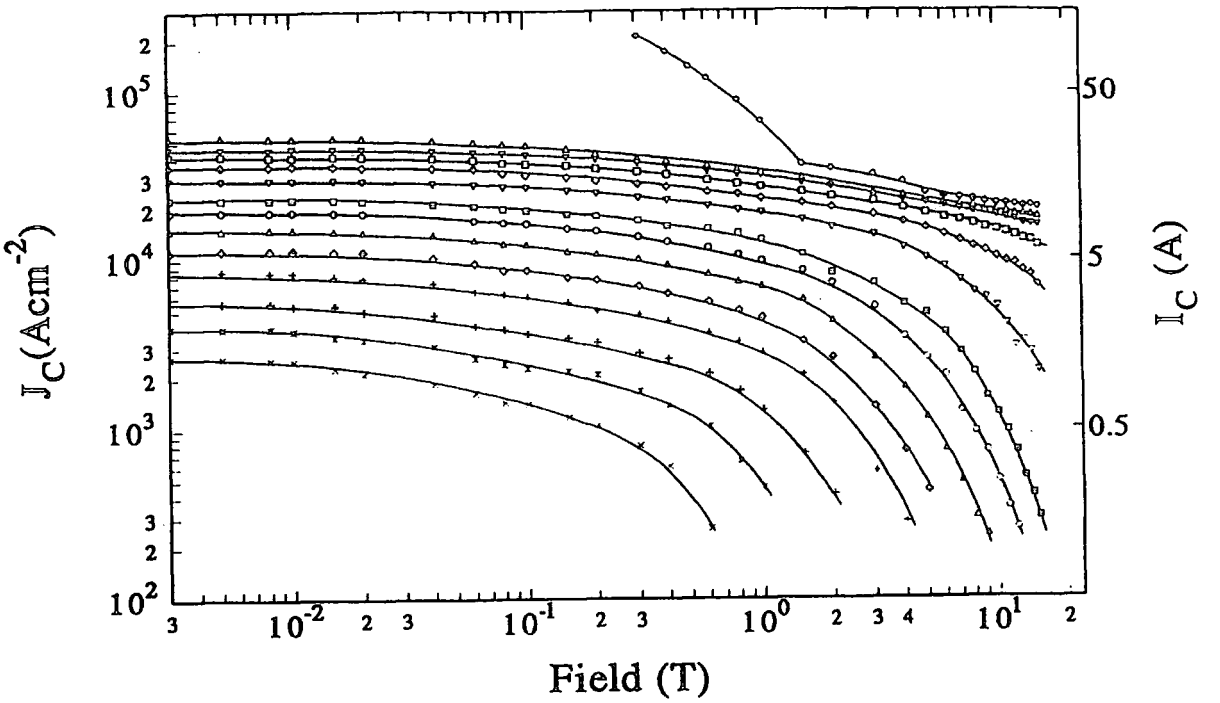

Figure 6.4: The critical current density of the tape for the LFF orientation on a log-log scale. The curves are measurements at constant temperatures of (from the top down): 4.2, 10, 20, 30, 40, 50, 60, 65, 70, 75, 80, 85, 90 and 95K respectively.

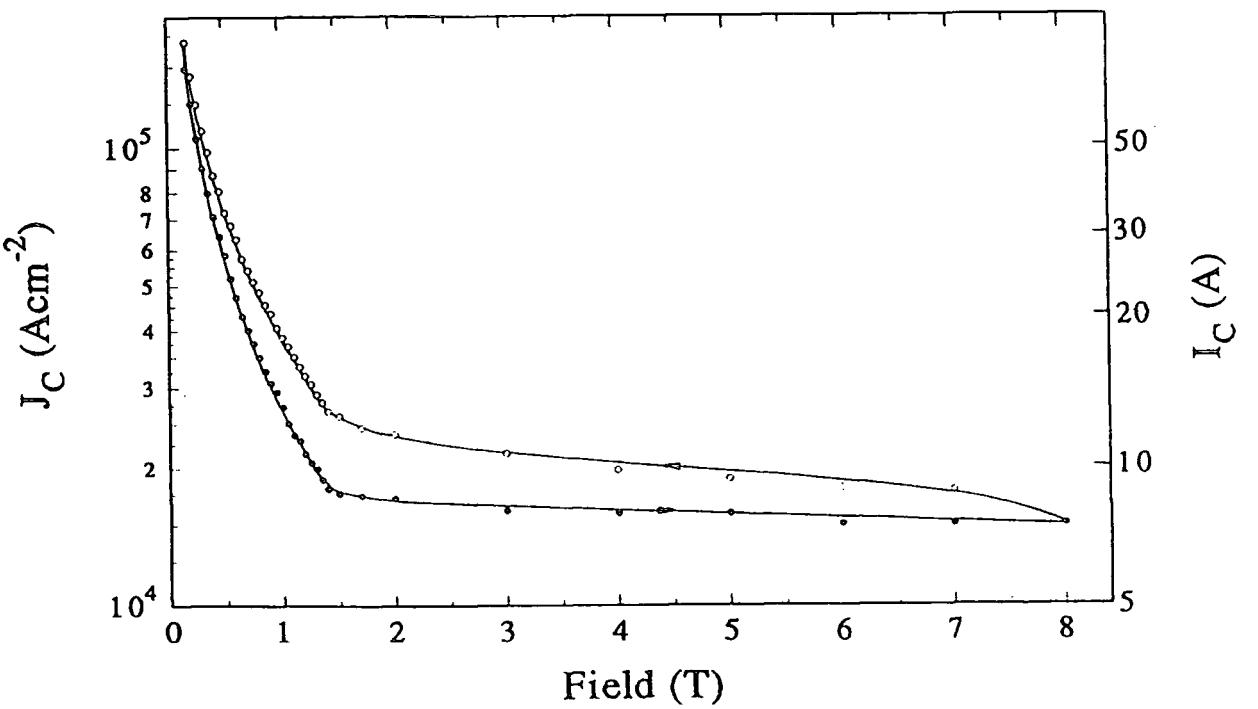

Figure 6.5 (a): for a description, see next page

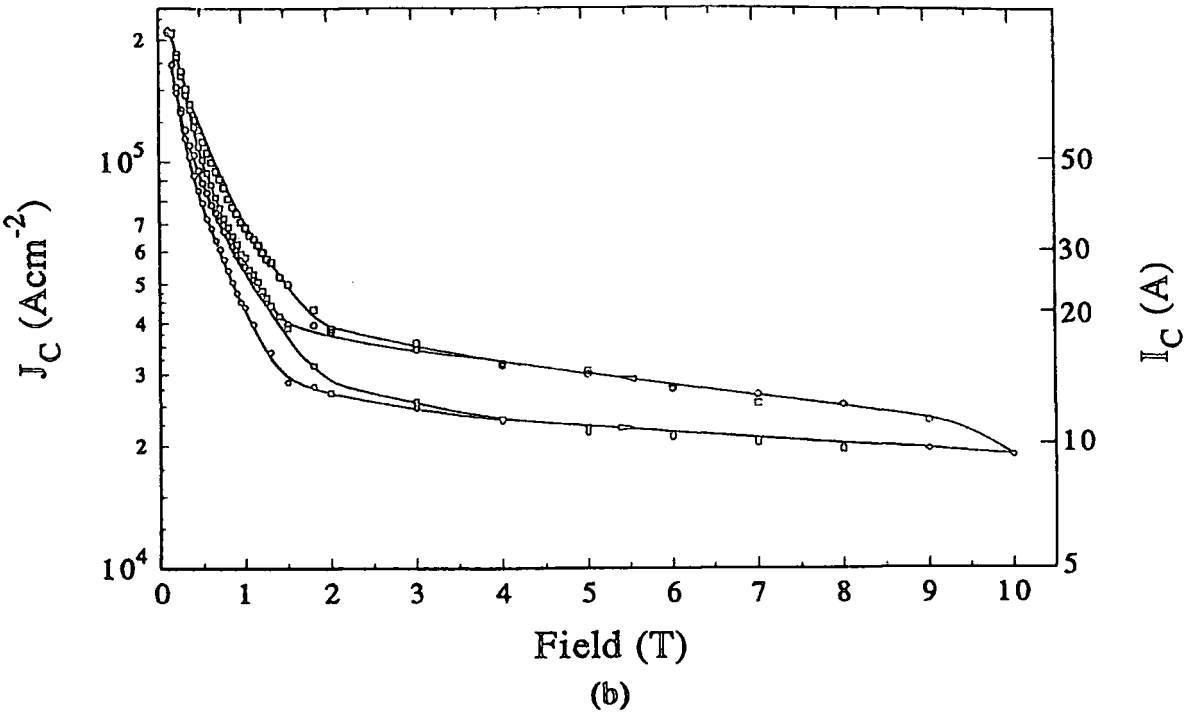

(b)

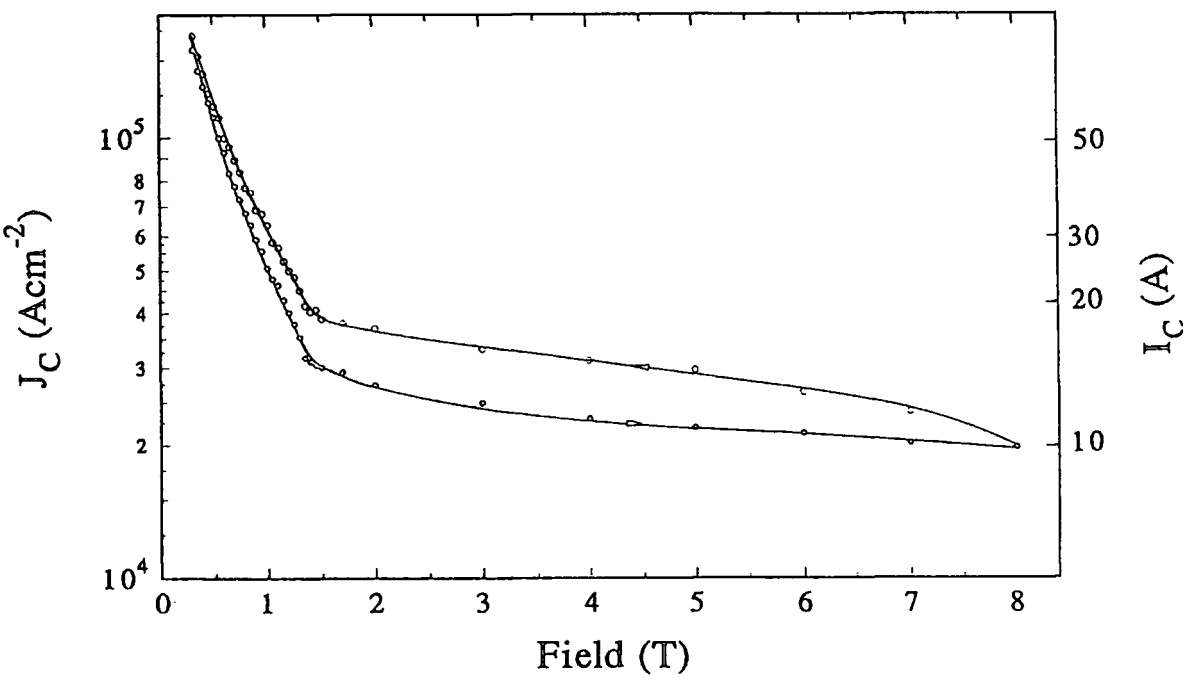

(c)

Figure 6.5: The critical current density at 4.2K in increasing and decreasing magnetic fields (as shown by the arrows). (a) (previous page) the BPC orientation; (b) the BPAB orientation including data at 2K where the circles correspond to 4.2K and the squares correspond to the 2K data; (c) the LFF orientation.

ii. for all three orientations at 4.2K, in an increasing *and* a decreasing field, the anomaly occurs at the same field, B_j = 1.5 T. At 2K however, for the BPAB orientation the anomaly has been shifted to a higher field, B_j = 2 T;

iii. from figure 6.6 it is seen that for the BPC orientation, J_c is much smaller than for the other two orientations. Above B_j, J_c for the LFF and BPAB orientations is the same. Below this field J_c for the LFF orientation is higher;

iv. above B_j the critical current density falls exponentially with field for the three orientations. Below B_j the data cannot be fitted to a single exponential function, except perhaps for the LFF orientation.

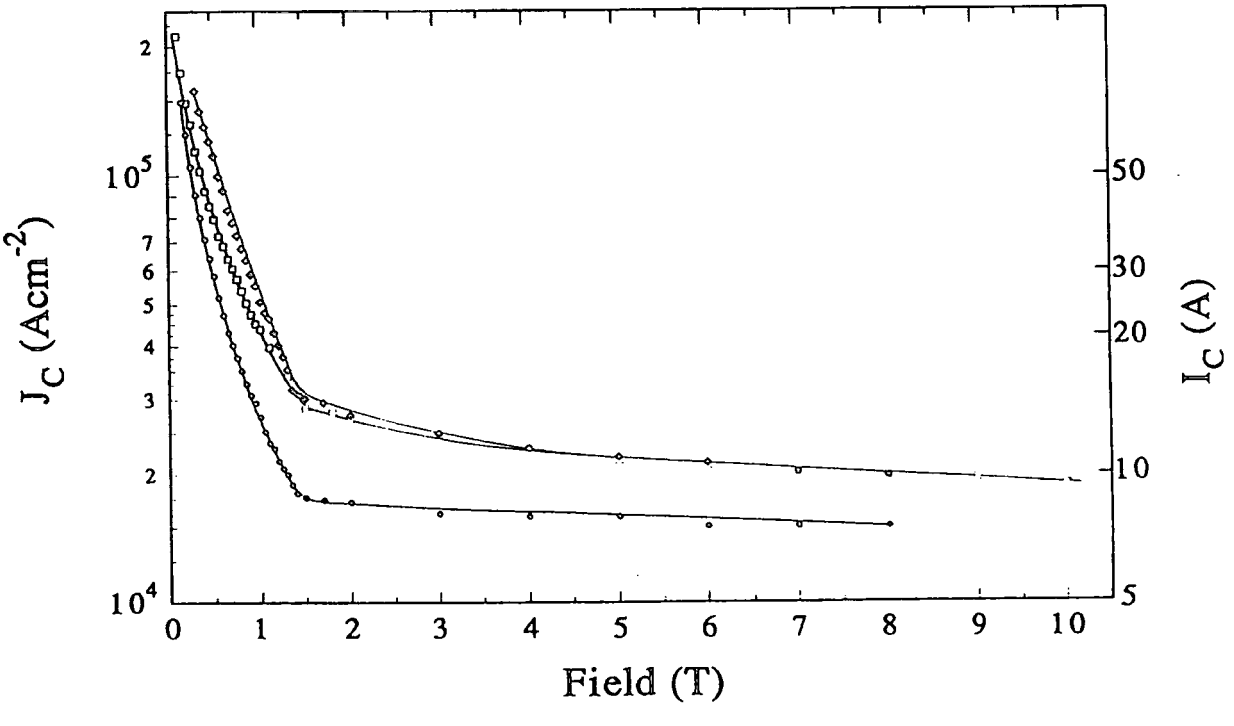

Figure 6.6: A comparison of J_c at 4.2K in an increasing field for the three orientations: ●, BPC; □, BPAB; ◊, LFF.

6.3.2. The data for fields less than 1T above 10K

In analyzing the $J_c(B,T)$ in the low field range of less than 1T, the data of figures 6.2-6.4 has been replotted in three different ways:

(a) The critical current density as a function of temperature at certain fixed magnetic fields is plotted in figure 6.7a,b for the BPC and BPAB orientations respectively. The data for the LFF orientation is similar to that for the BPAB orientation. All the curves have a similar shape. In medium fields (above 0.8T) at low temperatures J_c is only weakly dependent on temperature. Above 40K however it starts to fall more rapidly. The curve for a field of 1mT for the BPC orientation is replotted in the inset to figure 6.7a. The solid line is a fit to the function:

$$J_C(T) = J_C(0)(1 - 0.87t - 0.35t^2) \qquad (6.1)$$

with $J_c(0) = 5.62\times10^4$ Acm^{-2}.

(b) The data of figures 6.7a,b are replotted in the form $\log\{J_c\}$ against $\log\{1-t^2\}$ for the BPC and BPAB orientations in figures 6.8a,b, where t is the reduced temperature. For both orientations the data at low fields and low temperatures can be described by a straight line. That is,

$$J_C(B,T) = C(B)(1-t^2)^n \qquad (6.2)$$

For the BPC orientation, $n=2.0\pm0.1$ for all fields up to 2T and C(B) decreases from 4.9×10^4 Acm^{-2} at 1mT to 1.9×10^4 Acm^{-2} at 2T. For the BPAB orientation, at 1mT and 100mT, $n=2.6\pm0.05$ and at 800mT and 2T, $n=2.8\pm0.05$. The parameter C(B) decreases from 5.0×10^4 Acm^{-2} at 1mT to 2.8×10^4 Acm^{-2} at 2T.

For the BPAB orientation at 1mT there is no change in the exponent throughout the temperature range. This is not the case at other low fields for this orientation and for the BPC orientation: at higher temperatures there is a change in the $J_c(t)$ dependence and J_c decreases more quickly with temperature.

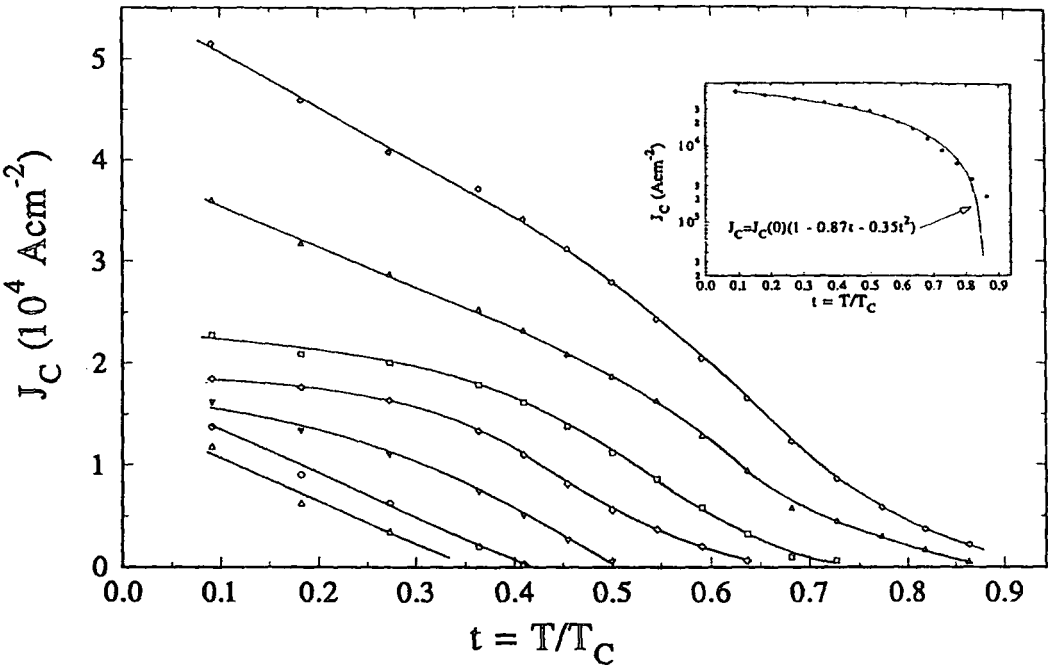

(a)

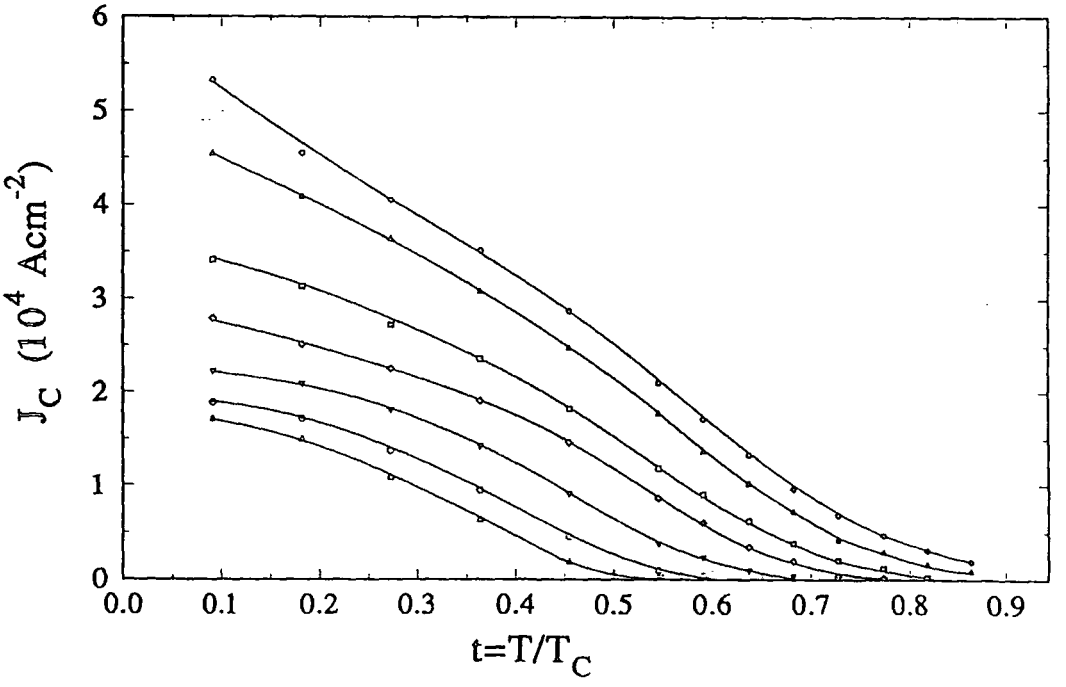

(b)

Figure 6.7: $J_c(T)$ for (a) the BPC orientation and (b) the BPAB orientation. For each figure the curves are data at fixed fields of (from top to bottom) 0.001, 0.1, 0.8, 2, 5, 10 and 15 Tesla. The inset in (a) shows $J_c(T)$ in a fixed field of 1mT -the solid line is a fit to equation 6.1.

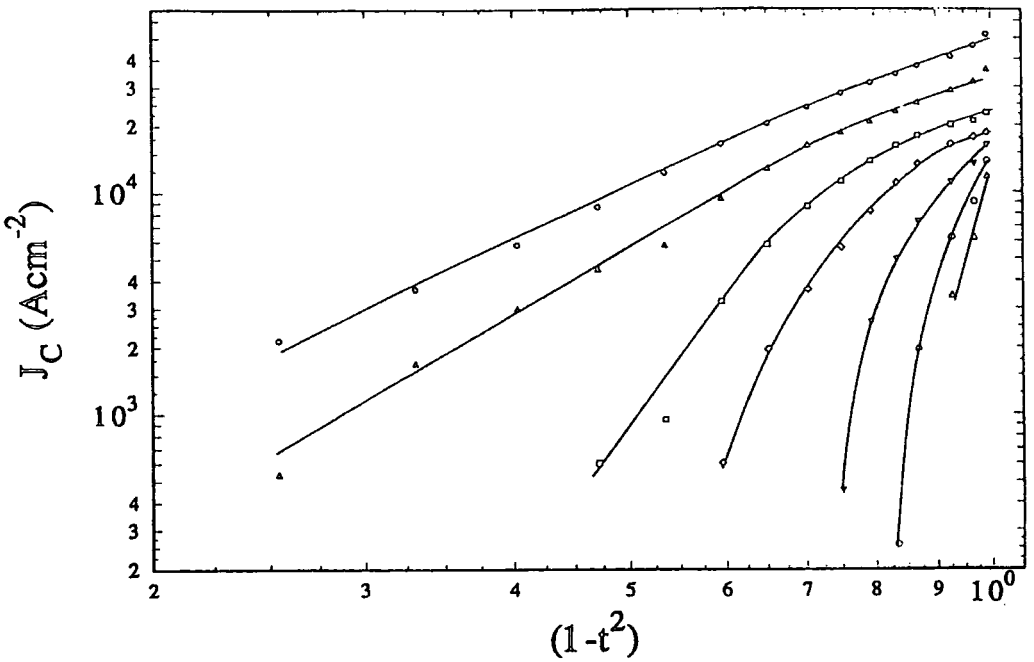

(a)

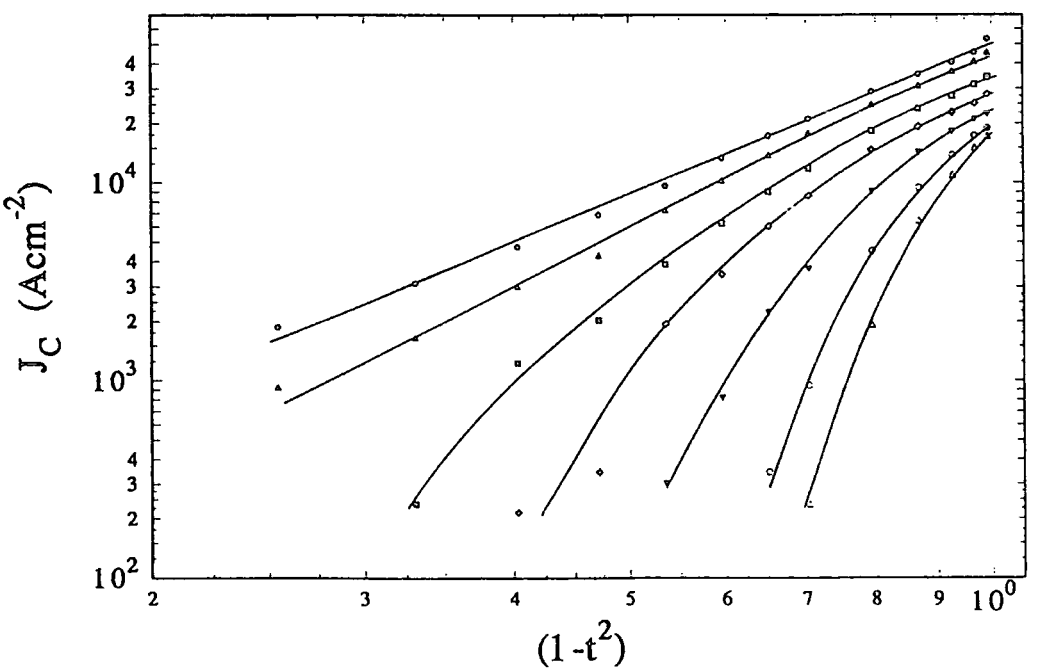

(b)

Figure 6.8: A plot of $\log\{J_c(T)\}$ vs $\log\{1-t^2\}$ for (a) the BPC orientation and (b) the BPAB orientation. For each figure the curves are data at fixed fields of (from top to bottom) 0.001, 0.1, 0.8, 2, 5, 10 and 15 Tesla.

(c) Figures 6.9a,b,c and d compare J_c with field for the three orientations at fields below 1T and at temperatures of 20, 40, 60 and 80K respectively on a log-log scale. The curves have the following common characteristics:

i. below a certain field, defined here as B_1, J_c is constant. For the BPAB and LFF orientations B_1 is the same and is 13-15mT up to 80K where it starts to fall towards zero at T_c. For the BPC orientation it is 8-10mT until 80K where it also starts to decrease;

ii. above the field B_1, in figures 6.10a-d there is no clear analytical form for the critical current density. A best fit, above B_1, up to a field of 1T (or less at the higher temperatures) is a power law of the form

$$J_C(B,T) = a(T)B^{-\gamma} \qquad (6.3)$$

where a(T) is a temperature dependent constant. For the BPC orientation between 10K and 60K, $\gamma = 0.16$. For the BPAB and LFF orientations in the same temperature range $\gamma = 0.13$. Above 60K, γ appears to increase slowly with temperature for each orientation.

It is also interesting to note the relative magnitudes of J_c for the three orientations. Although for the BPAB and LFF orientations B_1 and γ is the same, at 30K and above the magnitude of J_c for the LFF orientation is clearly higher than for the BPAB orientation. For the BPC orientation at the lower temperatures J_c is the same as for the other two orientations below B_1. At temperatures of 40K and above however, below B_1, the magnitude of J_c is *higher* than for the BPAB and LFF orientations. Once J_c starts decreasing according to the power law the magnitude of J_c for the BPC orientation quickly falls below that for the other two orientations.

The three sections, (a)-(c), present the $J_c(B,T)$ data in alternative ways. Either of the functional forms of equations 6.1 - 6.3 could be used to try and describe the field and temperature dependence of J_c at low fields. However, below the field B_1, J_c is best described by the form of equation 6.2 (or equation 6.1) and above B_1 (up to 1T) it is best described by the power law of equation 6.3.

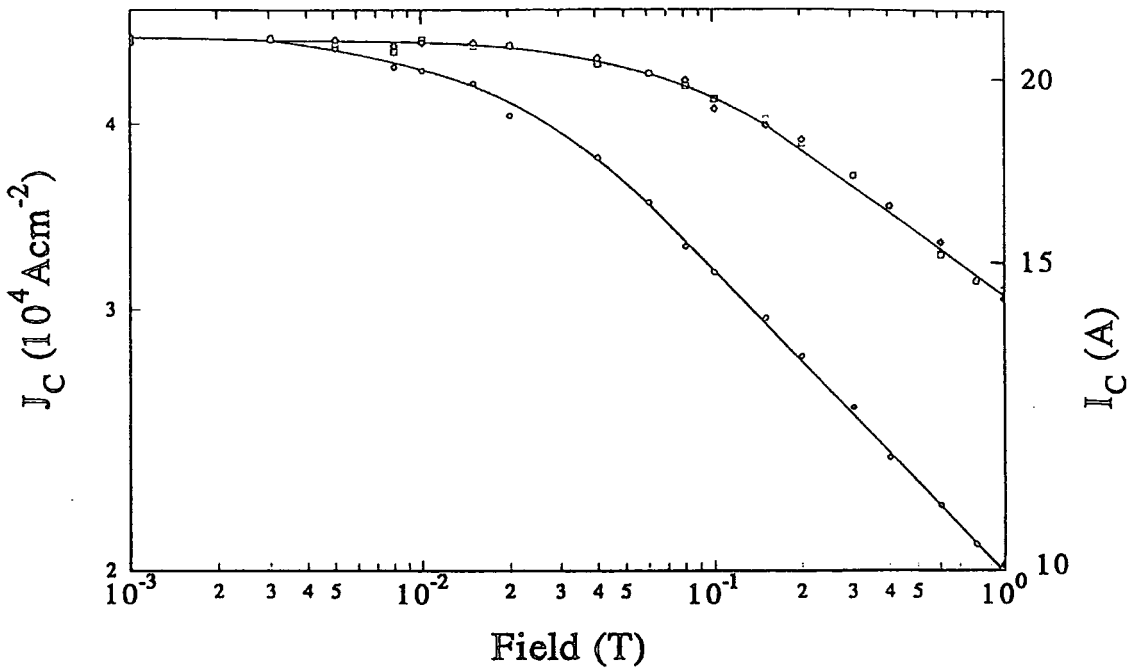

(a)

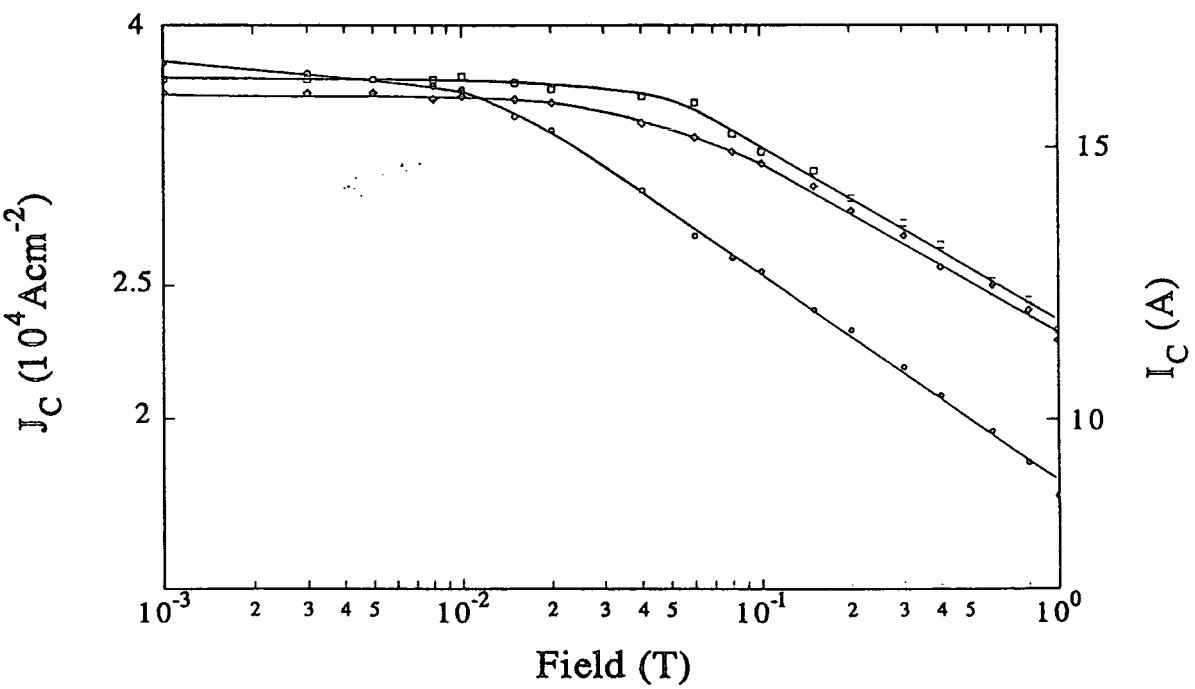

(b)

Figure 6.9: $J_c(B)$ below a field of 1T for the three orientations at a temperature of (a) 20K and (b) 40K. For each figure the orientations are as follows: ●, BPC; □, BPAB; ♦, LFF.

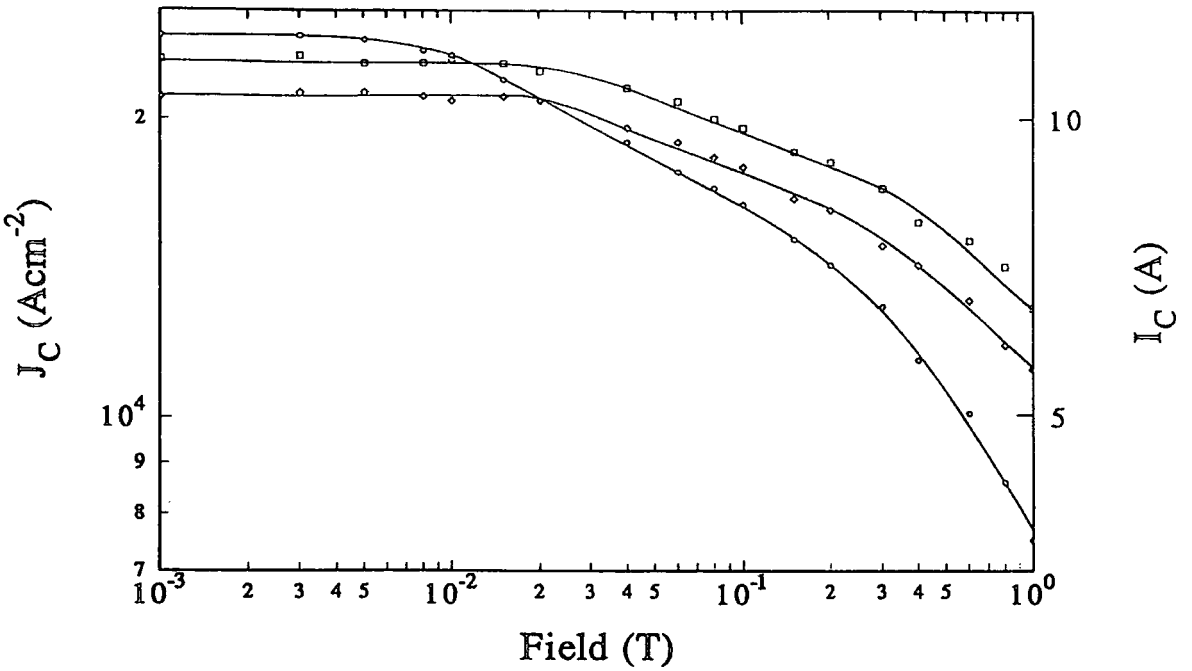

(c)

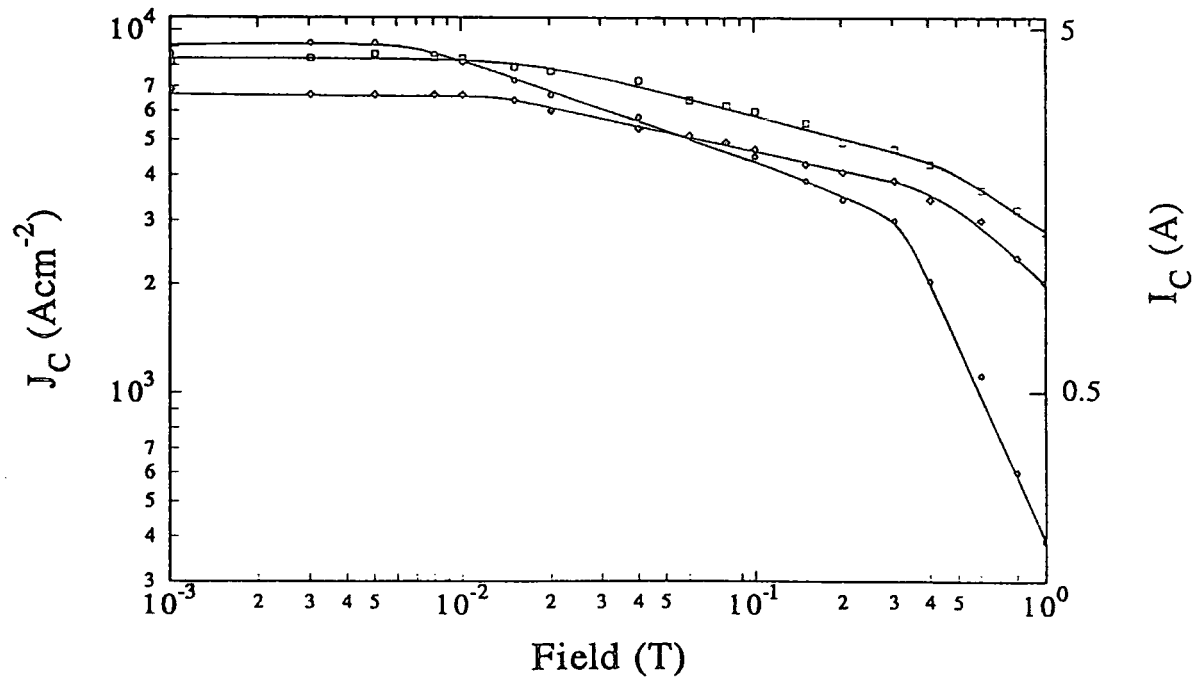

(d)

Figure 6.9: $J_C(B)$ below a field of 1T for the three orientations at a temperature of (c) 60K and (d) 80K. For each figure the orientations are as follows: ●, BPC; □, BPAB; ◈, LFF.

6.3.3. The data for fields higher than 1T above 10K

This section is in four parts. In part (a) the $J_c(B,T)$ data is described in terms of an exponential function. Alternatively a description of $J_c(B,T)$ can be made by considering the volume pinning force. This method is presented in part (b). Part (c) considers whether the functional form of equation 6.2 can be applied to the high field range. Finally part (d) analyses possible crossover effects in the field and temperature dependence of J_c. The data has been analyzed as such, in several alternative forms, to enable comparison to the literature.

(a) The data of figures 6.2-6.4 are re-plotted on log-linear scales in figures 6.10 - 6.12, demonstrating that the critical current density decreases exponentially with field at medium to high fields at all temperatures for the three orientations. The changeover from the low field dependence to this exponential dependence is not instantaneous. The data can only be described by an exponential function at fields above a value defined here as $B_{exp}(T)$. For the BPAB and LFF orientations the value of $B^{ab}_{exp}(T)$ is 4-5T between 4.2K and 30K then starts to decrease towards zero at T_c. For the BPC orientation the changeover from the low to high field behaviour is much quicker. J_c decreases exponentially above a field defined here as $B^{c}_{exp}(T)$ which is 1.5-2T up to 40K and then decreases to zero at T_c. At very high fields however (above 40K) J_c begins to decrease more rapidly with field than an exponential function and falls quickly to unmeasurably small values. In contrast, for the BPAB and LFF orientations the data remains exponential over the entire field range above $B^{ab}_{exp}(T)$ up to 15T. The field at which the rapid decrease of J_c, departing from the exponential form, begins for the BPC orientation has been called $B_d(T)$.

The data have been fitted to the function

$$J_C(B,T) = \alpha_J(T)\exp\{-B/\beta(T)\} \qquad (6.4)$$

above the field $B^{ab}_{exp}(T)$ for the BPAB and LFF orientations and between the fields $B^{c}_{exp}(T)$ and $B_d(T)$ for the BPC orientation. The parameters $\alpha_J(T)$ and $\beta(T)$ have been calculated

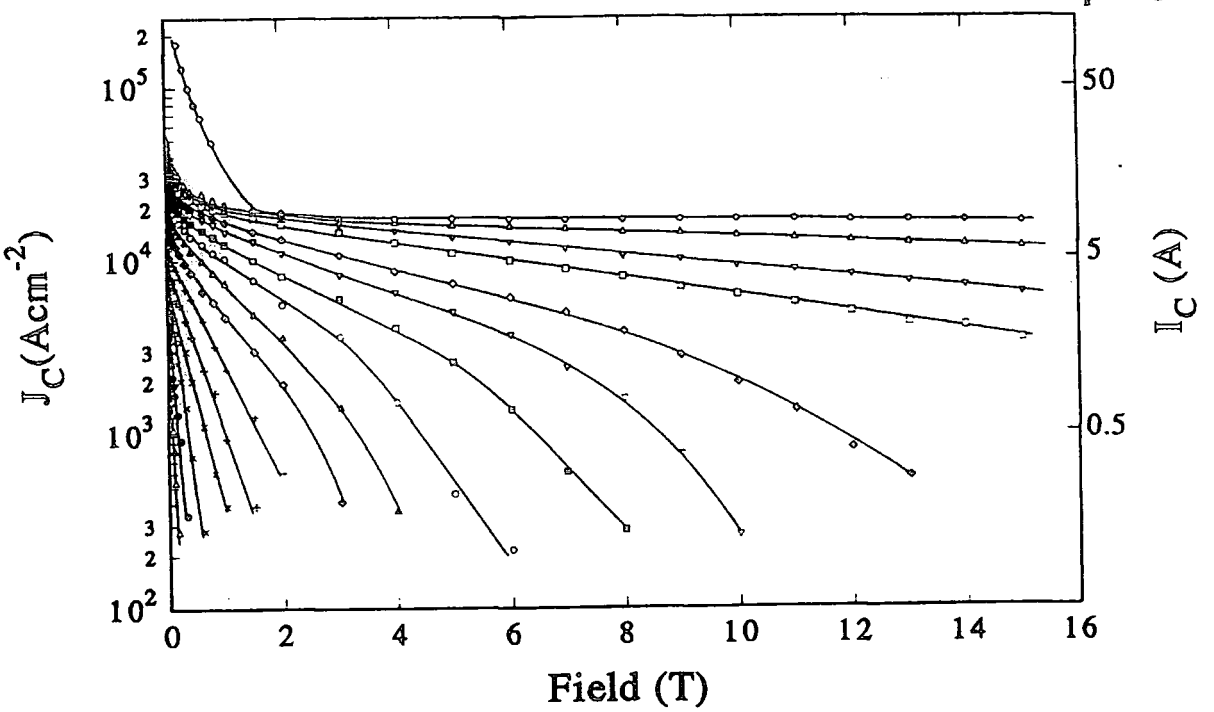

Figure 6.10: The critical current density of the tape for the BPC orientation on a log-linear scale. The curves are measurements at constant temperatures of (from the top down): 4.2, 10, 20, 30, 40, 50, 60, 65, 70, 75, 80, 85, 90 and 95K respectively.

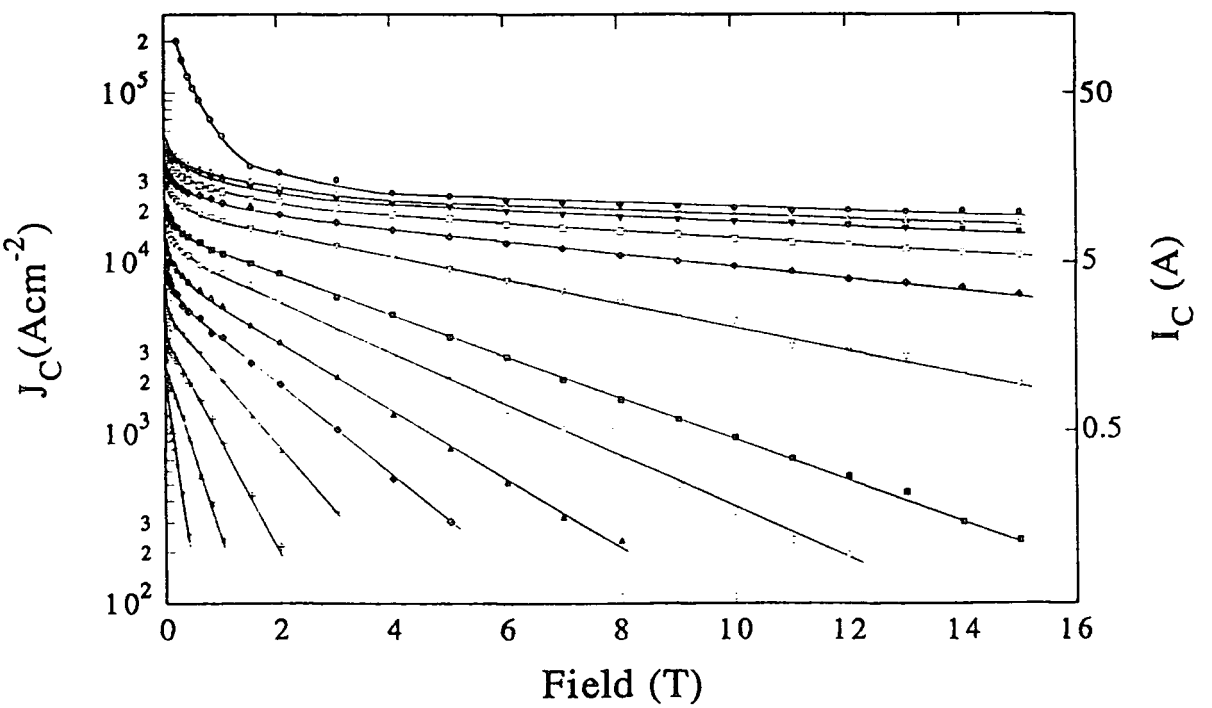

Figure 6.11: The critical current density of the tape for the BPAB orientation on a log-linear scale. The curves are measurements at constant temperatures of (from the top down): 4.2, 10, 20, 30, 40, 45, 50, 55, 60, 65, 70, 75, 80, 85, 90 and 95K.

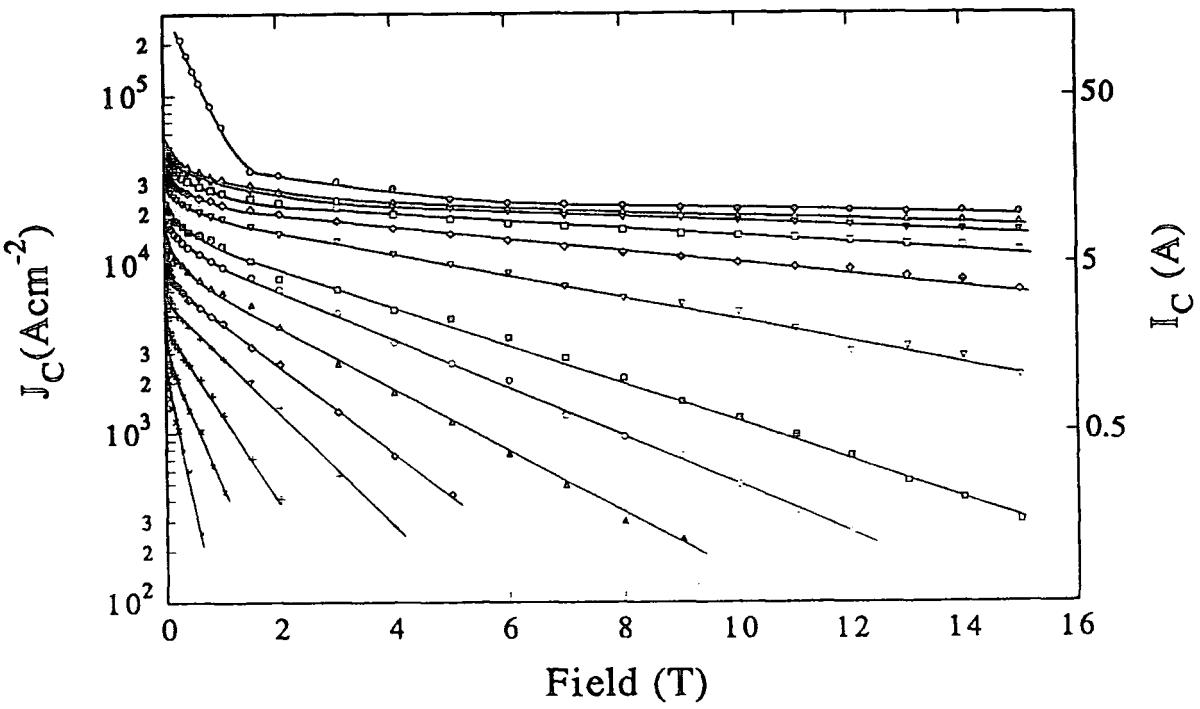

Figure 6.12: The critical current density of the tape for the LFF orientation on a log-linear scale. The curves are measurements at constant temperatures of (from the top down): 4.2, 10, 20, 30, 40, 45, 50, 55, 60, 65, 70, 75, 80, 85, 90 and 95K respectively.

for the three orientations and are plotted in figures 6.13 and 6.14 respectively. The following points should be noted:

i. the three curves for $\alpha_j(T)$ converge at 55K. Below this temperature, $\alpha_j(T)$ for the BPC orientation is approximately constant and $\alpha_j(T)$ is the same for the BPAB and LFF orientations but not temperature independent. Above 55K, $\alpha_j(T)$ for the BPAB orientation becomes less than the value for the LFF orientation. The $\alpha_j(T)$ curve for the BPC orientation crosses the BPAB line and lies on or just above the LFF line. The error in $\alpha_j(T)$ for each orientation is 5%.

ii. ß(T) for the BPAB and LFF orientations is the same. For the BPC orientation ß(T) is smaller throughout the temperature range. The relative error in ß(T) is 5% for all orientations and temperatures except at 4.2K and 10K for the BPC orientation where it is 20%. This is because at these temperatures the slope of log $\{J_c\}$ with B is close to zero and ß is inversely proportional to the slope.

In order to describe the functional form of $\alpha_j(T)$ and ß(T) more quantitatively their log value has been plotted against $\log\{1-t^2\}$, where t is the reduced temperature, in figures 6.15 and 6.16. A fit to a $(1-t^2)^n$ dependence has been attempted because of the similar theoretical temperature dependence of the important parameters: the coherence length; the magnetic penetration depth; the depairing critical current density and the upper critical field. An attempt to fit the data to a $(1-t)^n$ dependence is also justified but in this case a better fit was found with $(1-t^2)^n$.

As can be seen from figures 6.16 and 6.17, there is a significant change in the temperature dependence of both parameters at 55K. All three orientations have the same temperature dependence for ß(T) which is stronger below 55K than above it. However, the parameter $\alpha_j(T)$ has a stronger temperature dependence above 55K than it does below it. For the BPC orientation, below 55K, $\alpha_j(T)$ is independent of temperature.

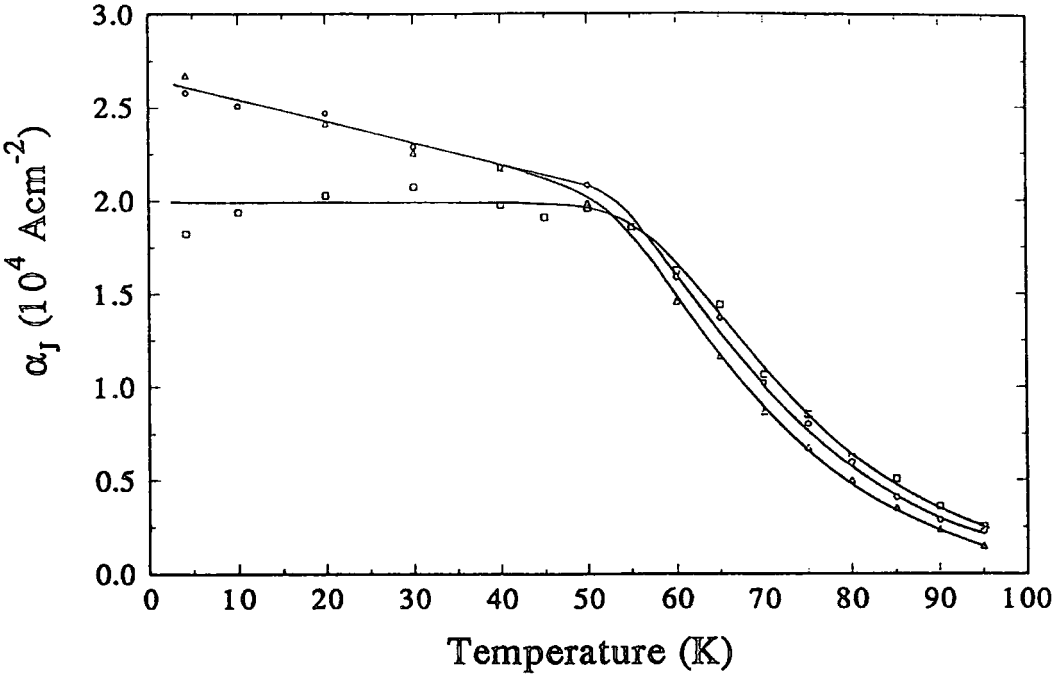

Figure 6.13: The parameter α_J(T) for the orientations: □, BPC; △, BPAB and ⊙, LFF.

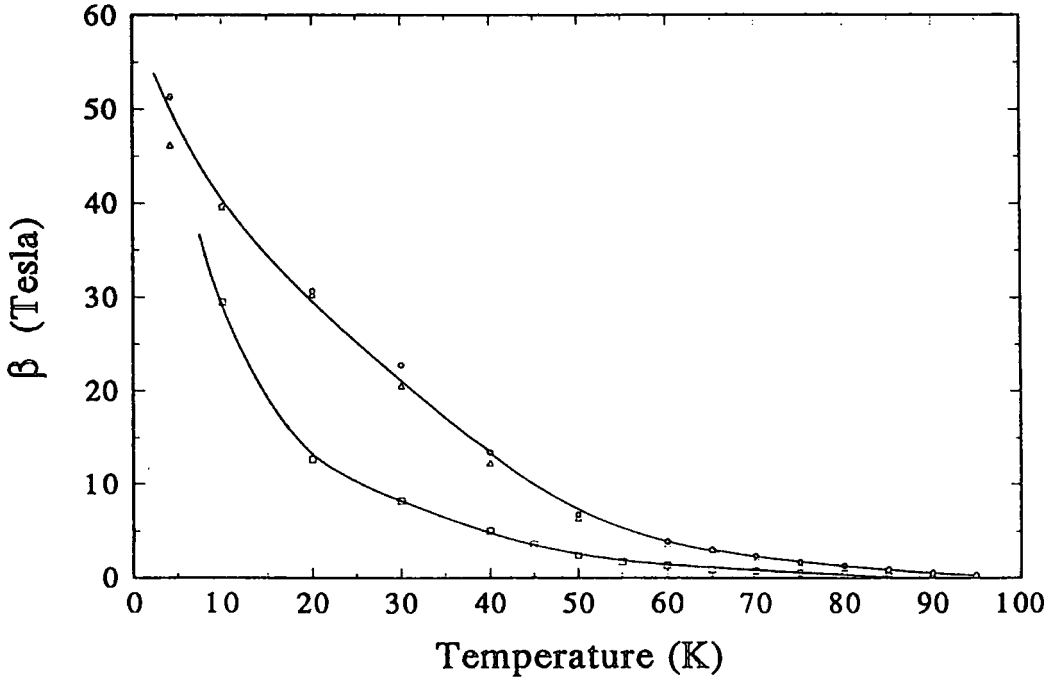

Figure 6.14: The parameter ß(T) for the orientations: □, BPC; △, BPAB and ⊛, LFF.

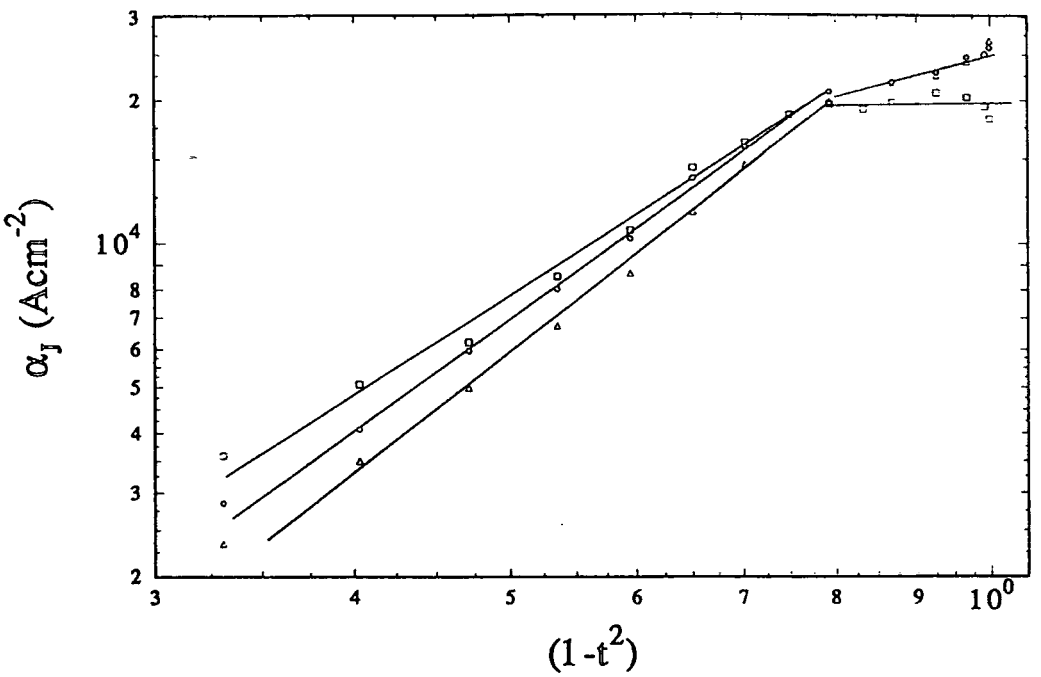

Figure 6.15: A plot of log{α_J(T)} vs log{1-t^2} for the orientations: □, BPC; ▵, BPAB and ⊜, LFF.

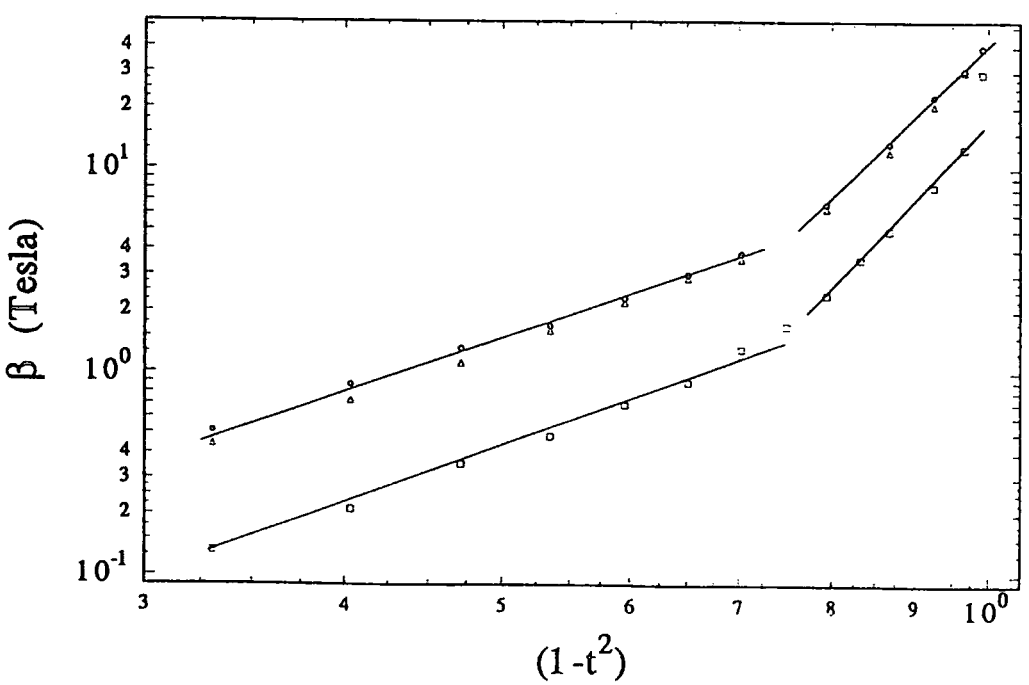

Figure 6.16: A plot of log{ß(T)} vs log{1-t^2} for the orientations: □, BPC; ▵, BPAB and ⊜, LFF.

Summarizing this part mathematically, $J_c(B,T)$ (in the regimes where it decreases exponentially with field) can be described by the functional forms:

below 55K,

$$J_C(B,T) = \alpha_{ab0}(1-t^2)\exp\left(\frac{-B}{\beta_{ab0}(1-t^2)^8}\right) \quad \textit{for BPAB, LFF} \qquad (6.5)$$

$$J_C(B,T) = \alpha_{c0}\exp\left(\frac{-B}{\beta_{c0}(1-t^2)^8}\right) \quad \textit{for BPC} \qquad (6.6)$$

where $\alpha_{ab0} = (2.5\pm0.3)\times10^4$ Acm^{-2}, $\beta_{ab0} = (40\pm2)$ T, $\alpha_{c0} = (2.0\pm0.2)\times10^4$ Acm^{-2} and $\beta_{c0} = (16\pm1)$ T;
and above 55K,

$$J_C(B,T) = \alpha'_{ab0}(1-t^2)^{5/2}\exp\left(\frac{-B}{\beta'_{ab0}(1-t^2)^3}\right) \quad \textit{for BPAB} \qquad (6.7)$$

$$J_C(B,T) = \alpha''_{ab0}(1-t^2)^{5/2}\exp\left(\frac{-B}{\beta''_{ab0}(1-t^2)^3}\right) \quad \textit{for LFF} \qquad (6.8)$$

$$J_C(B,T) = \alpha'_{c0}(1-t^2)^2\exp\left(\frac{-B}{\beta'_{c0}(1-t^2)^3}\right) \quad \textit{for BPC} \qquad (6.9)$$

where $\alpha'_{ab0} = (2.9\pm0.2)\times10^4$ Acm^{-2}, $\beta'_{ab0} = (9.3\pm0.5)$ T, $\alpha''_{ab0} = (2.95\pm0.2)\times10^4$ Acm^{-2}, $\beta''_{ab0} = (9.5\pm0.5)$ T, $\alpha'_{c0} = (2.5\pm0.3)\times10^4$ Acm^{-2} and $\beta'_{c0} = (3.1\pm0.2)$ T. The error on the $(1-t^2)$ indices is 10%. Note that in each temperature range the temperature dependence of ß is the same for all three orientations.

(b) The reduced pinning force (F_p/F_{pmax}) is plotted against $b = B/B_{irr}$ for the BPC orientation in figure 6.17. There is no evidence for scaling and none was found for the other two orientations.

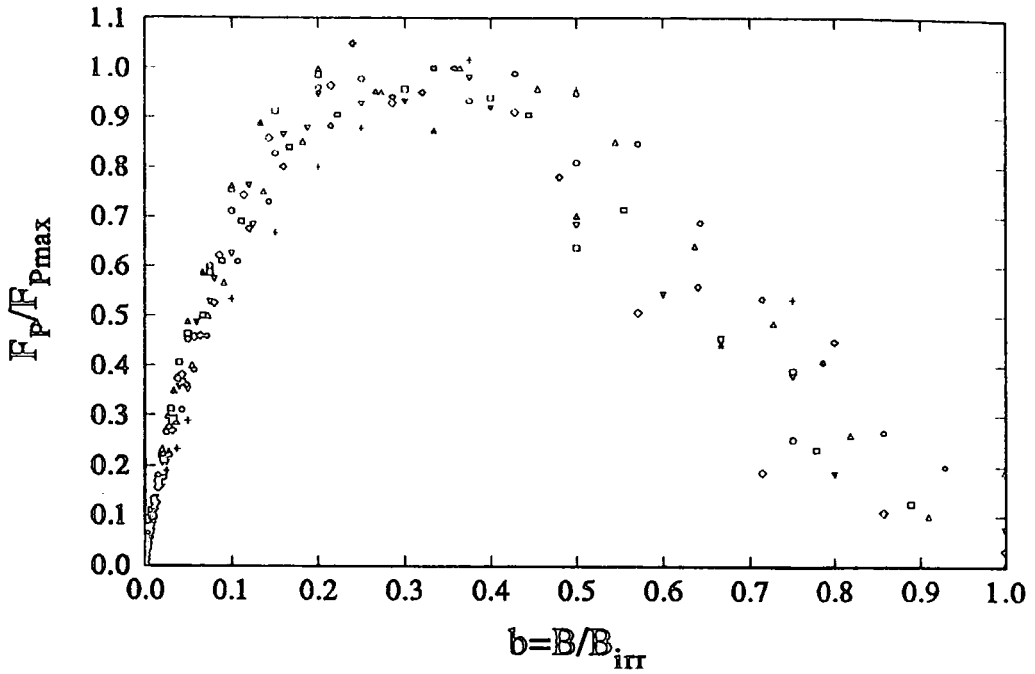

Figure 6.17: The reduced pinning force as a function of the reduced field for the BPC orientation.

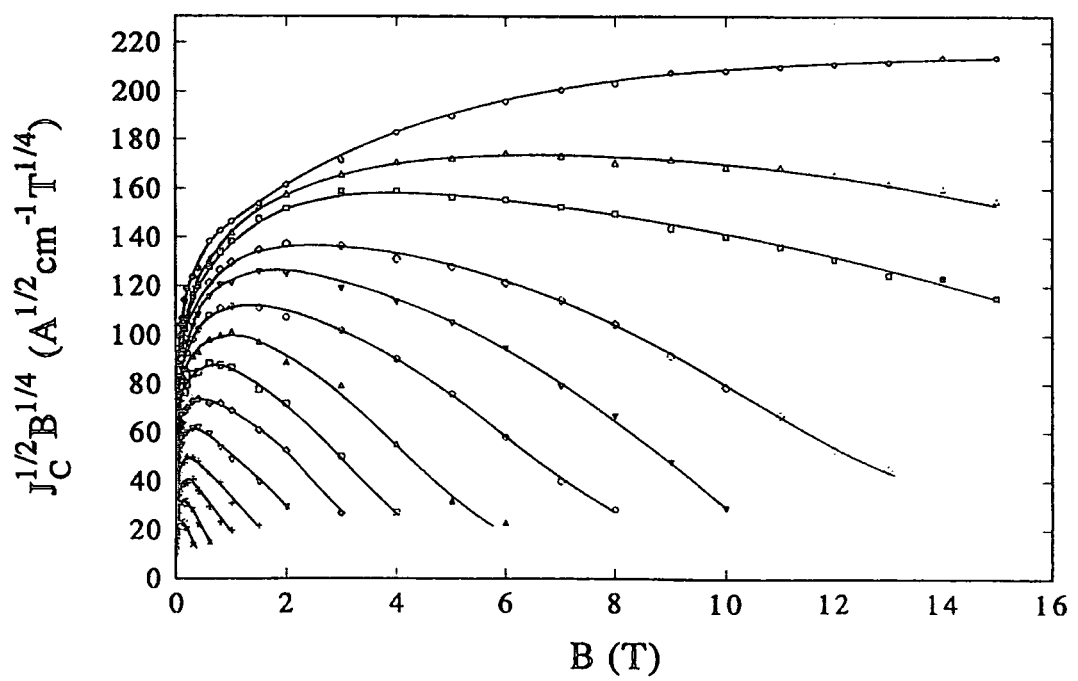

Figure 6.18a: A Kramer plot for the BPC orientation. The curves are at fixed temperatures of (top to bottom) 10, 20, 30, 40, 45, 50, 55, 60, 65, 70, 75, 80, 85 and 90 K.

An attempt has also been made to fit the data to the Kramer relation for depinning by shearing of the flux line lattice about the pinning centres[2]. His model predicts a pinning force of the form $F_P \propto b^{1/4}(1-b)^2$. Plotting $J_c^{1/2}B^{1/4}$ vs B should then give a straight line, which when extrapolated to $J_c^{1/2}B^{1/4} = 0$ gives the scaling field which is $B_{c2}(T)$ in Kramer's analysis. Figure 6.18 is a Kramer plot for the three orientations. For the BPC orientation (figure 6.18a) there is no clear fit to the Kramer relation. This is not the case however in figures 6.18b and 6.18c for the BPAB and LFF orientations. At 50K and above, except when close to B=0, the data at fixed temperatures form parallel straight lines. Extrapolating these lines to $J_c^{1/2}B^{1/4} = 0$ gives scaling fields just higher than the measured irreversibility line and clearly not equal to $B_{c2}(T)$. In comparing the BPAB and LFF orientations, the slopes of the straight lines in 6.18b and 6.18c are the same but for the same temperature the line for the LFF orientation is always higher. Kramer's model is an alternative form to the exponential function of equations 6.5-6.9 for describing $J_c(B,T)$. The two different forms are *not* compatible.

(c) In section 6.3.2(b), $J_c(B,T)$ was described using a $(1-t^2)^n$ dependence at fields close to zero. From figures 6.8a,b it is clear that such a description cannot be extended to high fields (above 2T).

(d) For each method of describing J_c, presented in parts (a) - (c), a crossover from a low to high temperature regime, at which the field and temperature dependence of J_c changes markedly, can be defined. In part (a), both parameters which describe the exponential function ($\alpha_j(T)$ and ß(T)) change their temperature dependence at 55K. This is seen clearly in figures 6.15 and 6.16 for all three orientations. In part (b), for the BPAB and LFF orientations, the Kramer analysis holds above 40K. Below this temperature however, the Kramer plot gives an unphysical curve with respect to this analysis. Finally, from the data of figures 6.8a and b, a crossover curve $T_\alpha(B)$ can be defined as follows: for a constant field, T_α is the temperature at which there is a clear change in the strength of the temperature dependence of J_c, as observed in the plots of $\log\{J_c\}$ vs $\log\{1-t^2\}$. For the BPC orientation $T_\alpha(B)$ goes from 30K at 15T to 40K at 2T then increases quickly to 60K at 1mT. $T_\alpha(B)$ for the BPAB orientation has the same functional form but with a larger magnitude.

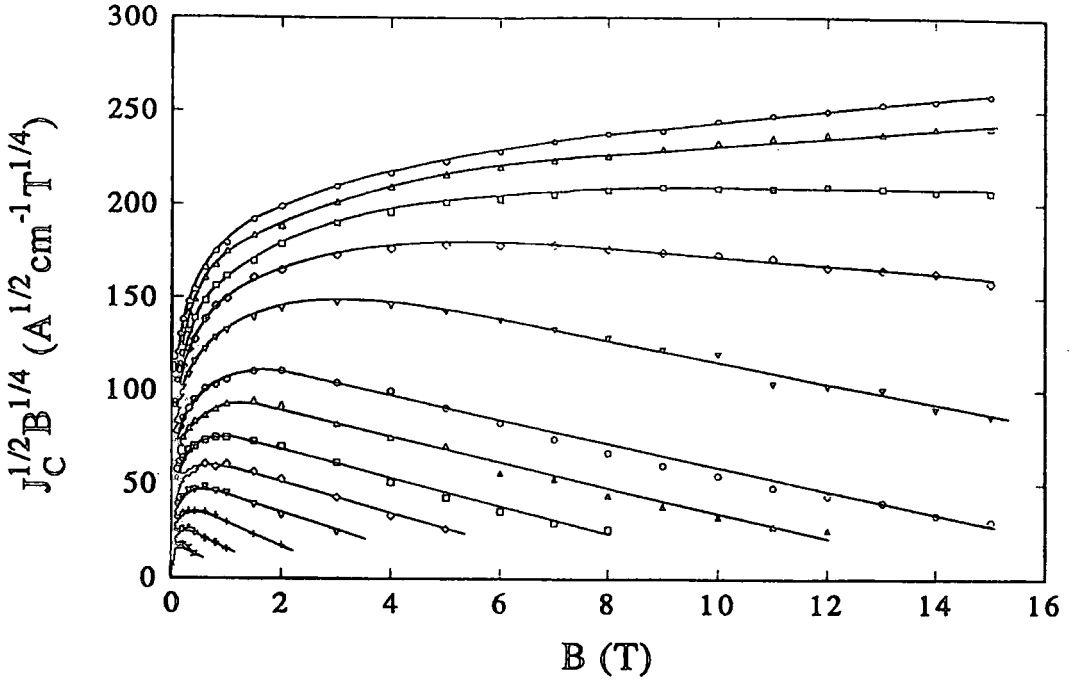

(b)

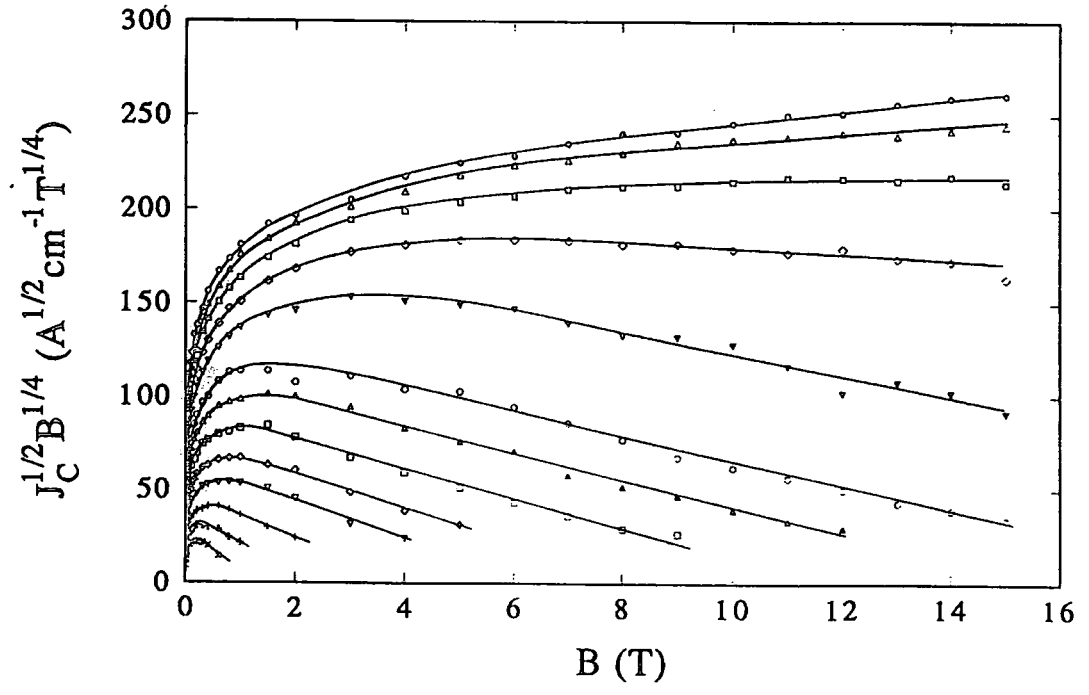

(c)

Figure 6.18: A Kramer plot for (b) the BPAB orientation and (c) the LFF orientation. The curves are at fixed temperatures of (top to bottom) 10, 20, 30, 40, 50, 60, 65, 70, 75, 80, 85 and 90 K.

6.3.4. The irreversibility line

The irreversibility field, $B_{irr}(T)$, has been defined as that field at which the critical current density became less than 200 Acm^{-2} (which corresponds to a critical current of 0.1 A). It is plotted for all three orientations in figure 6.19. $B_{irr}(T)$ for the BPC orientation is lower than $B_{irr}(T)$ for the BPAB and LFF orientations (which are equivalent). The inset of figure 6.19 shows the ratio B^{ab}_{irr}/B^{c}_{irr}, where the superscripts denote the BPAB and BPC orientations respectively. It is appears to be constant at a value of 3 throughout the range accessible with the measurements.

Figure 6.20 is a plot of $\log\{B_{irr}(T)\}$ vs $\log\{1-t\}$. The data can be described by two straight lines each with a slope 2.75 $\pm$ 0.05 for the BPAB and BPC orientations. A best fit line for the LFF orientation gives a slope of 2.4 $\pm$ 0.06. The smaller slope for the LFF orientation is probably an artifact of the analysis. By defining the irreversibility line using a finite critical current criterion the calculated values will be slightly smaller than the true values. Approaching the irreversibility field, J_c for the LFF orientation is higher than for the BPAB orientation. Although an extrapolation of J_c to zero may give the same value for B_{irr} using a finite criterion will give higher values of B_{irr} for the LFF orientation. A better fit is obtained with a (1-t) dependence than with a $(1-t^2)$ dependence.

The irreversibility line can then be represented by the following equations:

$$B^{ab}_{irr}(t) = B^{ab}_{irr}(0)(1-t)^{11/4} \qquad (6.10)$$

$$B^{c}_{irr}(t) = B^{c}_{irr}(0)(1-t)^{11/4} \qquad (6.11)$$

where $B^{ab}_{irr}(0) = (133 \pm 8)$ Tesla and $B^{c}_{irr}(0) = (47 \pm 2)$ Tesla.

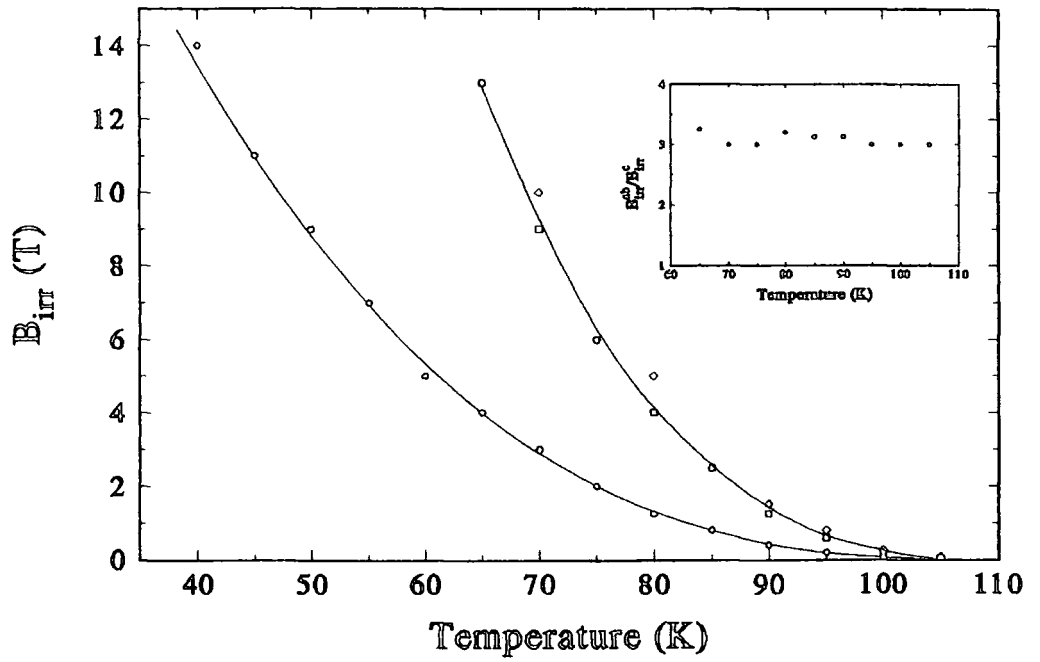

Figure 6.19: The irreversibility line for the orientations: ⊜, BPC; □, BPAB and ◇, LFF. The inset is a plot of the ratio B^{ab}_{irr}/B^{c}_{irr}.

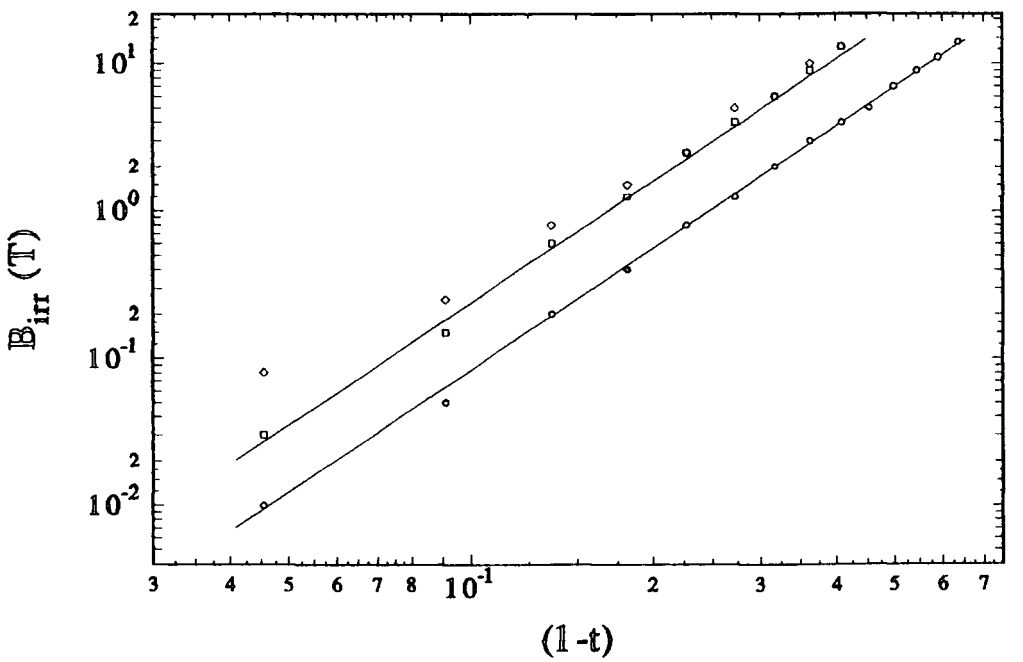

Figure 6.20: A plot of $\log\{B_{irr}(T)\}$ vs $\log\{1-t\}$ for the orientations: ⊜, BPC; □, BPAB and ◇, LFF. The lines are fits to the functional forms of eq. 6.10 and 6.11.

6.3.5. Summary description of the data

The fields and temperatures defined in the description of the data here are plotted on a B-T phase diagram in figure 6.21 for the BPC and BPAB orientations. The superscripts ab and c refer to the BPAB and BPC orientations respectively. This figure illustrates how the $J_C(B,T)$ characteristic varies across the B-T phase diagram. For example, $J_C(B,T)$ of the BPAB orientation is described by the exponential form of equations 6.3 and 6.7 above the line $B^{ab}_{exp}(T)$ until the irreversibility line, $B^{ab}_{irr}(T)$, is reached. By comparison, the BPC orientation can be described by the exponential functions of equations 6.6 and 6.9 in the region bounded by the curves $B^{c}_{exp}(T)$ and $B^{c}_{d}(T)$. Above $B^{c}_{d}(T)$, J_C starts to decrease rapidly until it becomes zero at $B^{c}_{irr}(T)$. The lines $T^{ab}_{cr}(B)$ and $T^{c}_{cr}(B)$ mark the crossover from a weaker temperature dependence of J_C at low fields to a stronger one at high fields for the respective orientations. For both orientations the low field anomaly below 10K is marked by the line $B_l(T)$.

The $J_C(B,T)$ is easier to visualise from the surface plots of figure 6.22 for the same two orientations. Note that the critical current density is plotted on a log scale. Figures 6.22a and 6.22b clearly illustrate the dramatic rise in J_C below the temperature 10K and the magnetic field 1.5T. For both orientations there is a plateau (broadest for the BPAB orientation) in J_C below approximately 40K. At higher temperatures J_C quickly reduces to zero.

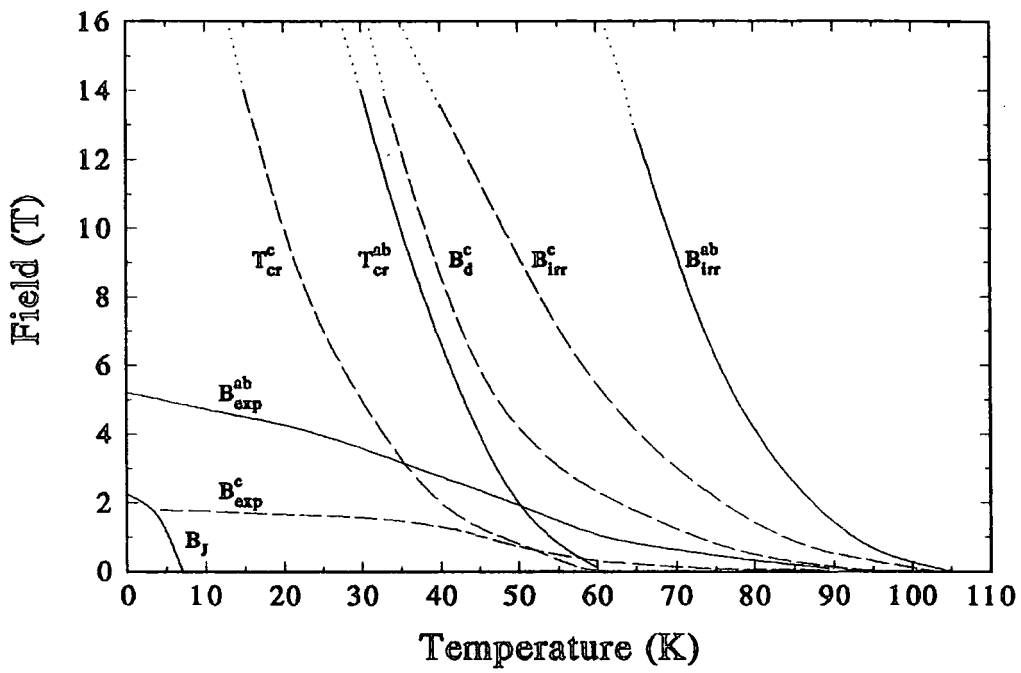

Figure 6.21: The B-T phase diagram for the tape for the BPC and BPAB orientations. For a description of the curves see the text.

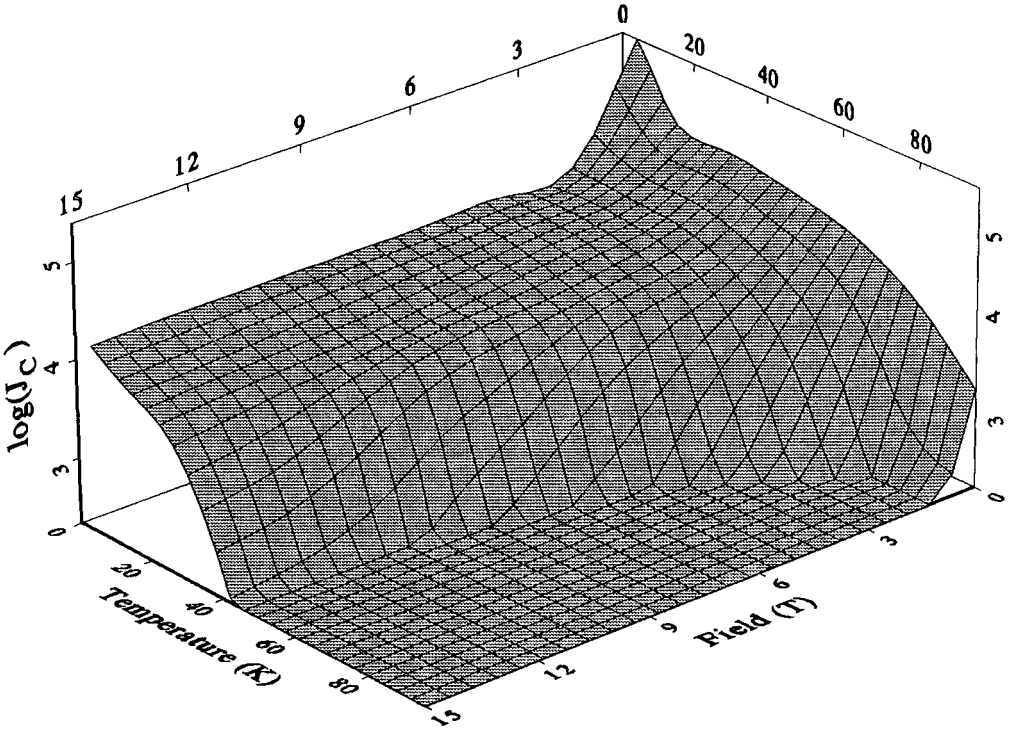

(a)

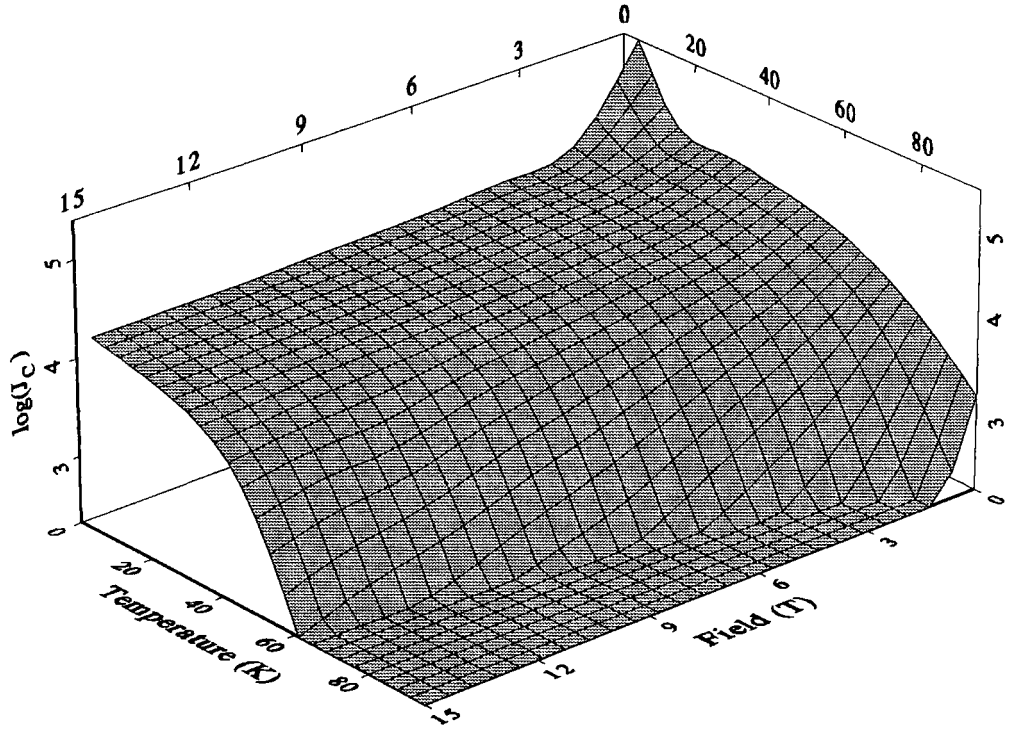

(b)

Figure 6.22: A $J_C(B,T)$ surface plot for (a) the BPC orientation and (b) the BPAB orientation.

6.4. Discussion

This section discusses the data in the same order in which it was analyzed in the previous section: the data below 10K; the data at fields below 1T; the data at fields above 1T and the irreversibility line.

6.4.1. The low temperature anomaly at $B_j(T)$

A similar anomaly in the transport J_c as found here at 4.2K in figure 6.10 was observed by Gurevich at al.[3] in a BSCCO-2223 tape. Since they measured J_c (with the field perpendicular to the tape surface) at 4.2K and 77K only they would be unaware of the possible disappearance of the anomaly at 10K. In their tape the discontinuity in J_c occurred at 1T. They also measured J_c for a BSCCO-2212 tape but no anomaly was observed. Such an feature has not been reported elsewhere in the literature for any HTSC materials. One reason for this may be the difficulty of measuring such high transport critical currents below 10K at these lower fields. Maeda and Hataya[4] have made comprehensive measurements of the magnetisation J_c for monocore and multifilamentary BSCCO-2223 tapes and found no anomaly at 4.5K.

The data presented here (figures 6.5-6.6) is the first to show this anomaly at a field, $B_j(T)$, independent of sample orientation and that it is not present at 10K and above. In addition the value of $B_j(T)$ is higher at 2K. Two possible causes for the existence of the anomaly are as follows:

i. a phase change of the flux line lattice.

Several theories[5,6,7,8] have predicted a phase change from single flux lines to pancake vortices at low fields for layered structures. For magnetically coupled layers Koshelev and Kes[7] suggest that for BSCCO compounds, depending on the magnitude of J_c, there may be such a 3D to 2D phase change between 1T and 5T at 4.2K (see section 3.7.1b). From the theory of collective pinning for Josephson coupled layers[6,8] (section 3.7.1c) the flux lines are expected to decompose into pancakes at a field $B_{2D} = \phi_0/s^2\Gamma$ (eq.3.17). Using the values for s and Γ for BSCCO-2223 in table

2.2, $B_{2D} \approx 0.7$ T. Cubitt et al.[9] claim to have observed this 3D to 2D phase transition at 60mT from SANS measurements on a BSCCO-2212 crystal. As the theory predicts, they found B_{2D} to be temperature independent.

Such theories as discussed here do not explain the anomaly observed in figures 6.5-6.6. The field at which the anomaly occurs, defined as B_j is not independent of temperature and the anomaly disappears altogether at 10K and above. $B_j(T)$ is the same for any orientation of the magnetic field with respect to the sample. For a change from a single flux line to pancakes it is only the field component parallel to the c-axis which is important and hence B_j would be expected to change with field orientation. Furthermore, below $B_j(T)$ it has been found that J_c is strongly dependent on field. Considering the pinning of single flux lines in layered structures (section 3.7.1a), J_c should be relatively independent of magnetic field. Other phase changes, such as singly pinned pancakes to collectively pinned pancakes, can also be discounted because they depend on the field component parallel to the c-axis and no orientation dependence is observed;

ii. decoupling of the grains

Although it is clear that BSCCO is a granular material, little is known in detail about its microstructure at or near the grain boundaries. The magnetic hysteresis in figures 6.5a,b,c is also observed in the highest quality BSCCO-2223 tapes[10] and is evidence for the existence of Josephson junctions at the grain boundaries (section 3.9).

Assuming that the grain boundaries in the BSCCO tape are S-N-S Josephson junctions then the field B_j can be related to the average upper critical field of the junctions. That B_j is equal for all orientations of the field infers that there is no preferred orientation for the dominant weak links. In addition however, the disappearance of the anomaly at 10K suggests that junction material is weakly *superconducting* with a T_c between 4.2K and 10K. This would also be consistent with the higher B_j at 2K. In this case $B_j(T)$ is actually the superconducting upper critical field of the junction material. Umezawa et al.[11] have investigated the microstructure of BSCCO-2223 tapes for different heat treatments. Even after the longest heat treatment they found a few layers of the lower

T_c BSCCO-2212 phase at the c-axis twist boundaries. It was shown that these layers of 2212 controlled the critical current in the range 75-105K. No other BSCCO phases were observed. For the tape studied here it is likely that at some or all of the grain boundaries there exists a BSCCO phase with a T_c between 4.2K and 10K. A rough estimate of the T_c, by extrapolating the measured B_j to zero, is 10.8 K. Possible candidates for the intergranular material are the BSCCO-2201 and 2011 phases which have maximum T_c's of 14K and 20K respectively. Whilst the intergranular material is still superconducting the individual grains are well connected.

In summary, the low temperature anomaly observed in figures 6.5a,b,c can best be explained as a decoupling of the grains. Some of the grain boundaries must contain a low T_c BSCCO phase (probably the 2201 or 2011 phase) producing strong connections between the grains for the transport current path. Above $B_j(T)$, the upper critical field of the low T_c BSCCO phase, J_c is determined by intergranular coupling. Below $B_j(T)$, J_c is initially high, because of the excellent connections between grains, but reduces quickly with field as the upper critical field of the junctions is approached, reducing the strength of the coupling between the grains. Figure 6.6, comparing J_c at 4.2K for the three orientations, agrees with this argument: below $B_j(T)$, J_c is higher for the LFF orientation than for the BPAB orientation - it is dependent on the direction of the Lorentz force within the grains. Above B_j however it is the same for these two orientations, being determined solely by the intergranular coupling. For the BPC orientation, where the field is perpendicular to the layers, the intergranular J_c is already much lower before B_j is reached.

6.4.2. $J_c(B,T)$ above 10K in fields less than 1T

i. the $(1-t^2)^n$ description below B_j

Hensel et al.[12] found J_c to decrease linearly with temperature, except very close to T_c, for a BSCCO-2223 tape in zero field. The 1mT curves in figures 6.7a,b cannot be fitted closely to a single straight line: instead the 1mT curve for the BPAB orientation is linear with $(1-t^2)^{2.6}$ for all temperatures and at 1mT for the BPC orientation, J_c varies as $(1-t^2)^2$ up to 65K. The temperature dependencies of BSCCO-

2223 thin films in zero field can be described by a 2-order polynomial in t (reduced temperature) according to the data of Yamasaki et al.[13]. The inset to figure 6.15a shows that such a polynomial can also describe the 1mT data for the BPC orientation except near to T_c. So contrary to what Hensel et al.[12] found, the zero field data for the BSCCO-2223 tape have a similar temperature dependence to a 2223 thin film.

Matsushita et al.[14] measured the temperature dependence of J_c for a multi-phase BSCCO tape in low fields parallel to the ab-plane and found it to vary with $(1-t^2)^n$. The parameter n was of the order of 10-16 below 30K and 2.5-3.5 below 30K. This is in contrast to the data of figures 6.8a,b where there is a weaker dependence in the lower temperature regime with n=2.5-3.

ii. the description above B_1

The transport J_c at low fields of various HTSC compounds has been measured by several authors who find the same general behaviour as observed in figures 6.9a-d: a constant value at very low fields and then a drop off with field as a power law followed by a plateau or much weaker field dependence at higher fields. In contrast magnetic measurements of $J_c(B)$ for BSCCO tapes have shown only an exponential dependence at these low fields[15].

Ekin et al.[16] found such a double step behaviour for several bulk Y-, Bi- and Tl-based compounds. In their samples J_c was constant up to approximately 1mT and then decreased as $B^{-3/2}$ before reaching a plateau around 300mT. The $B^{-3/2}$ dependence corresponds well to the theory of Peterson and Ekin[17] for a J_c determined by a network of Josephson junctions between grains at very low fields (10's mT). The field dependence of J_c at the Josephson junctions is given by the Airy diffraction pattern and is averaged over a distribution of the weakest links.

Nakamura et al.[18] have measured J_c for a BSCCO-2212 single crystal below 10mT. It was found to be a function of the field component parallel to the c-axis and was constant up to 1.3mT above which it decreased as B^{-1}. They fitted their data to the Kim critical state[19] after taking account of the self field and demagnetisation effects.

In comparison to the low field data on HTSC crystals[18] and bulk samples[16,17] the data in figures 6.9a-d is constant up to fields of B_l = 8-13mT and then decreases with a relatively weak field dependence of $B^{-(0.13-0.16)}$. At fields above 1T the field dependence becomes even weaker - the high field characteristics are not discussed here.

iii. interpretation

It is to be expected that above 10K, when the low T_c phase intergranular material is normal, at low fields the current flows through a network of S-N-S Josephson junctions. Even though J_c has a weaker field dependence than the theories suggest, the low field behaviour above 10K is still consistent with such a model as follows: the field $B_l(T)$ can be considered an effective penetration field. At this field the flux starts to penetrate into the intergranular material and grain surfaces and can be called the lower critical field of the weak links. The values of $B_l(T)$ measured here includes contributions from self-fields, remnant fields (produced by cycling of the high-field magnet during the measurements), trapped flux and demagnetisation effects. Because of these effects no significance can be made of the values and anisotropy of $B_l(T)$. Above $B_l(T)$ as the field penetrates further between the grains and into them, the junctions are increasingly decoupled and current flows through a network of Josephson coupled grains. The weak field dependence of J_c in this regime, compared to the theoretical models, can be ascribed to the large spread of junction sizes and orientations along with their non-uniformity in BSCCO tapes which the models cannot account for. Senoussi[20] suggests that the junctions are not ideal (where the current flows only to the junction penetration depth) but are highly inhomogeneous and contain flux trapping regimes. The current can now also be carried by the interior of the junctions. Such effects and a large distribution in the junction critical fields will weaken the field dependence of J_c. At fields around 1T, the flux has fully penetrated into the intergranular material and starts to penetrate deeper into the grains. The current flow is now via a few remaining strong connections between grains. The high field behaviour of J_c is discussed in the next section.

These 'strong connections', whose nature is not clear, need to be considered here as they do exist at fields below 1T, but with their low numbers are not assumed to affect

$J_c(B,T)$. Figures 6.9a,b,c,d however, show a strong orientation dependence below 1T. This indicates that either intragranular effects are always determining J_c to some small degree or the strongest connections have a preferred direction. In their railway-switch model, Hensel at al.[12] suggest that the current can transfer between grains via small angle c-axis grain boundaries such that it can remain in the ab-planes of the crystal. Other similar 'ab-plane connections' can be imagined such as ab-plane intergrowths across grain boundaries. It is also possible that these connections exist mostly in the region of the BSCCO-Ag interface in the tape, where grain alignment is best. $J_c(B,T)$ across these connections will be determined by the intrinsic properties of BSCCO. Below 1T, the orientational dependence observed in J_c (which gets stronger at high temperatures) is probably caused by the small number of ab-plane connections rather than any orientational dependence in the S-N-S Josephson junctions; the critical field of the S-S'-S Josephson junctions below 10K, $B_J(T)$ was found to be independent of orientation and it is the same junctions, though now S-N-S, that are thought to be determining J_c below 1T.

That the zero field temperature dependence of J_c is similar to that of a BSCCO-2223 thin film suggests that intrinsic properties may determine J_c to some degree. Alternatively, analyzing the data another way it has been shown that J_c varies as $(1-t^2)^n$ close to zero field. Such a temperature dependence is expected for an array of Josephson coupled grains[21] but with an exponent $n=1.5$ compared to $n=2$ and 2.6 for the BPC and BPAB orientations respectively, of the tape. It is concluded that the zero field behaviour of J_c is probably due to a combination of S-N-S junctions and ab-plane connections.

In summary, in low fields the current in the BSCCO tape flows through a network of S-N-S Josephson junction coupled grains. A minority of grains however, are connected such that the current can transfer between them without leaving the crystal ab-planes. The J_c at these connections is determined by the intrinsic properties of the BSCCO. At low fields however the Josephson junction network is dominant in limiting J_c. The field B_1 marks the point at which the flux first penetrates into the intergrain regions and as the field is further increased, the strength of the connection between S-N-S Josephson

coupled grains steadily decreases. In this regime the observed power law field dependence of J_c is weaker than predicted by standard junction network models. This is due to the large spread in the junction sizes, homogeneity and orientation in the tape. The orientation dependence observed in J_c below 1T is due to the small number of ab-plane connections.

6.4.3. The data above 10K at fields higher than 1T

It was seen from the analysis of section 6.3.3 that the high field $J_c(B,T)$ could be described by two alternative functional forms: one the exponential field dependence; and the other, Kramer's analysis. Both of these forms will be discussed in turn. It is not possible to describe J_c using a $(1-t^2)^n$ form at high fields. Possible crossover effects, from a low temperature to high temperature regime in the B-T phase diagram, will be discussed separately. Finally an interpretation of the high field data for the tape is given.

i. the exponential description

Many transport J_c measurements showing an exponential high field dependence at all temperatures, as found for the tape here, have been made on BSCCO tapes: the 2212 phase[22] and the 2223 phase [23,24,25,26]. In reference 25 the J_c of a BSCCO-2223 tape, with the field perpendicular and parallel to the surface, showed an exponential dependence before and after irradiation by heavy ions which increased J_c over most of the field range. The departure from the exponential law in very high fields for the BPC orientation, as seen in figure 6.10, has been observed in other BSCCO tapes[22,25]. Magnetisation measurements of J_c for BSCCO-2223 tapes also show the exponential dependence[15,25] but down to much lower fields. The same behaviour is also observed in $YBa_2Cu_3O_{7-\delta}$ thin films[27] (including the more rapid decrease of J_c in high fields parallel to the c-axis) and polycrystalline BSCCO-2212 wires (see chapter 7). A similar analysis as in section 6.3.3(a), where the parameters $\alpha_j(T)$ and ß(T) are calculated, has been carried out elsewhere. In reference 26 the parameters for a different 2223-tape have a similar temperature and orientation dependence as for the tape in figures 6.13-6.14. It was found however that ß(T) for a

2223 thin film had a different dependence. In reference 27, $\alpha_j(T)$ and ß(T) were calculated for an YBCO-123 thin film. The variation of $\alpha_j(T)$, with the field parallel and perpendicular to the c-axis, is again similar to that for the BSCCO-2223 tape (and the corresponding BPC and BPAB orientations). However ß(T) had a different functional form for each orientation.

In BSCCO-2212[28] and BSCCO-2223[13] thin films and in the best BSCCO-2223 tapes[17] at 4.2K, J_c is constant up to the highest obtainable fields parallel to the ab-plane. The weak field dependence at high temperatures in reference 13 is probably due to a distribution in T_c's throughout the sample. When measured in fields parallel to the c-axis, J_c decreases exponentially. By varying the angle θ that the field makes with the c-axis, it is found that J_c in the thin films scales with $B\cos\theta$[13,28]. In both references 13 and 28 it is concluded that J_c is not determined by grain boundary effects and that the angular dependencies are explained by intrinsic pinning (section 3.8). In a tape the grains are not perfectly aligned and there will be a distribution of angles between the c-axis and tape surface. In this case the flux lines will take the form of pancakes coupled by Josephson strings parallel to the layers (section 3.5). Whatever the orientation of the field there will always be a component parallel to the c-axis. In the model of intrinsic pinning, any reduction in J_c with increasing field is due purely to the field component parallel to the c-axis.

Most theories that attempt to explain the field and temperature dependence of J_c only consider the case where the field is parallel to the c-axis. Possible theories that may be able to explain the behaviour of J_c as described in this section are:

(a) pair-breaking

An exponential field dependence of J_c is observed for a single S-N-S Josephson junction (section 2.5). However, when a distribution of such junctions are considered, in modelling a J_c determined by Josephson coupling between grains, a power law dependence is usually found (section 6.3.2). Alternatively the crystal structure may contain intrinsic S-N-S or S-I-S Josephson junctions. For a stack of Josephson coupled superconducting layers in a perpendicular field Daemen et al.[29] have calculated

J_c along the c-axis to be exponential with field for pinning induced disorder. They consider the lattice to be composed of pancake vortices which when displaced relative to their neighbours in adjacent layers cause a reduction in the local critical current. Applying their theory to the brick-wall model, where the current must transfer between grains along the c-axis, for a tape in a perpendicular field they predict a power law dependence of J_c. Such a dependence is not observed in high fields for the tape studied here, except possibly at the lowest temperatures over a limited range. Since J_c measured by magnetic measurements is also exponential at high fields, it is reasonable to assume that its field and temperature behaviour is determined by intrinsic properties of the BSCCO rather than intergranular coupling effects.

(b) softening of the lattice constants

For the field parallel to the c-axis, Yamafuji et al.[30] show that an exponential field dependence of the form

$$J_C(B,T) = J_{C0} \exp\{-B/f(T)\} \qquad (6.12)$$

is obtained for a layered superconductor if the tilt modulus softens for high values of k, the wavevector of lattice distortions and $C_{44}(k=0)$ is proportional to B. J_{c0} is the zero field critical current density in the absence of thermal fluctuations. For a 3D lattice $C_{44}(0)$ is proportional to B^2 (section 3.3.2) but Yamafuji et al. suggest that a 2D layered structure may produce a $C_{44}(0) \propto B$ dependence, as for a superconducting transformer.

(c) collective pinning and vortex glass theories

Collective pinning and vortex glass theories of the flux line lattice do not directly predict the observed field dependence of J_c - assumptions need to be made about the variation of the pinning potential with B, T and J (see sections 3.7.1a-c, in particular equations 3.14 and 3.19). It cannot be discounted though that a distribution of pinning potentials, by the thermal fluctuations described in these theories, leads to the observed exponential dependence of J_c.

(d) flux creep theories

Assumptions about the B and T dependence of pinning potentials are also made in

models which explain an exponential $J_C(B)$ by a flux creep argument[31,32]. Such models give an exponential behaviour of the form

$$J_C(B,T) = J_{C0}(T) \exp\{-B \ln(E_0/E_C) \ln(J_{C0}/J^*)/f(T)\} \qquad (6.13)$$

where $J_{C0}(T)$ is the critical current density in the absence of thermal fluctuations, E_0 and J^* are a characteristic electric field and current density respectively for the material, E_C is an electric field criterion and the function f(T) includes the temperature variation of the average pinning potential.

(e) the curve $B_d(T)$

Finally, the departure from the exponential law for the BPC orientation in high fields at 40K and above (defined by the curve $B_d(T)$) must be considered. When the field is parallel to the tape surface, $J_C(B)$ is exponential at all temperatures down to the lowest measurable value of J_C. This indicates that when the field component parallel to the c-axis reaches a certain value the critical current is quickly reduced to zero. If there was perfect alignment of the tape this decrease in J_C would be even more sudden. Two possible explanations of the curve $B_d(T)$ are:

1. a decoupling phase transition of the pancakes as predicted by various models of Josephson coupled layers (ref 25 and section 3.7.4) and sometimes referred to as melting. This happens when the mean square thermal displacement of the flux pancakes, $<u^2>$, becomes equivalent to the square of the vortex spacing $a_0^2 \approx (\phi_0/B)$ and there is no longer any correlation between vortices in adjacent layers. At this point J_C parallel to the c-axis becomes zero;
2. alternatively, the change in the field dependence can be attributed to a vortex glass to liquid transition. Changes in the curvature of log{E}-log{J} traces, in fields parallel to the c-axis, for BSCCO-2223 tapes[33] and BSCCO-2223 thin films[34] has been interpreted in terms of the vortex glass theory(section 3.7.2). Such a change in the E-J traces also corresponds to a change in the form of the field dependence of $J_C(B,T)$. Li et al.[29] calculated a glass-liquid transition line $B_g(T)$ which corresponded to a departure of J_C from an exponential to a much stronger field dependence. Their $B_g(T)$ was only measured between 55-75K and below 2T and lies just below the curve

$B_d(T)$ as plotted in figure 6.21. Yamasaki et al.[30] calculated $B_g(T)$ for a BSCCO thin film. Their $B_g(T)$ was much lower than that of Li et al. and than $B_d(T)$ for the tape here but their irreversibility line was also much lower.

ii. scaling of the pinning force and Kramer's analysis

This part discusses the alternative method used to describe the field and temperature dependence of J_c at high fields: via models of the volume pinning force. Fietz-Webb scaling of the pinning force for BSCCO using $B_{irr}(T)$ as the scaling field has been claimed by several authors[35,36]. But the data was over a limited temperature range and the scaling was imperfect, similar to that in figure 6.17 for the BPC orientation. Rose et al.[36] found that the pinning force of bulk BSCCO-2212 fitted the Kramer model[2] above 1T at all temperatures. The data for the BPAB and LFF orientations in figures 6.18b,c only fits the Kramer model above 40K.

The lack of scaling for the HTSC materials is not surprising if J_c is strongly affected by thermal fluctuations[37] which is expected to be the case for most measurements of the reduced pinning force. Even if perfect scaling is observed over a limited field range it is not necessarily correct. Hampshire[38] has shown that if J_c varies exponentially with field and the scaling field is calculated by a critical current criterion or an extrapolation of the $J_c(B)$ curve to zero then scaling following the Kramer dependence is just an artifact of the analysis. The true effective upper critical field is needed to test for scaling of the pinning force. The Kramer plots of figures 6.18a,b,c do not involve any scaling fields. They show that for the BPAB and LFF orientations above 40K the data is consistent with the Kramer model of pinning in high fields. That is, the data suggests that J_c is determined by a depinning mechanism - by a shearing of the flux lattice round a few strong line pins. Below 40K the negative or zero slope of the curves is not consistent with such flux lattice shearing. This is an alternative description to the one offered by the exponential form of $J_c(B,T)$ discussed in part i. For the BPC orientation, $J_c(B,T)$ cannot be described by Kramer's model in any part of the B-T phase diagram.

iii. crossover effects

Using an exponential field description of $J_c(B,T)$, a change in the temperature dependence of the parameters $\alpha_j(T)$ and ß(T) has been observed in other materials. Le Lay et al.[26] found a distinct change in both parameters for the BPC and BPAB orientations of a BSCCO-2223 tape at a temperature of 55-60K. Hampshire and Chan[27] calculated $\alpha_j(T)$ and ß(T) for an YBCO-123 thin film. No clear changes in ß(T) were observed: for a field parallel to the ab-plane ß decreased linearly with T up to T_c. At 50K however, the $\alpha_j(T)$ curve for the field parallel to the ab-planes crosses over the $\alpha_j(T)$ curve for the field parallel to the c-axis. In references 26 and 27 very little or no measurements were taken for the Lorentz force free orientation. It should be noted that for our tape, when the field is parallel to the surface, the parameter $\alpha_j(T)$ is Lorentz force independent below 55K but not above it. In contrast, ß(T) is the same for the BPAB and LFF orientations at all temperatures.

Analysis of $J_c(B,T)$ for BSCCO-2223 in terms of Kramer's model is rare. Rose et al.[36] fitted their data on bulk BSCCO-2212 to the Kramer model at temperatures of 6K and above. No 'crossover' effects were observed.

Metlushko et al.[39] observed a distinct change in the B and T dependence of J_c for a $Tl_2Sr_2Ca_2Cu_3O_x$ (TSCCO-2223) single crystal (B parallel to c-axis). They plotted their data as J_c vs T for fixed fields. Below 40K, J_c was almost field independent but had a strong temperature dependence. Above 40K, J_c had a strong field dependence but its temperature dependence was not as strong. This is different to the crossover effects observed in the BSCCO-2223 tape. At high temperatures it has a stronger temperature and field dependence (though the functional form of the field dependence does not change). From figures 6.7a,b it is clear that J_c is not field independent at less than 55K. The curve $T_\alpha(B)$ is constructed rather qualitatively from the $J_c(B,T)$ data and does not rely on a mathematical description of J_c. It is odd though, that the field dependence of the crossover line $T_\alpha(B)$ is not reflected in the crossover observed using the exponential field description of $J_c(B,T)$. This form defines a field independent crossover temperature in the B-T phase diagram.

The B,T dependence crossover is related in some way to a change in pinning, via a phase change in the FLL or a physical change in the pinning centres. Possible mechanisms to consider are:

(a) a distribution in T_c's

It has already been shown that the tape has an approximately 10K phase material at its grain boundaries. It is reasonable to assume that there will be a distribution of T_c's at higher temperatures as well. Umezawa et al.[11] found traces of the BSCCO 2212 phase with T_c's from 75-105K at the grain boundaries in some BSCCO-2223 tapes. It is possible that 55K phase material exists at the grain boundaries in our tape. As below 10K, discontinuities in J_c would be expected at fields equal to the upper critical field of the 55K phase near the crossover. A wide distribution of T_c's of the intragranular material would not cause such a sharp change in the B,T dependence. Also, a variation in T_c does not explain the Lorentz force dependence of $\alpha_J(T)$.

(b) a change in collective pinning

Metlushko et al.[39] were able to explain the crossover in J_c for their TSCCO-2223 crystal using the 3D collective pinning theory of Feigel'man and Vinokur (section 3.7.1a). They identified 40K as the crossover temperature from small to large flux bundle pinning. It is not clear whether the 3D collective pinning theory can be applied to a highly anisotropic superconductor such as TSCCO-2223. It does not describe the data for the BSCCO-2223 tape (which has a very similar crystal structure to TSCCO-2223). In collective pinning theory for layered superconductors (sections 3.7.1b,c), thermal fluctuations are expected to reduce J_c when the mean squared displacement of a flux line ($<u^2>$) becomes larger than the square of the coherence length (ξ^2). This occurs at a temperature $T_p(B)$. $T_p(B)$ is an increasing function with field and temperature - see figure 3.5. Vinokur et al.[8] have calculated the effect of thermal fluctuations on the shape of the $J_c(T)$ curve at constant B for collective pinning. At the temperature $T_p(B)$, J_c should start to decrease rapidly to zero. The $J_c(T)$ curves of figures 6.7a,b are similar in shape to the $J_c(T)$ curve without thermal fluctuations from Vinokur et al. No evidence for the existence of the line $T_p(B)$ is found for the BSCCO tape measured here, though the sudden drop in J_c at $T_p(B)$ could be disguised by the

imperfect texturing of the grains. Alternatively, the B,T dependence crossover could be attributed to a 2D-3D pinning phase transition (see 3.7.1). This is a change from the pinning of vortex pancakes in isolated 2D layers at low temperatures, to pinning determined by vortex-vortex interactions between adjacent layers. Without knowing how the pinning potentials change with B,T and J in this theory, it is difficult to predict whether a 2D-3D pinning change would produce the B,T crossover changes observed in the tape. For magnetically coupled layers (section 3.7.1b), Koshelev and Kes predict that a 2D-3D pinning change would not change the form of the J_c field dependence.

A vortex glass has similar properties to a collectively pinned FLL. A vortex glass to liquid transition would almost certainly cause a change in the form of the J_c field dependence.

(c) flux creep, lattice softening

A change in pinning would be reflected in a change of the parameters in the lattice-softening theory of Yamafuji et al. (equation 6.12) and the flux creep theory of equation 6.13. A change in ß(T) corresponds to a change in f(T) in both equations. In equation 6.12, f(T) includes the temperature dependence of several pinning parameters (the interaction distance, the Labusch pinning parameter etc.). In equation 6.13, f(T) includes the temperature dependence of the pinning potential. J_{c0} in both equations, corresponding to $\alpha_j(T)$, is related to the pinning potential at zero field in the absence of thermal fluctuations. Such a change in J_{c0} at 55K, as observed for $\alpha_j(T)$, can only be explained by a physical change in the tape's pinning centres. As for collective pinning, these theories are incomplete and it is difficult to explain the crossover in the B,T dependence of J_c for the tape with them.

iv. interpretation

It has been shown that at high fields, $J_c(B,T)$ can be described by either an exponential field function or by Kramer's pinning model. The exponential form provides the best description of the data over all fields and temperatures for all orientations. Therefore, any interpretation of $J_c(B,T)$ for the tape should be made in terms of the exponential functional form.

Following on from the conclusions of section 6.4.2, for $J_c(B,T)$ below 1T, it is expected that above 1T, J_c is determined by the ab-plane connections between grains. Coupling across S-N-S Josephson junction grain boundaries is not expected to play a major role. It is useful at this point to recap on the reasons why this conclusion is drawn: theories that explain J_c by a network of S-N-S Josephson junctions predict a power law field dependence but above 1T an exponential field dependence is observed; there is a strong orientation dependence of J_c which appears to depend mainly on the field component parallel to the c-axis. Such orientation dependence would be unusual if $J_c(B,T)$ was determined by S-N-S coupling, especially as below 10K at low fields, when it is thought that J_c is determined by S-S'-S coupling, the upper critical field of the intergranular material is independent of field orientation; and if other superconducting phases, with T_c's higher than 10K, are present at the grain boundaries and are strongly influencing J_c then more discontinuities in J_c at their upper critical fields would be observed.

It is assumed therefore, that the field, temperature and orientational dependence of $J_c(B,T)$ is due to the intrinsic crystal properties of BSCCO-2223. The parameter $\alpha_J(T)$ can be equated to the zero field J_c in the absence of S-N-S junctions below 1T, i.e. it describes the temperature variation of the zero field J_c of the ab-plane connections. The parameter ß(T) describes the field sensitivity of J_c.

It is suggested that flux lines parallel to the ab-plane are intrinsically pinned. Any reduction in J_c with increasing field is caused by the field component parallel to the c-axis. This means that the exponential field function only describes the field and temperature variation of J_c for a field parallel to the c-axis (but with the current parallel to the ab-planes). The similar functional forms for all three orientations of the parameters $\alpha_J(T)$ and ß(T) support this conclusion. A rough estimate of the tape texture can be obtained from the anisotropy in ß(T) below 55K. If the average misalignment angle is θ then for the BPAB orientation the effective field is $B\cos\theta$ and for the BPC orientation it is $B\sin\theta$. For constant J_c, $B\sin\theta/ß_c = B\cos\theta/ß_{ab}$ which gives $\tan\theta = 0.4$ and a misalignment angle of $\theta = 21^\circ$. This is typical for a tape of this quality. The same angle is obtained by assuming that the fields B_{exp} are determined by the component parallel to the c-axis. This is a reasonable assumption if J_c is not determined solely by

Josephson junctions but also by a few ab-plane connections at fields just below B_{exp} .

It seems unlikely, that a pair breaking mechanism determines $J_c(B,T)$ at these high fields. The model of Daemen at al. (section 6.4.3i(a)) or, for reasons outlined above, S-N-S Josephson coupling between grains is inconsistent with the proposed model where current is transferred via ab-plane connections. The other theories that can be considered to explain the exponential form of $J_c(B,T)$ (collective pinning, flux creep or lattice softening) are incomplete. The proper B,T and J dependence of the pinning potentials need to be theoretically derived or measured. There will be a wide distribution of pinning potentials in BSCCO. It is this distribution in energies that probably leads to the exponential form of $J_c(B,T)$.

The quick departure from the exponential form of J_c for the BPC orientation at fields $B_d(T)$ is most likely caused by a phase transition in the FLL. It is not possible to prove conclusively which predicted phase transition is occurring - again because of the incomplete nature of the theories and also the experimental data. An analysis of the E-J characteristics near $B_d(T)$ may have provided more information.

Whatever mathematical description is used to represent the $J_c(B,T)$ data, it is clear that there is a crossover in the field and temperature dependencies as you go from low to high temperatures in the B-T phase diagram. The curve $T_\alpha(B)$ predicts a field dependence of the crossover temperature whilst the change in the $\alpha_J(T)$ and ß(T) parameters provides a single, field independent, crossover temperature. If the crossover is caused by a change in pinning or a phase transition, a field dependent crossover temperature would be expected. The pinning potential must have some field dependence, as it is modified by vortex-vortex interactions and in the theories of collective pinning, flux creep and lattice softening, the parameter ß(T) would depend on the variation of the average pinning potential. The change in $\alpha_J(T)$, which represents a zero field J_c, at 55K can be equated to T_α at B=0. The parameter ß(T) is calculated from data above the field B_{exp}. From the phase diagram of figure 6.21 it can be deduced that, if there was a field dependent change in ß(T) it would only be observed in the $J_c(B,T)$ data at temperatures below 50K. At these temperatures, J_c vs B has only a

small slope (figures 6.10-6.12). The parameter ß(T) would have to change by a relatively large amount for a change in slope to be detectable. It is possible therefore that the parameter ß could have a field-dependent crossover temperature. The value of ß measured would be an average of two slopes below 50K but only one above 50K - causing the observed crossover at 55K.

Without invoking a phase transition of the FLL, it is difficult to describe the crossover in terms of the flux creep or lattice softening theories. The crossover could be a 2D-3D pinning transition in a collectively pinned layered superconductor, but the theory does not explicitly predict the exponential field dependence of $J_c(B,T)$. The change in the Lorentz force dependence at the crossover suggests that $J_c(B,T)$ is determined by some depinning mechanism. The collective pinning theory is probably the best framework in which to describe J_c in BSCCO-2223. Then: for the BPAB and LFF orientations J_c is reduced to immeasurably small values by thermal depinning and $T_\alpha(B)$ can be raised by better texturing; whilst for the BPC orientation, J_c is reduced at $B_\alpha(T)$ by a phase transition and it is not clear if $T_\alpha(B)$ can be increased by better fabrication.

Summing up, above 1T, a function of the form $J_c(B,T)=\alpha_j(T)\exp\{-B/ß(T)\}$ best describes the field, temperature and orientational dependence of the critical current density for the BSCCO-2223 tape. The parameter $\alpha_j(T)$ is the zero field J_c of the ab-plane connections which couple the grains in high fields. The parameter ß(T) describes the field sensitivity. The variation of J_c is determined by the intrinsic properties of BSCCO. Flux parallel to the ab-planes is pinned intrinsically and causes no reduction in J_c with field. When the field is parallel to the c-axis, J_c reduces exponentially with field. Because the tape is imperfectly textured there is always a field component parallel to the c-axis which determines the variation of $J_c(B,T)$ for all three tape orientations. The average misalignment angle of the grains in the tape has been estimated as 21°.

There is no complete theory which can describe the exponential field decrease of J_c. More information is needed on the B,T and J dependence of the pinning potential. A distribution of pinning potentials also needs to be summed. Collective pinning theory in layered superconductors appears to offer the best framework for describing $J_c(B,T)$.

In the B-T phase diagram of J_c there is a crossover from a weak field and temperature dependence at low temperatures to a stronger field and temperature dependence at high temperatures. This crossover is probably due to a pinning phase transition but more work on the theory is needed to explain completely the observed changes. By comparing the methods for determining the crossover line, it is suggested that ß(T) may have a field dependent change which is not detected in the exponential analysis of the data. This is expected if ß(T) describes changes in the average pinning potential.
For the BPAB and LFF orientations, J_c approaches zero by thermal depinning. For the BPC orientation, J_c is reduced suddenly by a FLL phase transition when the field parallel to the c-axis is large.

6.4.4. The irreversibility line

i. The irreversibility line

The irreversibility line for BSCCO-2223 from transport measurements is commonly shown to vary as $(1-t)^n$ or $(1-t^2)^n$. Hikata et al.[40] measured $B_{irr}(T)$ above 40K for a Pb-doped BSCCO-2223 tape and found it varied as $(1-t)^n$ with $n=3$ for the field perpendicular to the tape surface and $n=2.8$ for the field parallel to the surface. These results are very similar to those in figure 6.18 (where $n=2.75$). Matsushita and co-workers[41,42] have found $B_{irr}(T)$ for a BSCCO-2223 tape to vary as $(1-t^2)^n$ with n taking values between 1.5 and 4.5. Miu[43] has measured the intergranular value of $B_{irr}(T)$ in bulk polycrystalline BSCCO-2223 by comparing the V-I traces of field-cooled and zero field-cooled samples. Contrary to other results Miu found $B_{irr}(T)$ below 100K to decrease exponentially with temperature.

It is well known that the irreversibility line depends to some extent on the type of measurement and criterion employed[44]. The theories put forward to explain this phenomenon (Lindemann melting, thermally activated depinning, fluctuation induced melting - see sections 3.6.2, 3.7.3 and 3.7.4 respectively) have several free parameters or require assumptions on the temperature dependence of the activation energy. It is therefore not possible to support any theory for the irreversibility line with the data in this thesis, especially as the calculated $B_{irr}(T)$ for the three orientations is only an upper

bound (given the finite J_c criterion). It is interesting to note however that $B_{irr}(T)$ for the BPAB and BPC orientations has the same functional form and the ratio between the two orientations is constant throughout the range of measurement. This is true even though the field dependence of J_c just below $B_{irr}(T)$ for the two orientations is markedly different indicating different depinning mechanisms.

Finally a rough estimate of the field range over which a BSCCO-2223 tape may be useful can be calculated from equations 6.10 and 6.11. If the temperature dependence of $B_{irr}(T)$ does not change below 55K (which is by no means certain considering the crossover in ß(T) at this temperature, but can be assumed so for a lower bound value) then at 4.2K with the field parallel to the surface the tape can carry a critical current in fields up to 120T. Acceptable levels of J_c for applications would probably be available for fields up to half this value.

Summarizing this section, the irreversibility line has the same functional form for all three orientations even though close to it, there is a marked difference in the field dependence of J_c when the field is perpendicular or parallel to the tape surface. It is estimated that at 4.2K the tape should be able to sustain a J_c high enough for applications in fields up to at least 60T.

6.5. Summary of main conclusions

The B-T phase diagram of the BSCCO-2223 tape is complicated and $J_c(B,T)$ depends on the texture, connectivity, intrinsic and extrinsic pinning and possible phase changes in the flux line lattice throughout the superconducting phase. The main characteristics are:

i. (a) it is suggested that the intergranular regions in the tape contain a low T_c superconducting BSCCO phase. This phase has an estimated T_c of 10.8K and an upper critical field at 4.2K of 1.5T; it is most probably the 2201 or 2011 phase of BSCCO. The anomaly marks the change from a J_c determined by intergranular coupling via S-S'-S junctions at low fields to a J_c determined by

intrinsic BSCCO properties at high fields;

(b) the experimental evidence in support of this conclusion is a discontinuity in J_c for all three orientations at a field $B_j(T)$. The field $B_j(T)$ is independent of orientation but has a temperature dependence. No discontinuities in J_c are observed above 10K;

ii. (a) in fields less than 1T above 10K, $J_c(B,T)$ is mainly determined by a network of S-N-S Josephson junction links between grains which are gradually weakened as the field is increased. Some grains however are connected by a different mechanism;

(b) the evidence for this conclusion is the rapid decrease of J_c in low fields, obeying a power law dependence. In addition the existence of S-N-S junctions at the grain boundaries is to be expected above 10K where the intergranular, low T_c BSCCO phase material is normal. The existence of other types of intergrain connections is suggested by the orientation dependence of J_c in these low fields;

iii. in fields above 1T, $J_c(B,T)$ could be described by an exponential field function or alternatively, by Kramer's pinning model. The exponential function, $J_c(B,T)=\alpha_j(T)\exp\{-B/\beta(T)\}$ best describes J_c for all orientations, temperatures and fields above 1T;

iv. (a) above 1T, J_c is not determined by S-N-S Josephson coupling between grains, but by intergrain connections such that the current can transfer between grains without leaving the crystal ab-planes (called ab-plane connections). It is these connections that are responsible for the orientation dependence in low fields mentioned in part ii above. $J_c(B,T)$ is then determined by the intrinsic properties of BSCCO-2223. It is suggested that flux parallel to the ab-planes is pinned intrinsically and hence any reduction in J_c with increasing field is due to the field component parallel to c-axis. The parameter $\alpha_j(T)$ is the zero field J_c if the grains were connected only by the ab-plane connections;

(b) the experimental evidence for this argument is as follows: the Lorentz force independence of J_c at low temperatures and similar functional form of the

parameter ß(T) for all three orientations is consistent with the model of intrinsic pinning of flux by the ab-planes. In addition, above 1T, the field dependence does not follow a power law, which is expected for a network of Josephson junctions. Considering these results and other data in the literature from BSCCO-2223 films (with no observed grain boundaries) it is reasonable to assume that at high fields, $J_c(B,T)$ is being determined by the intrinsic properties of BSCCO;

v. (a) there is a low to high temperature crossover in the field and temperature dependence of J_c which, it is suggested, indicates a change in the type of pinning. A crossover was observed for each form of analysis used to interpret the data: there was a marked change in the temperature dependence of the parameters $\alpha_i(T)$ and ß(T); above, but not below 40K, for the field parallel to the tape surface the data fitted the Kramer model for flux shear; and a field dependent crossover line, $T_\alpha(B)$, was defined by investigating the temperature dependence of J_c in fixed magnetic fields. It is proposed that ß(T) has a field dependent crossover temperature which is not detected in the exponential description;
(b) the observed change in the Lorentz force dependence of J_c at the crossover supports the conclusion that it defines a change in pinning;

vi. (a) it is tentatively suggested that in a field parallel to the c-axis, the irreversibility line is due to phase transition in the flux line lattice. In a field parallel to the ab-planes it is due to thermal depinning. More information is needed on the variation of the pinning potential before the irreversibility line can be fitted to any flux melting or depinning theories;
(b) this conclusion is suggested by the following: when the field is perpendicular to the tape surface, at a field $B_d(T)$ just below the irreversibility line, J_c starts to decrease more rapidly with field than an exponential. However, when the field is parallel to the tape surface, J_c continues to decrease exponentially with field down to unmeasurably small values;

vii. Unfortunately, no theory is complete enough to fully explain $J_c(B,T)$. More knowledge of the distribution in the pinning potential and its B,T and J dependence is required. Because of the complex structure of the B-T phase diagram, collective pinning theory in layered superconductors offers the best framework for describing $J_c(B,T)$ in BSCCO-2223. In the context of this theory, the parameter ß(T) describes the temperature variation of the average pinning potential;

These results demonstrate the importance of fabricating tapes with improved texture and connectivity for better J_c values at all temperatures. Figure 6.21 shows the complicated B-T phase diagram for the tape. The surface plots of figures 6.22a,b clearly demonstrate the depression of J_c at high temperatures at the line $T_\alpha(B)$. To increase the temperature range over which useful values of J_c can be obtained, $T_\alpha(B)$ and not $B_{irr}(T)$ needs to be raised. Better texturing will increase $T_\alpha(B)$ for the BPAB and LFF orientations. It is not clear if it would be possible however, to raise $T_\alpha(B)$ for the BPC orientation.

The very high values of J_c below 10K, when the intergranular material is superconducting, illustrates how better connectivity can dramatically increase the critical current density in these tapes. Better connectivity through a higher proportion of grains connected via 'ab-plane' connections will raise $\alpha_j(T)$. The parameter ß(T) can be raised by introducing stronger pinning centres as is found from measurements on irradiated samples[25]. At 4.2K it is estimated that the tape could produce useful values of J_c up to 60T, showing great potential for high field applications if J_c can be raised sufficiently in long lengths of tape.

To decide which models of the flux line lattice best describe $J_c(B,T)$ in BSCCO, more experimental measurements of the activation energies and elastic constants are needed. Extensive measurements of $J_c(B,T)$ made over a wide range of B and T on crystals or thin films will help to explain the role of texture. For the BSCCO tapes, a correlation of $J_c(B,T)$ variations to changes in the microstructure, particularly at the grain boundaries, would be very useful.

References for Chapter 6

1. Beales T.P., Appl. Phys. Comm. 12(2), 205 (1993).

2. Kramer E.J., J. Appl. Phys. 44(3), 1360 (1973).

3. Gurevich A., Pashitski A.E., Edelman H.S. and Larbalestier D.C., Appl. Phys. Lett. 62(14), 1688 (1993).

4. Maeda T. and Hataya K., presented at the 1994 International Workshop on Superconductivity, Kyoto, June 1994.

5. Clem J.R., Phys. Rev. B 43(10), 7837 (1991).

6. Feigel'man M.V., Geshkenbein V.B. and Larkin A.I., Physica C 167, 177 (1990).

7. Koshelev A.E. and Kes P.H., Phys. Rev. B 48(9), 6539 (1993).

8. Vinokur V.M., Kes P.H. and Koshelev A.E., Physica C 168, 29 (1990).

9. Cubitt R., Forgan E.M., Yang G., Lee S.L., Paul D. McK., Mook H.A., Yethiraj M., Kes P.H., Li T.W., Menovsky A.A., Tarnawski Z. and Mortenson K., Nature 365, 407 (1993).

10. Sato K., Hikata T. and Iwasa Y., Physica C 185-189, 2341 (1991).

11. Umezawa A., Feng Y., Edelman H.S., High Y.E., Larbalestier D.C., Sung Y.S. and Hellstrom E.E., Physica C 198, 261 (1992).

12. Hensel B., Grivel J.-C., Jeremie A., Perin A., Pollini A. and Flükiger, Physica C 205, 329 (1993).

13. Yamasaki H., Endo K., Kosada S., Umeda M., Misawa S., Yoshida S. and Kajimura K., IEEE Trans. Appl. Supercond. 3(1), 1536 (1993).

14. Matsushita T., Otabe E.S., Ni B., Hikata T. and Sato K., Cryogenics 31, 949 (1991).

15. Maeda T. and Hataya K., presented to The 1994 International Workshop on Superconductivity, Kyoto, Japan.

16. Ekin J.W., Larson T.M., Hermann A.M., Sheng Z.Z., Togano K. and Kumakura H., Physica C (1989).

17. Peterson R.L. and Ekin J.W., Physica C 157, 325 (1989).

18. Nakamura N., Gu G.D., Murakami M. and Koshizuka N., submitted to *The 1994 International Workshop on Superconductivity*, Kyoto, Japan.

19. Kim Y.B., Phys. Rev. 129, 528 (1963).

20. Senoussi S., submitted to J. de Phys. III, (1992).

21. Clem J.R., Bumble B., Raider S.I., Gallagher W.J. and Shih Y.C., Phys. Rev. B 35(13), 6637 (1987).

22. Takahashi C., Komatsu M., Yaegashi Y., Nagano M. and Takahashi H., IEEE Trans. Appl. Supercond. 3(1), 957 (1993).

23. Sato K., Hikata T., Mukai H., Ueyama M., Shibuta N., Kato T., Masuda T., Nagata M., Iwata K. and Mitsui T., IEEE Trans. Mag. 27(2), 1231 (1991).

24. Fuchs G., Gladun A., Fischer K., Staiger T., Reissner M., Hadaier G. and Steiner W., *Applied Superconductivity* - Proc. EUCAS 1993, ed. Freyhardt H.C. (DGM, Germany 1993), p.827.

25. Kummeth P., Struller C., Neumüller H.-W., Ries G., Kraus M., Wirth G., Wiesner J., Eibl O. and Saemann-Ischenko G., *Applied Superconductivity* - Proc. EUCAS 1993, ed. Freyhardt H.C. (DGM, Germany 1993), p.685.

26. Le Lay L., Friend C.M., Maruyama T., Osamura K. and Hampshire D.P., Accepted by J. Phys. C., July 1994.

27. Hampshire D.P. and Chan S.-W., J. Appl. Phys. 72(9), 4220 (1992).

28. Schmitt P., Kummeth P., Schultz L. and Saemann-Ischenko G., Phys. Rev. Lett. 67(2), 267 (1991).

29. Daemen L.L., Bulaevskii L.N., Maley M.P. and Coulter J.Y., Phys. Rev. B 47(17), 11291 (1993).

30. Yamafuji K., Fujiyoshi T., Toko K., Matsuno T., Kobayashi T., Shimoyama J. and Kishio K., preprint 1994.

31. Zeldov E., Amer N.M., Koren G., Gupta A., McElfresh M.W. and Gambino R.J., Appl. Phys. Lett. 56(7), 680 (1990).

32. Gladun A., Fuchs G., Fischer K., Busch D., Eujen R. and Huedepohl J., IEEE Trans. Appl. Supercond. 3(1), 1390 (1993).

33. Li Q., Wiesmann H.J., Suenaga M., Motowidlow L. and Haldar P., submitted to Phys. Rev. B. (rapid comm.) 1994.

34. Yamasaki H., Endo K., Kosaka S., Umeda M., Yoshida S. and Kajimura K., presented at the 1994 International Workshop on Superconductivity, Kyoto, Japan 1994.

35. Kottman P., Jones H., Plecháeek V. and Polák M., Cryogenics 32(11), 1005 (1992).

36. Rose R.A., Ota S.B., de Groot P.A.J. and Jayaram B., Physica C 170, 51 (1990).

37. Niel L., Cryogenics 32(11), 975 (1992).

38. Hampshire D.P., *Applied Superconductivity* - Proc. EUCAS 1993, ed. Freyhardt H.C. (DGM-Germany 1993).

39. Metlushko V.V., Güntherodt G., Moshchalkov V.V., Bruynseraede Y., Thomas H. and Winzer K., *Applied Superconductivity* - Proc.EUCAS 1993, ed. Freyhardt H.C. (DGM, Germany 1993), p.853.

40. Hikata T., Sato K. and Iwasa Y., Jap. J. Appl. Phys. 30(7B), L1271 (1991).

41. Matsushita T., Otabe E.S., Kiuchi M., Ni B., Hikata T. and Sato K., Physica C 201, 151 (1992).

42. Matsushita T., Otabe E.S. and Ni B., Supercond. Sci. Technol. 5, S73 (1992).

43. Miu L., Phys. Rev. B 46(2), 1172 (1992).

44. Brandt E.H., Intl. J. Mod. Phys. B 5(5), 751 (1991).

7. The Critical Current Density of Monocore and Multifilamentary $Bi_2Sr_2Ca_1Cu_2O_x$ Wires in High Magnetic Fields

It was with $Bi_2Sr_2Ca_1Cu_2O_x$ (BSCCO-2212) wires that Heine et al.[1] first demonstrated that the Bi-based cuprates were the most promising HTSC materials for high field applications. Although the 2223 phase of BSCCO has the high intrinsic values of J_c, wires made with it do not have high J_c values. The 2212 phase can be made via a partial melting which leads to some alignment of the grains at the Ag-BSCCO boundary (although the wire core is untextured) and decreases the number of weak links, greatly increasing J_c. It is difficult to form the 2223 phase in this way: mechanical alignment, as in silver sheathed tapes, is needed to obtain high values of J_c. For magnet applications however, a wire is the preferred form of the superconductor for mechanical strength and ease of winding into compact coils. Further work is therefore warranted to see if the J_c values of BSCCO-2212 wires can improve enough for them to be used in the world of real applications. In addition, a comparison of $J_c(B,T)$ with that for BSCCO-2223 and the effect of increasing the number of filaments can give insight into the problems of granularity and anisotropy as already discussed in the previous chapter.

The next section describes the three wires, supplied by J.Tenbrink of Vacuumschmelze GmbH, which were measured. Section 7.2 gives brief experimental details and presents the $J_c(B,T)$ data. This data is analyzed in section 7.3 in terms of a pinning force model and an exponential field description. The variation of $J_c(B,T)$ with the number of filaments and field orientation is also investigated. Section 7.4 discusses and interprets this analysis and the chapter finishes with the main conclusions in section 7.5.

7.1. The $Bi_2Sr_2Ca_1Cu_2O_x$ wires

The BSCCO-2212 multifilamentary wires were made by the standard powder-in-tube method. For details on the fabrication see Tenbrink and Krauth[2]. Pure silver tubes were drawn down to about 1mm diameter for monocore wires. For multifilamentary wires they were drawn down to 2-4mm, bundled into a larger tube and drawn again

down to 1mm. The wires were then annealed during which there was partial melting of the powder.

Short straight sections (10mm length) of three different wires were measured: one monocore; one with 19 filaments and one with 37 filaments. Figures 7.1-7.3 are optical micrographs of the cross-sections of these three samples respectively. Note the uniformity of the wires which also had a relatively high mechanical strength. Table 7.1 lists the wire diameter, fraction of the area that is BSCCO material and the critical current at 4.2K in a field of 10 Tesla for each wire.

Type of wire	Wire Diameter (mm)	Fraction of superconducting area	I_c(4.2K,10T) B∥I/B⊥I (A)
Monocore	1.04	59%	25.3/18.7
19 Filament	1.04	34%	46.0/21.8
37 Filament	1.04	34%	47.0/33.2

Table 7.1: Sample dimensions and critical currents of the BSCCO-2212 wires. I_c at 4.2K was measured with a 1.5μVcm^{-1} criterion in a magnetic field of 10T parallel and perpendicular to the wire axis.

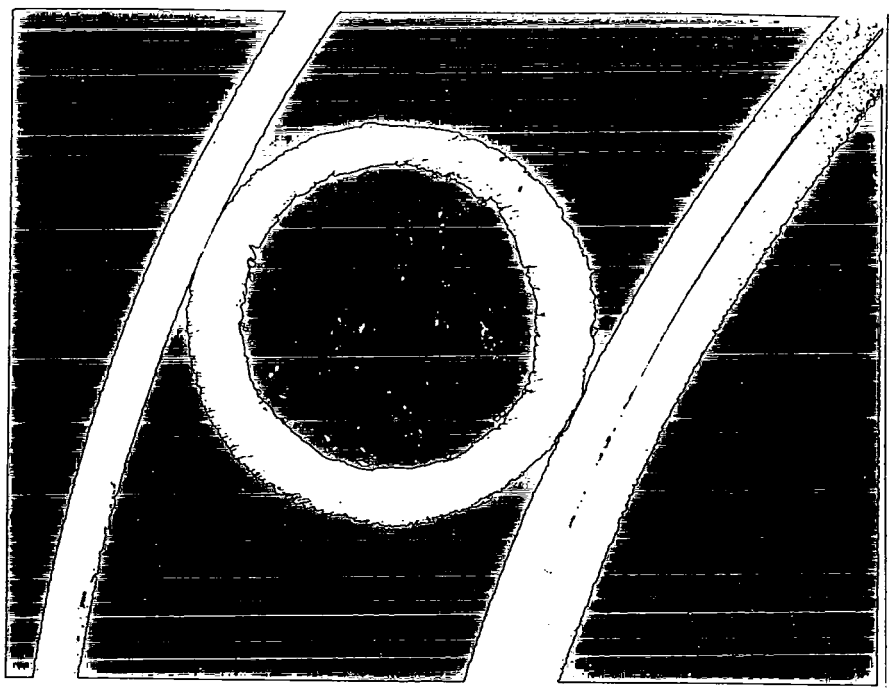

Figure 7.1: An optical micrograph of the cross-section of the monocore BSCCO-2212 wire. The wire has an outer diameter of 1.04 mm.

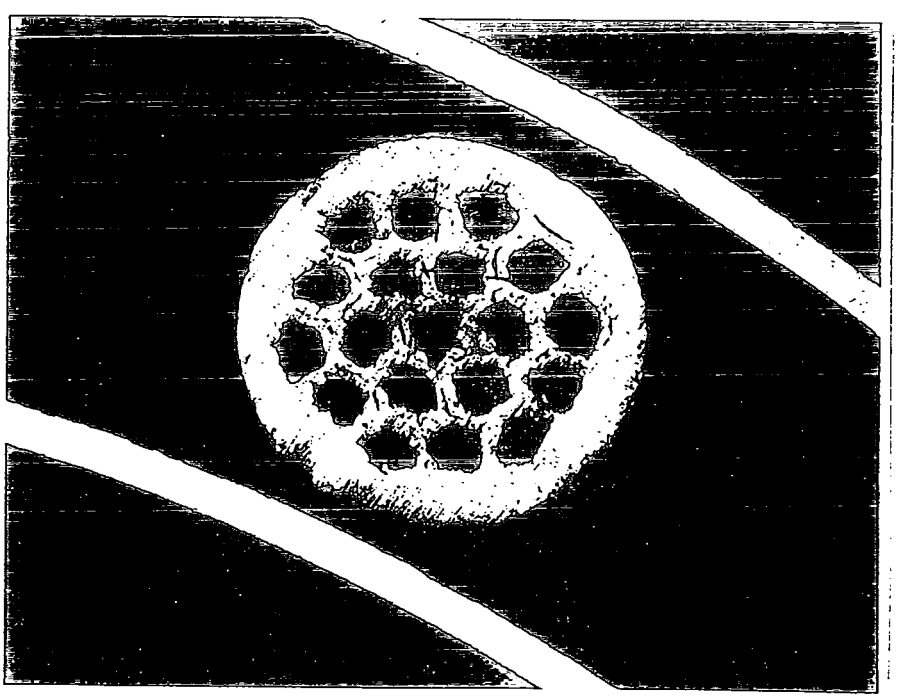

Figure 7.2: An optical micrograph of the cross-section of the 19 filament BSCCO-2212 wire. The wire has an outer diameter of 1.04 mm.

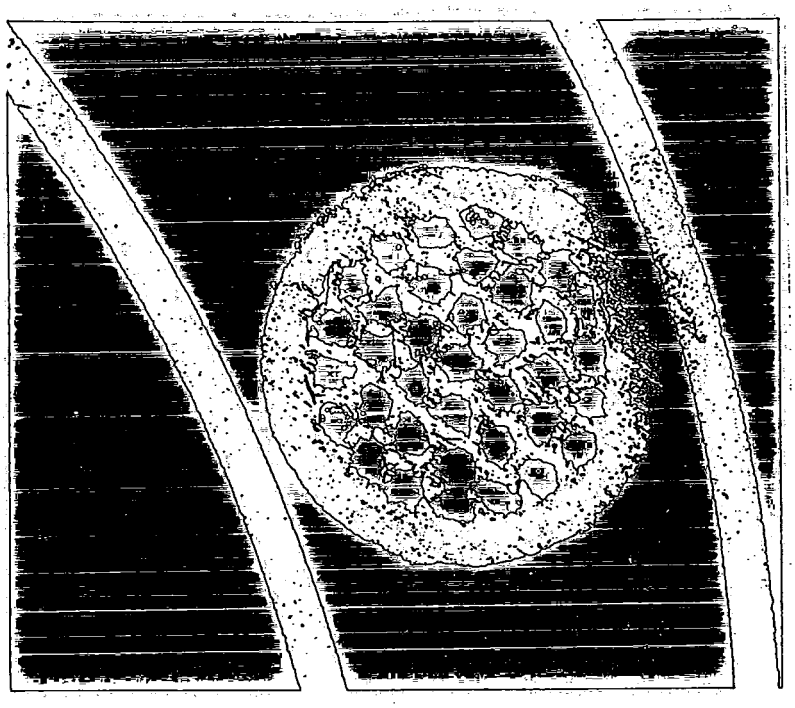

Figure 7.3: An optical micrograph of the cross-section of the 37 filament BSCCO-2212 wire. The wire has an outer diameter of 1.04 mm.

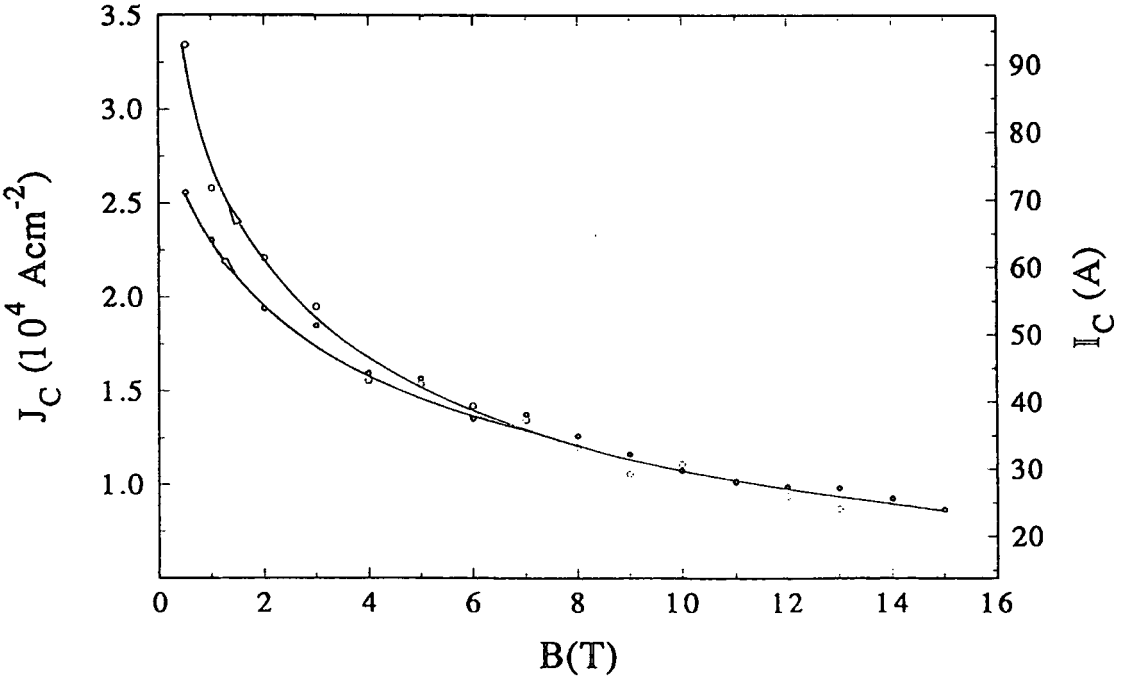

Figure 7.4: J_c for the 19 filament BSCCO-2212 wire at 4.2K in an increasing (closed circles) and decreasing field (open circles).

7.2. Experimental details

7.2.1. Experimental techniques

The wire samples were mounted in the $J_c(B,T)$ probe in a similar way as for the $Bi_2Sr_2Ca_2Cu_3O_x$ tape, described in section 4.1.2d. The voltage taps were soldered from 1.5 - 2.5 mm apart using Indium solder (the temperature of the soldering iron was kept below 100°C). After each change of orientation the critical current of the wire was measured in liquid nitrogen but no variation was found for any of the samples. The $J_c(B,T)$ measurements were taken at temperatures of 4.2K, 20K, 40K, 60K and 80K for each wire for two orientations of the magnetic field. For the *parallel orientation* the field was parallel to the wire axis and hence also to the macroscopic transport current. Similarly for the *perpendicular orientation* the field was perpendicular to the axis of the wire. A 1.5 $\mu V.cm^{-1}$ criterion was used to calculate J_c from the E-J characteristics.

7.2.2. $J_c(B,T)$ for the three wires from 4.2K - 80K

In figure 7.4, J_c for the 19 filament wire at 4.2K is plotted for an increasing and decreasing field. J_c is hysteretic below 4 T but not above. Figure 7.5 presents $J_c(B,T)$ for the monocore wire in (a), the perpendicular orientation and (b), the parallel orientation. Similarly figures 7.6a,b and 7.7a,b show the $J_c(B,T)$ data of the 19 and 37 filament wires respectively for the two orientations. A brief look reveals that, except at low fields and at 40K for the 37 filament wire, J_c decreases exponentially with field for all temperatures and orientations.

7.3. Analysis of the data

7.3.1. A description of $J_c(B,T)$ in terms of the pinning force

The bulk volume pinning force, $F_p=J_c \times B$ is plotted for the three wires in figures 7.8a,b,c. The pinning force characteristics are similar for each wire. F_p is higher for the parallel orientation at all temperatures than the perpendicular orientation and

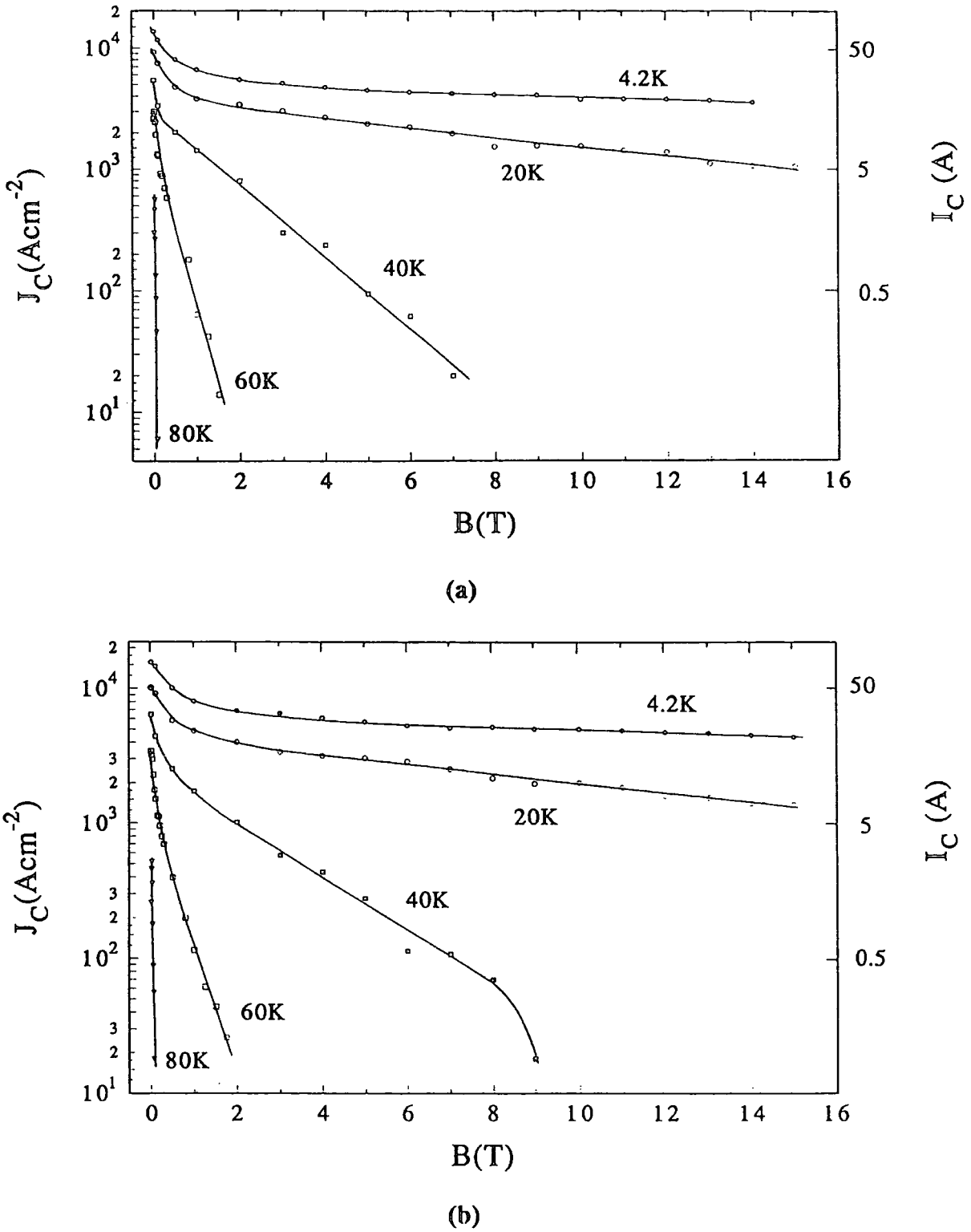

Figure 7.5: $J_c(B,T)$ of a monocore BSCCO-2212 wire with (a), the field perpendicular to the wire axis and (b), the field parallel to the wire axis. Each curve is at a constant temperature as indicated in Kelvin.

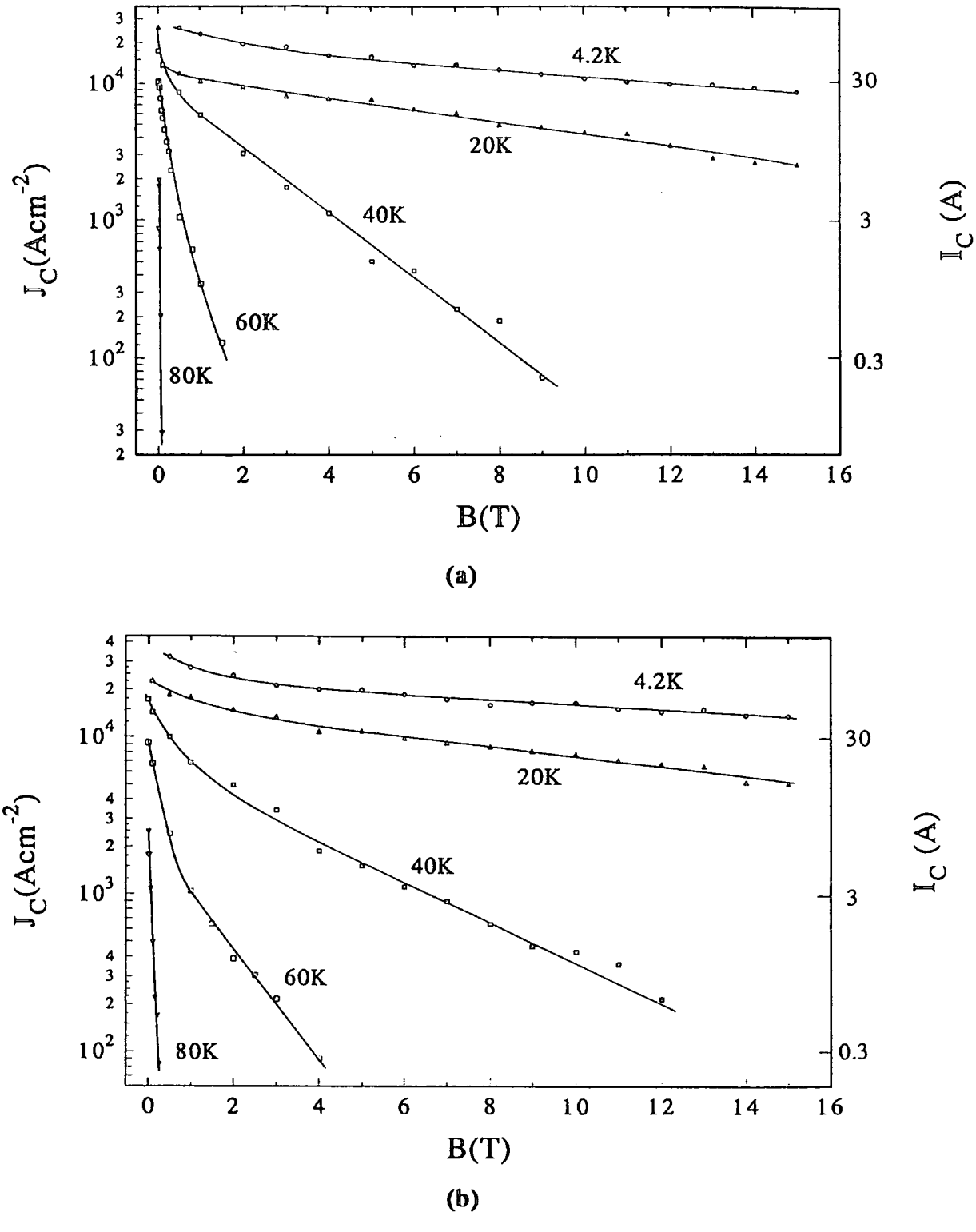

Figure 7.6: $J_c(B,T)$ of a 19 filament BSCCO-2212 wire with (a), the field perpendicular to the wire axis and (b), the field parallel to the wire axis. Each curve is at a constant temperature as indicated in Kelvin.

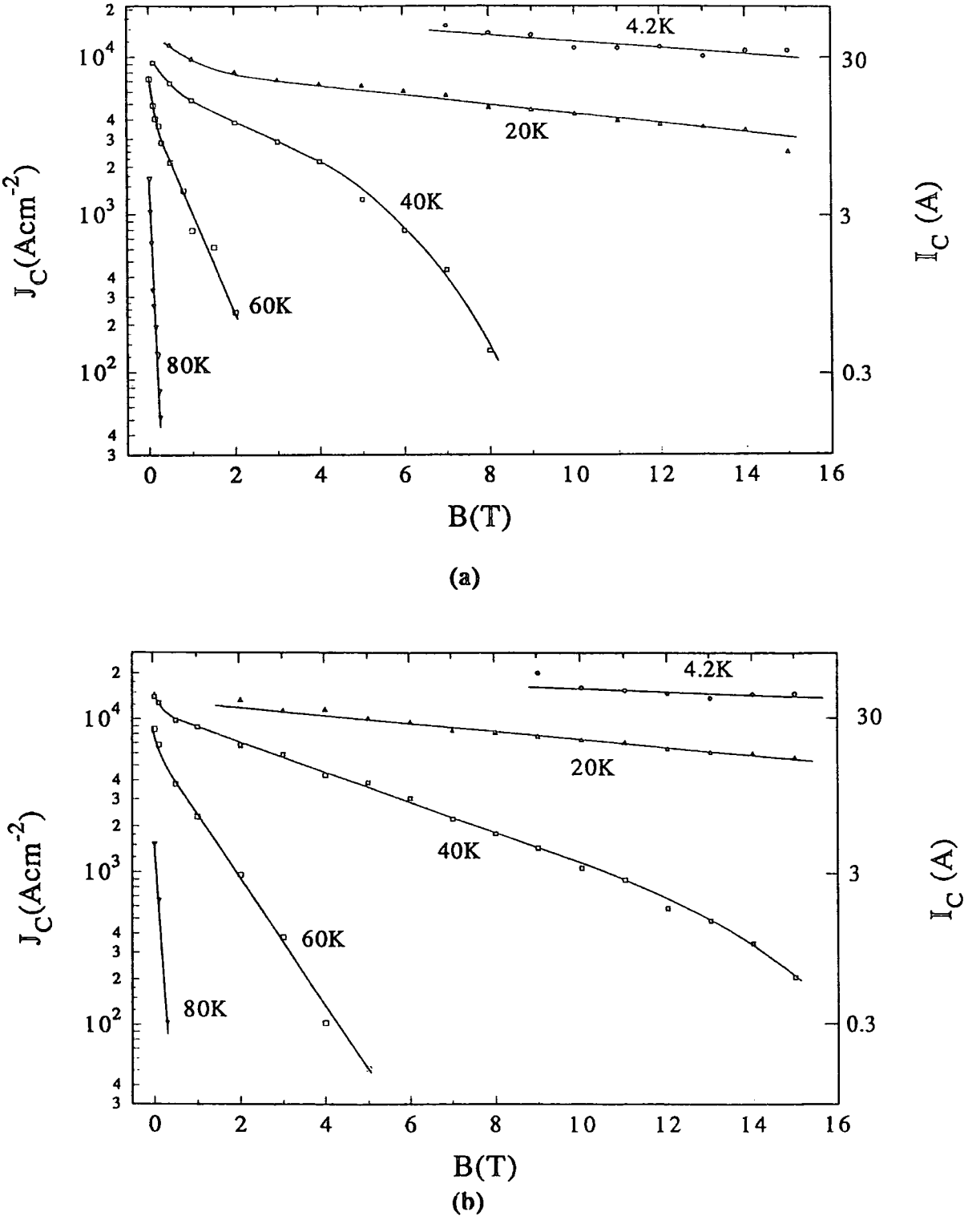

Figure 7.7: $J_c(B,T)$ of a 37 filament BSCCO-2212 wire with (a), the field perpendicular to the wire axis and (b), the field parallel to the wire axis. Each curve is at a constant temperature as indicated in Kelvin.

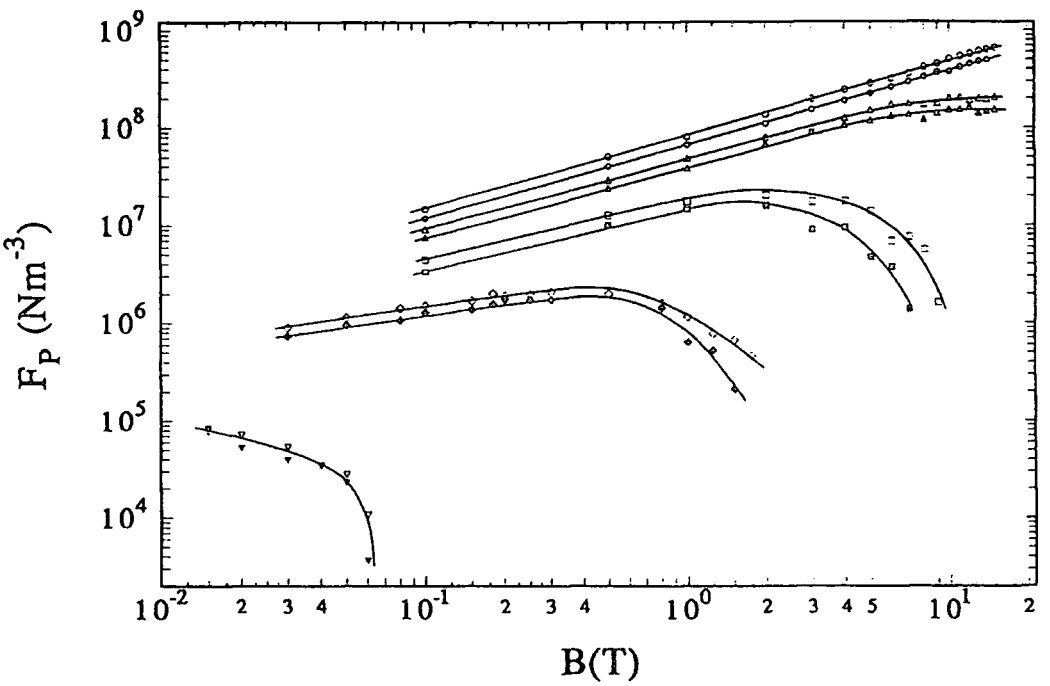

(a)

Figure 7.8: The bulk volume pinning force for (a) the monocore wire, (b) (next page) the 19 filament wire and on the next page, (c) (next page) the 37 filament wire. The open symbols refer to the parallel orientation and the corresponding closed symbols to the perpendicular orientation at the temperatures: ○, 4.2K; △, 20K; □, 40K; ◇, 60K; and ▽, 80K.

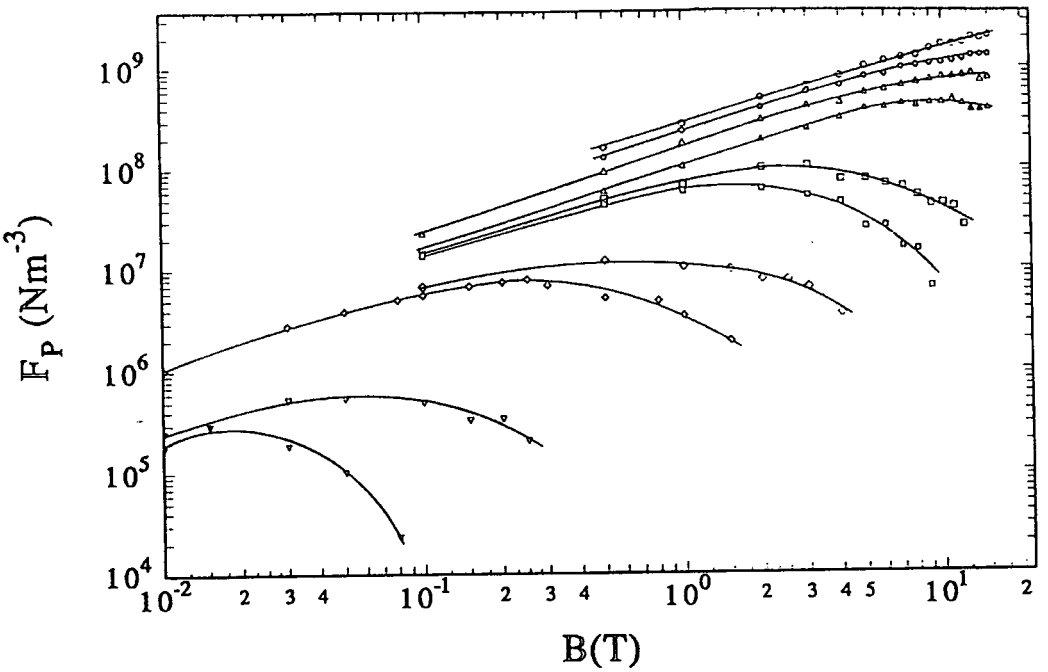

(b)

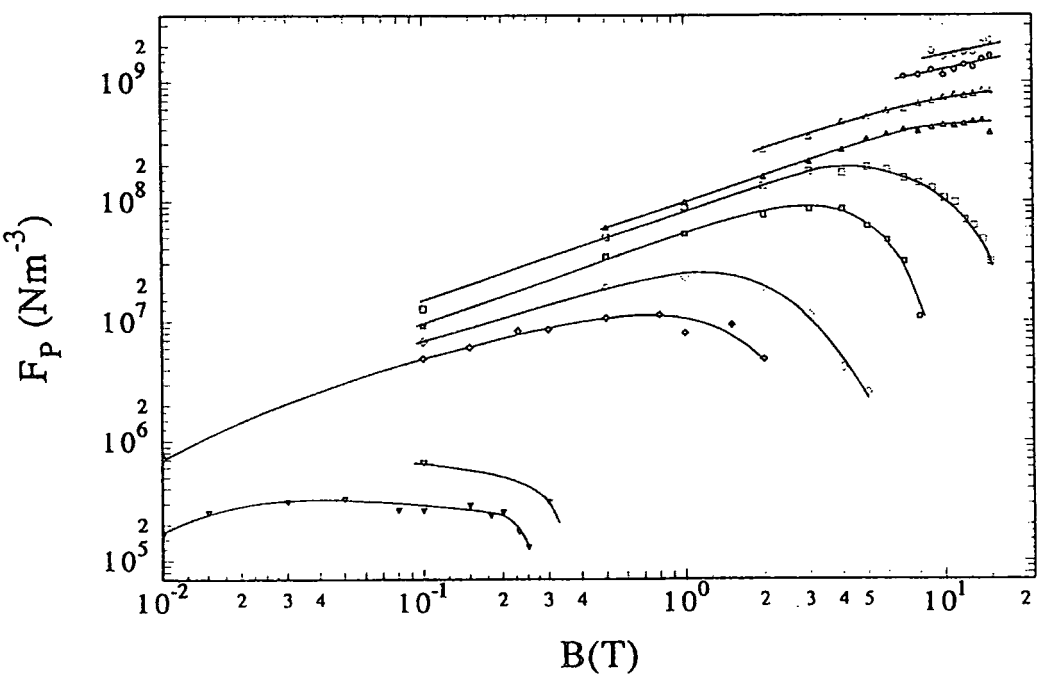

(c)

Figure 7.8: see the previous page for a description.

increases with the number of filaments. The peak in F_P shifts to lower fields very quickly with increasing temperature above 20K though it is at a higher field for the parallel orientation. At 4.2K, F_P for both orientations of the monocore wire and for the parallel orientation of the 19 filament wire is well represented by the relation

$$F_P \propto B^{3/4} \tag{7.1}$$

This relation also holds at fields less than 4T for both orientations of the monocore wire at 20K and the perpendicular orientation of the 19 filament wire at 4.2K. The limited set of data at 4.2K for the 37 filament wire precludes any fitting to such a power law.

The $J_C(B,T)$ data has also been fitted to the Kramer model[3] for each wire in figures 7.9a,b,c. For flux motion by shearing of the flux line lattice Kramer predicted that $J_C^{1/2}B^{1/4}$ should vary linearly with B with a negative slope. The Kramer plots of figures 7.9a,b,c form straight lines at high fields for all temperatures, orientations and wires. At 4.2K and 20K however, the lines have unphysical slopes for each wire. It is concluded that the data fits the Kramer dependence, at fields higher than that corresponding to the peak in F_P, for all three wires above 20K.

7.3.2. An exponential field description of $J_C(B,T)$

As an alternative to the pinning force description, $J_C(B,T)$ can be described by an exponential field function, as for the BSCCO-2223 tape in chapter 6. From figures 7.5-7.7 it can be seen that field dependence of J_C is similar for each wire at all temperatures and orientations: at low fields (<1T), $J_C(B,T)$ decreases quickly then the rate of decrease slows and the field dependence becomes exponential. An exception to this behaviour is at 40K for the 37 filament where J_C decreases more rapidly than the exponential function above 4T and 10T for the perpendicular/parallel orientations respectively. The $J_C(B,T)$ data above 1T has been fitted to the function:

$$J_C(B,T) = \alpha_J(T)\exp\{-B/\beta(T)\} \tag{7.2}$$

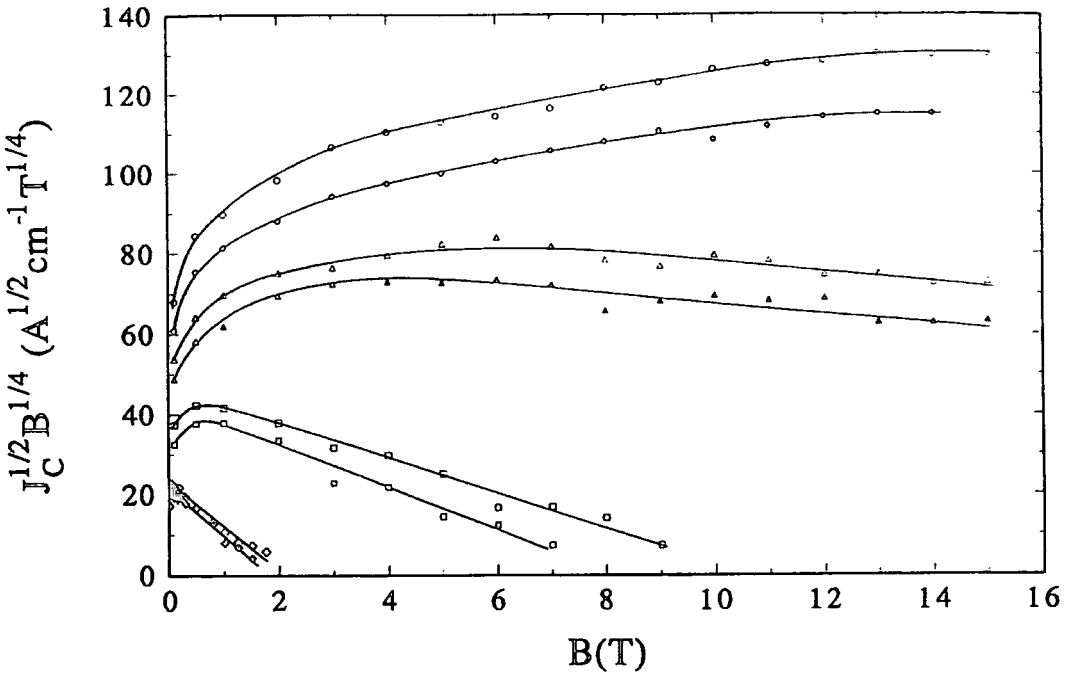

(a)

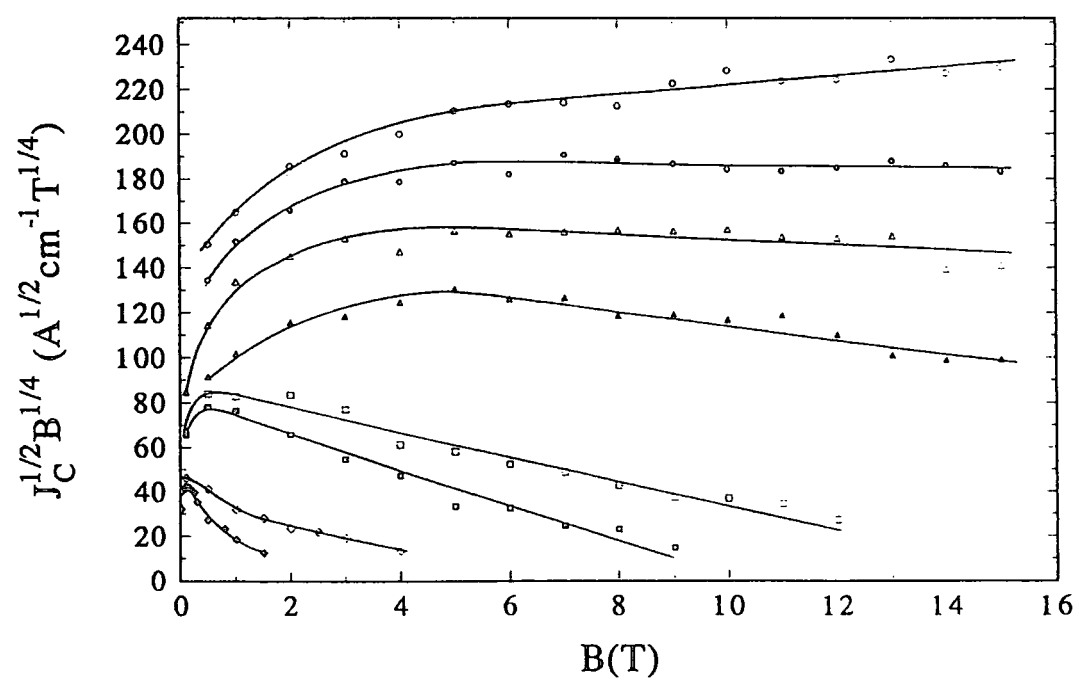

(b)

Figure 7.9: A Kramer plot for (a) the monocore wire, (b) the 19 filament wire and (c) (next page) the 37 filament wire. The open symbols refer to the parallel orientation and the corresponding closed symbols to the perpendicular orientation at the temperatures: ○, 4.2K; △, 20K; □, 40K; and ◇, 60K.

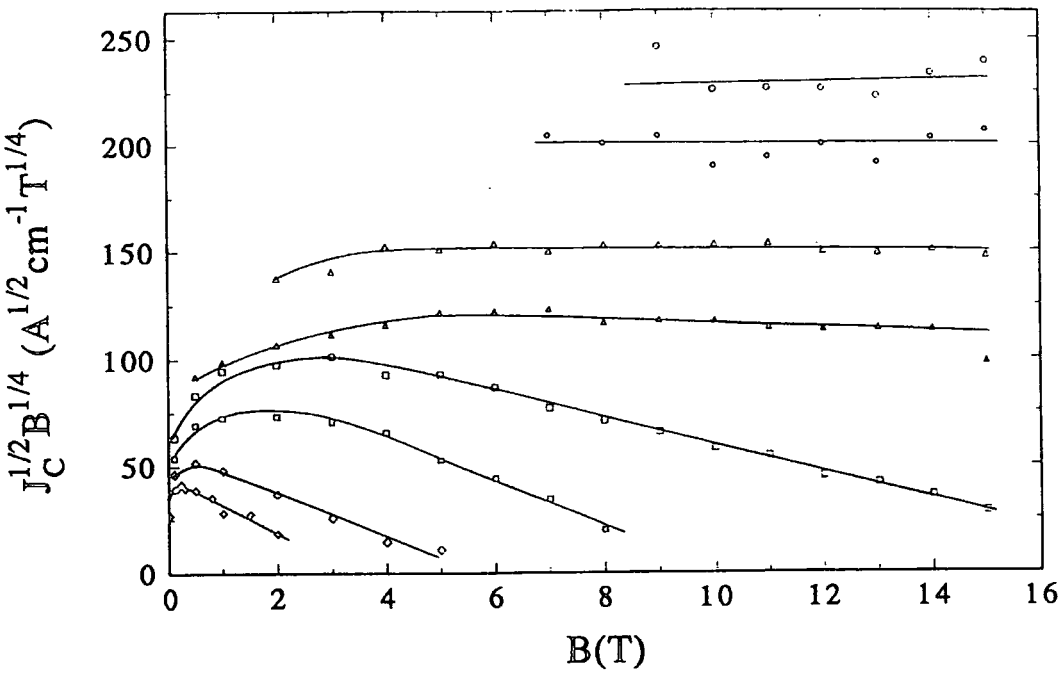

Figure 7.9(c): for description see previous page.

The parameters α_j(T) and ß(T) are plotted in figures 7.10 and 7.11 for each wire and field orientation. Also plotted in these figures are α_j(T) and ß(T) for the BPAB and BPC orientations of the BSCCO-2223 tape of chapter 6. Because of the small number of data points it is not possible to draw smooth curves for each wire but the following trends can be observed:

i. α_j(T) for the monocore wire is clearly smaller than for the multifilamentary wires. In general the parallel orientation has a higher α_j(T) at each temperature than the perpendicular orientation. α_j(T) for the BSCCO-2223 tape has a different temperature dependence to the wires (BPAB and BPC orientations). Its value is close to that for the wires at the lowest and highest temperatures but is considerably higher in the range 30-60K.

ii. above 20K all the wires have a similar ß(T) but at and below this temperature the curves are markedly different from each other. For a particular orientation the 37 filament wire has a higher ß(T) than the 19 filament wire whilst at 4.2K the monocore wire has the highest ß(T) for both orientations. ß(T) for the BPAB and BPC

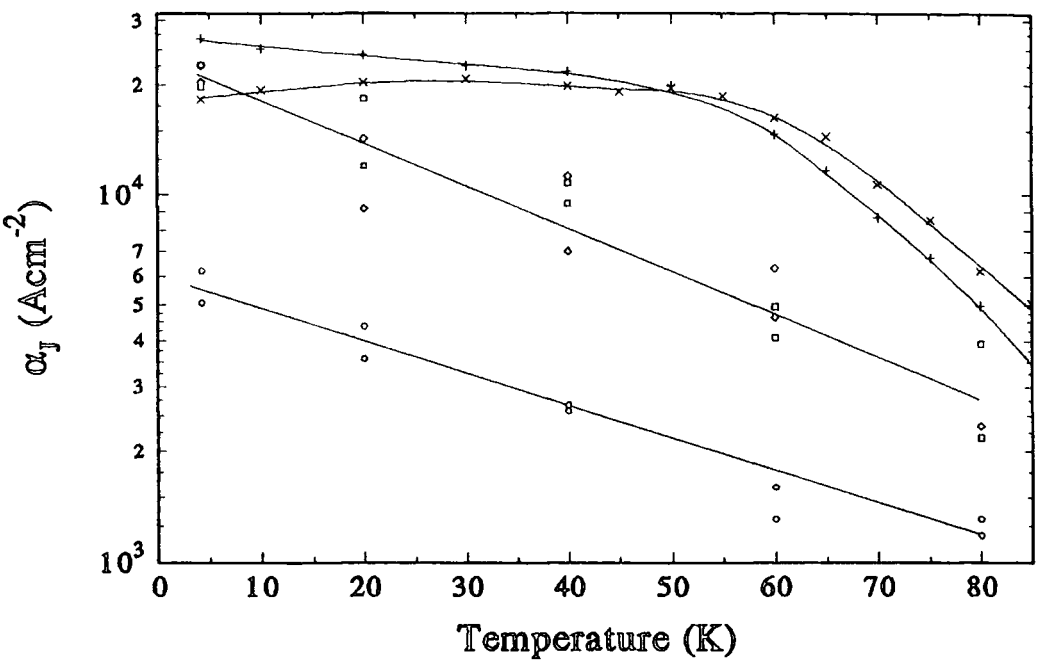

Figure 7.10: The parameter $\alpha_j(T)$ for the: ⊜,○ monocore; ⊟,□ 19 filament; ◊,◇ 37 filament wire. Closed symbols signify a perpendicular field, open symbols signify a parallel field. Also included is $\alpha_j(T)$ for the BSCCO-2223 tape of chapter 6: +, BPAB orientation and ×, BPC orientation. The lines are drawn as a guide to the eye only.

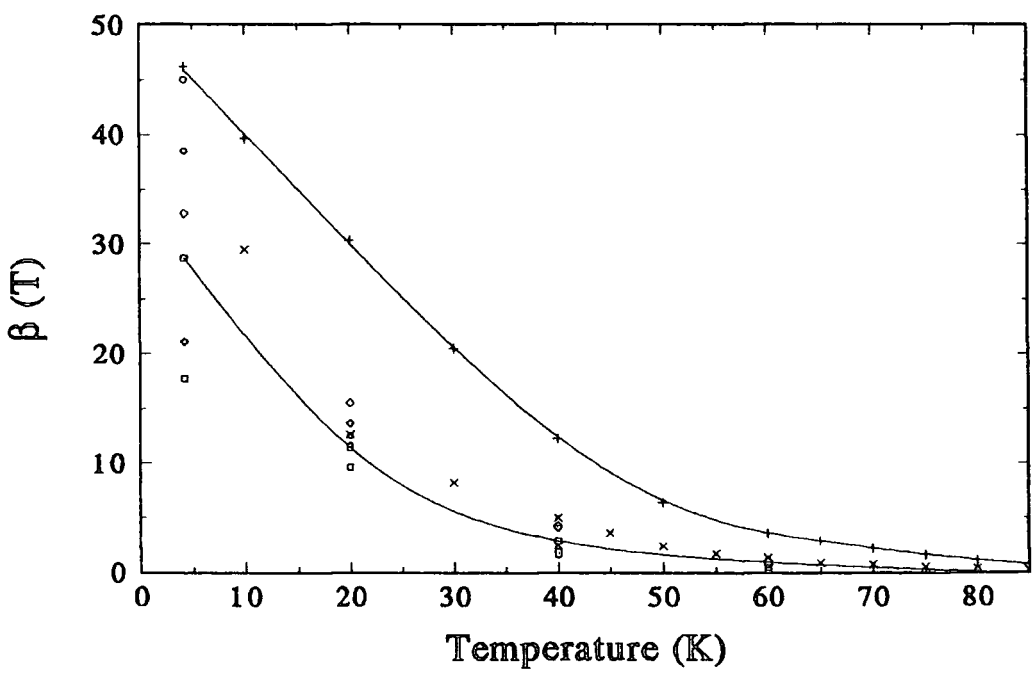

Figure 7.11: The parameter ß(T) for the BSCCO-2212 wires and the BSCCO-2223 tape. The symbols are the same as in figure 7.10. The lines are drawn as guides to the eye only.

orientations of the BSCCO-2223 tape has a similar temperature dependence as the wires. For the BPAB orientation, it is noticeably higher than it is for the wires in the medium temperature range. As is seen from figure 7.11, the BPC orientation of the 2223 tape has values of ß(T) close to that of the three wires.

7.3.3. Comparisons of J_c with respect to the number of filaments and field orientation.

The data of figures 7.6 and 7.7 have been replotted in figures 7.12a,b to compare the relative values of J_c for the 19 and 37 filament wires. Figure 7.12a compares the two wires in the perpendicular orientation whilst figure 7.12b compares them in the parallel orientation. At 4.2K and 20K for both orientations there is no difference in J_c in the field range measured. At temperatures of 40K and above this similarity ends. In fields above 1T, J_c for the 37 filament wire is higher than for the 19 filament wire for both orientations. Below 1T however this behaviour is reversed and the 19 filament wire has the higher J_c at a fixed field.

For the perpendicular field orientation the ratio of J_c for the 37 filament wire to J_c for the 19 filament wire is plotted in figure 7.13a, agreeing with the observations above. For the same orientation figures 7.13b,c show the J_c ratio between the 37 and 19 filament wires with the monocore wire respectively. At 4.2K and 20K the monocore wire has a J_c 2-3 times smaller than the multifilamentary wires. Above 20K the difference in J_c rises rapidly with field and temperature. At 4.2K and 20K the ratio between the 19 filament and monocore wires decreases at high fields because at these temperatures the monocore has a flatter slope in its $J_c(B)$ characteristic (see figure 7.11).

Figure 7.14 compares the relative values of J_c for the 19 filament wire in the parallel and perpendicular field orientations. Even at 4.2K J_c is higher for the parallel and the difference increases with temperature. At the lower temperatures (4.2K/20K) the ratio varies little with magnetic field but at 40K and above it starts to rise quickly with field. A similar orientation dependence is observed for the monocore and 37 filament wires.

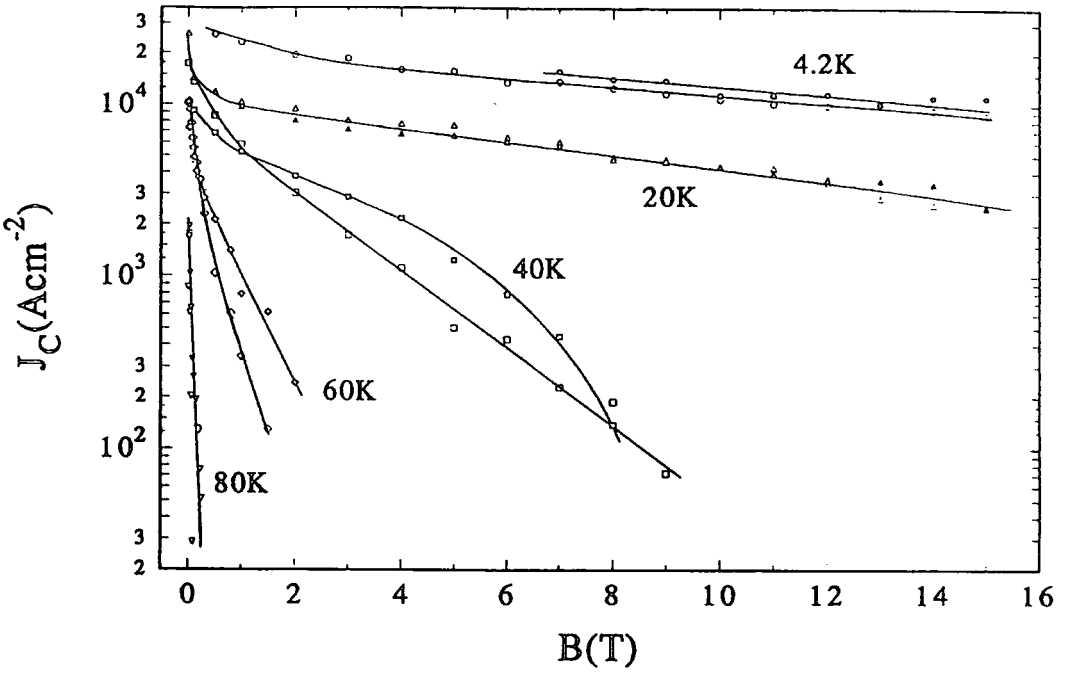

(a)

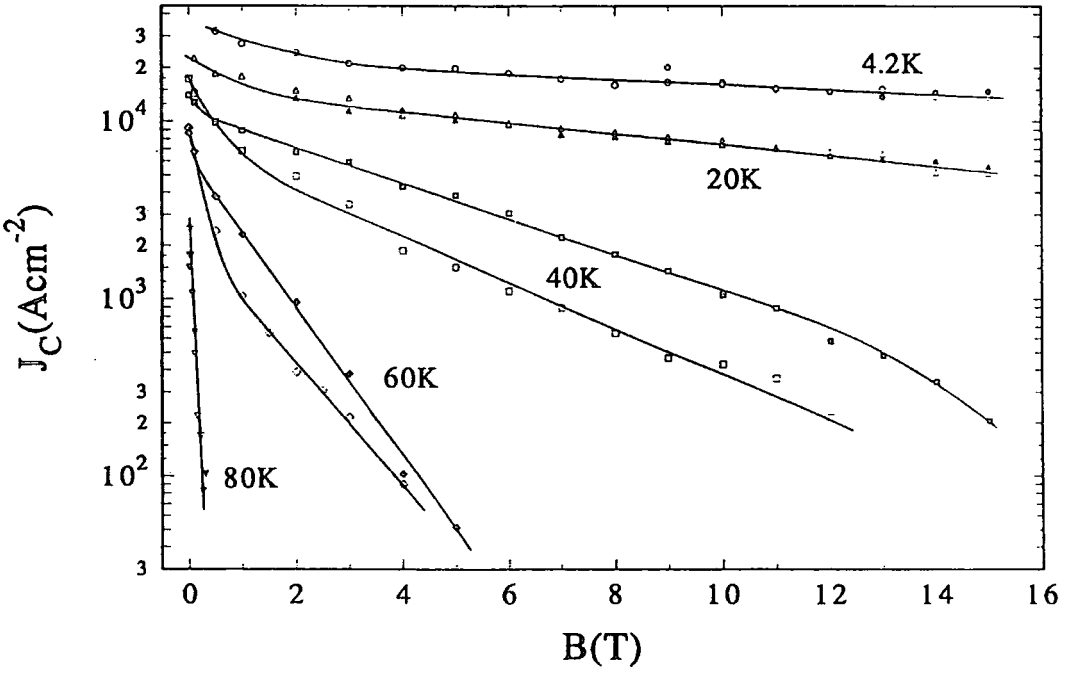

(b)

Figure 7.12: J_c for the 19 filament wire (open symbols) and 37 filament wire (closed symbols) for (a) the perpendicular field orientation and (b) the parallel field orientation.

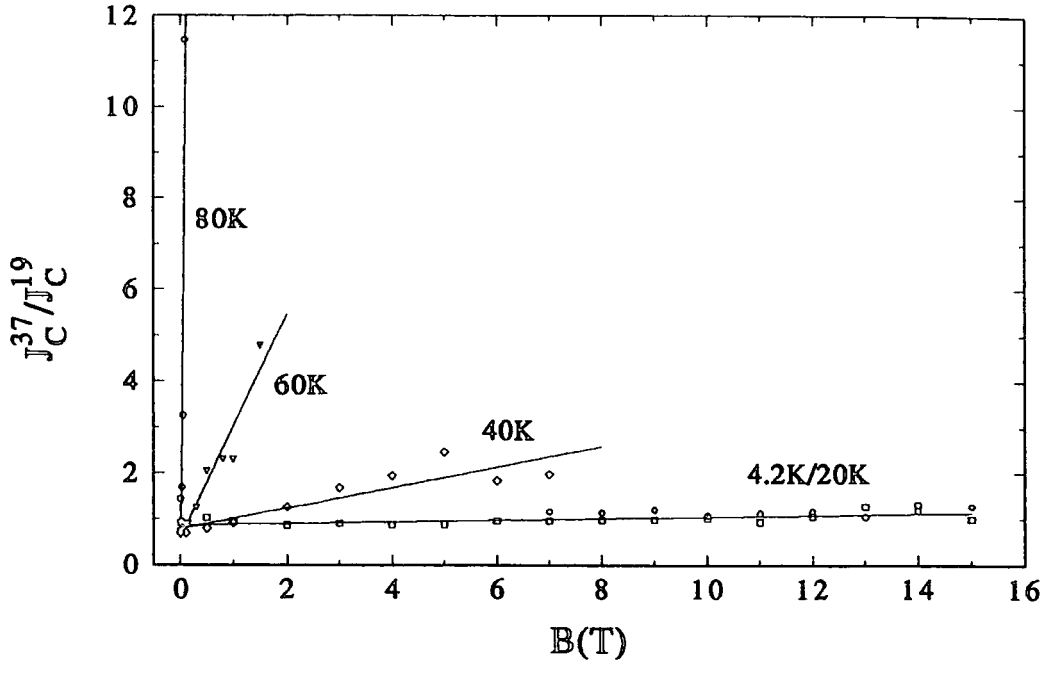

(a)

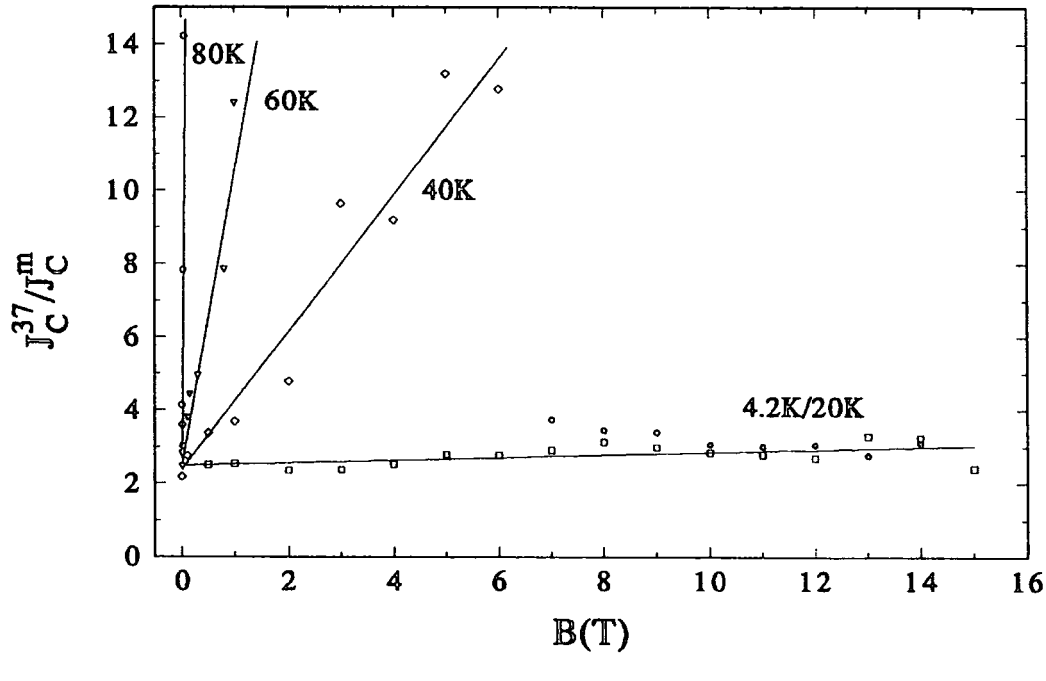

(b)

Figure 7.13: The ratios of J_c with perpendicular field between: (a) the 37 and 19 filament wires; (b) the 37 filament and monocore wires; and on the next page, (c) the 19 filament and monocore wires. In each case the 4.2K data is represented by the symbol ○.

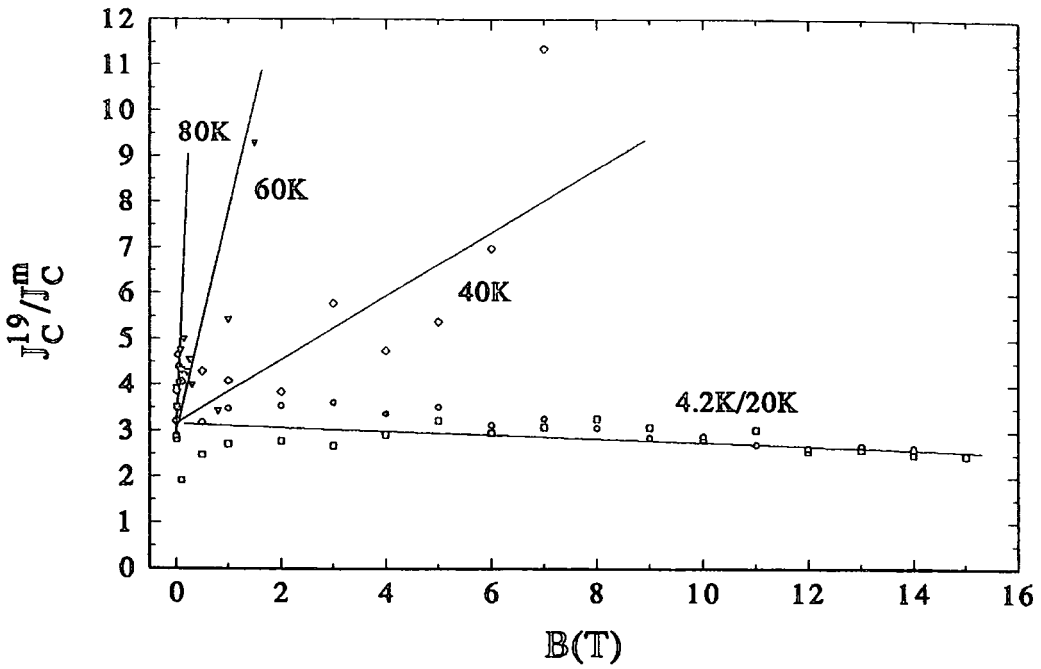

Figure 7.13 (c): see previous page for a description.

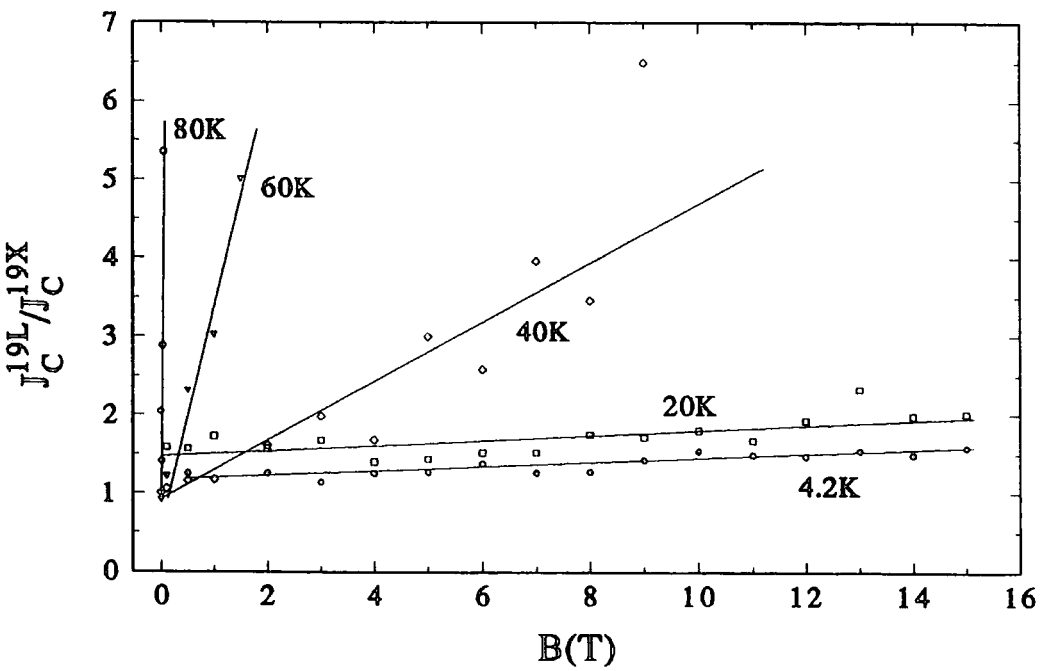

Figure 7.14: Ratios of J_c between the parallel orientation (J_C^{19L}) and the perpendicular orientation (J_C^{19X}) for the 19 filament BSCCO-2212 wire.

7.4. Discussion

7.4.1. The performance of the wires

Table 7.2 lists some values of $J_c(B,T)$ for the wires and for comparison includes J_c for the 2223 tape of chapter 6 at the same fields and temperatures. Heine et al.[1] and Tenbrink et al.[4] have also measured the J_c of monocore and multifilamentary Vacuumschmelze wires. They quote 5.5×10^4 Acm^{-2} at 4.2K in self field (ref. 1) and 1.6×10^4 Acm^{-2} at 4.2K and 9T (ref. 4): approximately 30% higher than the 19 and 37 filament wires here. Tenbrink et al.[4] found no difference in the transport J_c between the monocore and multifilamentary wires at 4.2K but here the performance of the monocore is poorer. All of these measurements were on short sections of wire. Löhle et al.[5] quote a zero field value of 1.4×10^4 Acm^{-2} at 4.2K for a 2m length of multifilamentary 2212 wire. By comparison, $J_c(B,T)$ in 2212 thin films is found to be two orders of magnitude higher than in the wires[6]. It can be seen that at 4.2K/10T the BSCCO-2223 tape in the BPAB orientation has a J_c a factor of two higher than the 2212-multifilamentary wires (and J_c for the BPC orientation is 1.5 times larger). For both wires and tape, J_c at 60K in the self field has similar values to that at 4.2K and 10T. However increasing the field to just 1T at 60K reduces J_c for the wires considerably. By comparison, because of its higher T_c, the 2223 tape in the BPAB orientation still has a J_c of 10^4 Acm^{-2} at this field and J_c for the BPC orientation is 75% of this.

The 2212 wires then, are only suitable for applications at 4.2K or possibly 20K but exhibit excellent field dependencies at these temperatures. By extrapolating the $J_c(B)$ curve for the 19 filament wire at 4.2K and in the perpendicular orientation, it is estimated that a value of 10^4 Acm^{-2} is sustainable up to at least 25 T.

7.4.2. The pinning force description of $J_c(B,T)$

Löhle et al.[5] have calculated the volume pinning force for their multifilamentary 2212 wires and found a $B^{3/4}$ dependence at 4.2K, similar to the wires here. The magnitudes

Sample	J_c(4.2K,10T) 10^3 Acm^{-2}	J_c(60K,self field) 10^3 Acm^{-2}	J_c(60K,1T) 10^3 Acm^{-2}
2212-monocore	3.7	2.6	0.063
2212-19 filament	11	10	0.34
2212-37 filament	11	7.3	0.79
2223-tape, BPAB	21	21	11
2223-tape, BPC	17	24	7.5

Table 7.2: Some values of the transport critical current density of the BSCCO-2212 wires and the BSCCO-2223 tape. BPAB refers to the tape orientation where the field is parallel to the tape surface and BPC refers to when the field is perpendicular to the tape.

of their pinning force were a factor of; two for the monocore and at least six for the multifilamentary wires; less than for the wires measured here. As in figures 7.8a,b,c, when the temperature was increased above 20K for the wires of Löhle et al., the peak in the pinning force quickly moved to lower fields.

Rose et al.[7] have measured J_c(B,T) of bulk polycrystalline BSCCO-2212 and found that their data fitted the Kramer dependence for flux motion by lattice shear at 6K and above. By comparison, the data of figures 7.9a,b,c is only consistent with Kramer's model at 20K and above. It should be noted from observing figures 7.8 and 7.9 that the field at which the pinning force first deviates from a power law dependence ($B^{3/4}$ at low temperatures) corresponds to the field at which the straight lines in the Kramer plot begin.

This analysis, in which the pinning force dependence has been investigated, suggests the following scenario: at low temperatures and fields the pinning is not described by the Kramer model and any movement of flux occurs from the depinning of single flux lines. As the magnetic field is increased and more flux lines are depinned there comes a point at which the FLL shears around a few very strong pinning sites (and the data fit the Kramer functional form). At higher temperatures the lattice shears at increasingly smaller fields. $J_c(B,T)$ above 20K can then be improved by increasing the density of *strong* pinning centres.

The combination of equation 7.1 and Kramer's model does not provide a comprehensive description of $J_c(B,T)$ for the 2212 wires. The crossover from the power law of equation 7.1 to the Kramer model is not distinct. At high temperatures the low field data is not accurately described by either model. Furthermore, the index of 3/4 in equation 7.1 is not predicted by any standard pinning model. The large Lorentz force dependence of the pinning force though, does indicate that J_c is determined by a depinning mechanism.

7.4.3. The exponential field description of $J_c(B,T)$

The high field $J_c(B,T)$ characteristics for the BSCCO-2212 wires have the familiar exponential field dependence, as exhibited by most bulk HTSC materials (c.f. Chapter 6). Because of the similarity of BSCCO-2212 and BSCCO-2223 it is reasonable to assume that the 2212 wires can be described using the same model of intergrain connections as proposed for the 2223 tape in chapter 6. Namely that, at low fields $J_c(B,T)$ is determined by S-N-S Josephson coupling between grains but in high fields it is determined by ab-plane connections between the grains (where the current can transfer between grains without leaving the crystal ab-planes). The sharp drop in J_c at low fields and the hysteretic behaviour observed in figure 7.4 supports the idea of a network of S-N-S Josephson junctions between grains. Note that the field at which J_c for the 19 filament wire ceases to be hysteretic at 4.2K (at 4T) is also the field at which J_c can first be described by the exponential function of equation 7.2, indicating a different

mechanism limiting J_c at high fields. The differences in $\alpha_j(T)$ and ß(T) for the wires and tape in the context of the ab-plane connection model can be explained as follows:

Figures 7.10 and 7.11 compare the exponential parameters for the 2212 wires and 2223 tape. The amount of scatter in the $\alpha_j(T)$ data and the low number of data points for both parameters for the wires makes it hard to compare to the tape data. The 2223 tape has a distinct change (or 'crossover') in the temperature dependencies of $\alpha_j(T)$ and ß(T) at 55K, yet no such change is seen for the wires. The 2223 tape is highly aligned yet the 2212 wires are mostly untextured. Therefore, for the wires, $\alpha_j(T)$ is an average of all possible orientations of the ab-plane connections. It is possible that in the averaging of $\alpha_j(T)$, any crossover has been smeared out and is not observed. For example, the average slope of $\alpha_j(T)$ before the crossover is similar to the average slope of $\alpha_j(T)$ after the crossover, giving a linear form of $\alpha_j(T)$ for the wires. The parameter ß(T) has the same functional form for all orientations of the 2223-tape. For a random orientation of grains, as in the wires, the functional form would not change and ß(T) for the wires has a similar dependence to that for all three orientations of the tape. It is tentatively proposed that there may be a marked change in the temperature dependence of ß(T) for the wires between 20K and 40K. Further data is necessary however to show if this suggestion is correct or not.

It is concluded then that the ab-plane connection description is consistent with the $J_c(B,T)$ data of the 2212 wires. Figures 7.10 and 7.11 highlight the better properties of the BSCCO-2223 tape compared to the BSCCO-2212 wires. Only at 4.2K do the values of $\alpha_j(T)$ and ß(T) for the wires start to approach those for the tape. As the calculated values of the parameters for the wires are an average of all field orientations, direct comparison between the *intrinsic* properties of BSCCO-2223 and BSCCO-2212 is not easy. If there is a crossover in the field and temperature dependence of J_c for BSCCO-2212 it would be expected to occur at a lower temperature than it does in BSCCO-2223. BSCCO-2212 has a lower T_c and higher superconducting anisotropy, $\Gamma \approx 3000$[8] than BSCCO-2223 ($\Gamma \approx 960$) which could strongly affect the crossover temperature if it is due to a pinning phase transition.

The marked departure from the exponential dependence for the 40K data of the 37 filament wire is similar to that observed for the BPC orientation of the 2223 tape, attributed to a FLL phase transition. This departure is not observed for the other two wires. For a broad distribution in grain orientation though, it would be expected that such a phase transition has little effect on the field dependence of J_c. A better explanation is that the 37 filament wire contains some material of a weaker superconducting BSCCO phase with a lower irreversibility line or that it has a lower density than the 19 filament wire.

Summing up, $J_c(B,T)$ of the 2212 wires can be described by the same exponential function as for the 2223 tape in chapter 6: at low fields the grains are coupled by S-N-S Josephson junctions and at high fields J_c is determined by ab-plane connections between grains. No crossover in the $J_c(B,T)$ dependence of the wires can be clearly defined due to the large distribution in grain orientations and small number of data points. The BSCCO-2212 material in the 37 filament wire is of poorer quality than in the other two wires. The data gives no further evidence as to which theory of the FLL best describes $J_c(B,T)$ in BSCCO.

7.4.4. Increase of $J_c(B)$ with number of filaments

Tenbrink et al.[4] found that the magnetically determined J_c of a 49 filament 2212 wire was up to seven times larger than for a monocore wire. They detected no difference from transport measurements. Figures 7.13b and 7.13c show that the multifilamentary wires have a transport J_c a factor of 2-3 higher than the monocore wire at zero field.

Tenbrink et al. attributed the increase in magnetic J_c to an increase in texture because of the larger area of 2212-Ag interface in the multifilamentary wires: it is known that in the region near a boundary with a silver sheath the BSCCO grains grow highly aligned. This leads to a region of highly textured BSCCO-2212 around the circumference of each filament and an untextured core. From the large difference in the values of $\alpha_j(T)$ for the monocore and multifilamentary wires it can be concluded that the highly textured 2212-Ag interface region has a high density of ab-plane connections

compared to the untextured core of a filament. This is to be expected from a physical viewpoint: for two grains to have an ab-plane connection they can only be mis-orientated with respect to each other by a small angle.

Since there is little difference between the 19 and 37 filament wires at 4.2K and 20K in high fields, $J_c(B,T)$ is not purely determined by the amount of 2212-Ag interface area and the resulting larger number of ab-plane connections. The phase purity and density of BSCCO-2212 material in the wires is also important. Further evidence for this obtained by noting the performance of the 37 filament wire in relation to the 19 filament wires at high temperatures. In high fields the 37 filament wire has the higher J_c yet in low fields the 19 filament wire has the higher J_c (see figures 7.12a,b). This can be explained by the following argument: the 19 filament wire has a better phase purity and/density than the 37 filament wire. At low fields, grains are connected by S-N-S Josephson coupling. Large voids and weakly superconducting areas going normal as the field is increased will reduce the number of high J_c percolative paths available for the transport current in the 37 filament wire. However the 37 filament wire has more ab-plane connections (from the larger 2212-Ag interface area) and hence a higher J_c in high fields. The rapid reduction in J_c in high fields at 40K is due to a lower average irreversibility field because of the poorer phase purity of the BSCCO.

In summary, because of the better alignment of grains at a 2212-Ag interface the majority of the ab-plane connections, which determine J_c at high fields, lie in the outer region of each wire filament. Increasing the number of filaments further should increase J_c as long as the quality (as in phase purity) of the BSCCO-2212 material can be maintained.

7.4.5. The force free orientation

In chapter 6 it was found that for the BSCCO-2223 tape, at low temperatures when the field was parallel to the tape surface, J_c was Lorentz force independent. This was explained by intrinsic pinning of flux by the ab-planes. The same analysis cannot be carried out on the 2212 wires. In high fields, J_c is determined by the ab-plane

connections which mostly lie in the 2212-Ag interface region. They will therefore be orientated so that the c-axis is perpendicular to the surface of each filament. If we take the most simple assumptions, that at the surface of each filament the grains are perfectly aligned and that the filaments are perfectly straight, then in the parallel orientation the field will be parallel to the current for all the ab-planes. In a perpendicular field there will be a distribution of angles that the field makes with each ab-plane connection: from the field parallel to the ab-plane to the field perpendicular to the ab-plane. In all cases however the field is always perpendicular to the current. The difference in J_c with field orientation observed for the wires (c.f. figure 7.14) is then to be expected. The stronger orientation dependence as the field and temperature is increased is due to the poorer field and temperature dependence of J_c when the field is perpendicular to the c-axis (which is the case for some of the grains in the perpendicular orientation).

7.5. Main conclusions

The critical current density of three BSCCO-2212 multifilamentary wires (monocore, 19 filaments and 37 filaments) has been measured in high magnetic fields and at temperatures from 4.2K to 80K. From the data the following observations and conclusions have been drawn:

i. As for the BSCCO-2223 tape of chapter 6, $J_c(B,T)$ can be described by either a Kramer flux shear model or an exponential field function. The latter description is more comprehensive and allows, through the parameters $\alpha_j(T)$ and ß(T), better comparison with the 2223-tape;

ii. The variation of J_c with field and temperature for the BSCCO-2212 wires can be explained by the same model as applied to the 2223-tape in chapter 6: J_c is determined by S-N-S Josephson coupling between grains in low fields and by ab-plane connections between grains at high fields;

iii. The values of $J_c(B,T)$ for the BSCCO-2223 tape are considerably better than for the 2212 wires. A comparison between the intrinsic pinning properties of

BSCCO-2223 and 2212 is difficult because of the different texturing in the wires and the tape. Further data is required to determine if there is a crossover in the field and temperature dependencies of J_c for BSCCO-2212;

iv. From the increase in $J_c(B,T)$ and the parameter $\alpha_i(T)$ with the number of filaments, it is concluded that the majority of ab-plane connections lie in the 2212-Ag interface region of each filament. However, as well as the number of filaments, the phase purity and density of the BSCCO-2212 material is still important in obtaining high $J_c(B,T)$;

These measurements demonstrate that at temperatures of 4.2K and 20K multifilamentary BSCCO-2212 wires have great potential for use in high field applications, especially in superconducting magnets where the wire form and high mechanical strength is preferred. It appears that at 4.2K, J_c can only be increased by better fabrication procedures to obtain better density, stoichiometry and connectivity or an increase in the number of filaments. Above 20K the wires have poor J_c in high fields as thermal effects become important. It is possible that J_c at these higher temperatures can be increased by stronger pinning (by irradiation for example).

References for Chapter 7

1. Heine K., Tenbrink J. and Thöner M., Appl. Phys. Lett. 55(23), 2441 (1989).

2. Tenbrink J. and Krauth H., paper presented at ICMC 93, Albuquerque USA.

3. Kramer E.J., J. Appl. Phys., 44(3), 1360 (1973).

4. Tenbrink J., Wilhelm M., Heine K. and Krauth H., IEEE Trans. Appl. Supercond. 3(1), 1123 (1993).

5. Löhle J., Mattenberger K., Vogt O. and Wachter P., Cryogenics 33(3), 287 (1993).

6. Schmitt P., Kummeth P., Schultz L. and Saemann-Ischenko G., Phys. Rev. Lett. 67(2), 267 (1991).

7. Rose R.A., Ota S.B., de Groot P.A.J. and Jayaram B., Physics C 170, 51 (1990).

8. Farrell D.E., Bonham S., Foster J., Chang Y.C., Jiang P.Z., Vandervoort K.G. and Lam D.J., Phys. Rev. Lett. 63(7), 782 (1989).

8. Main Summary and Concluding Remarks

This thesis has presented extensive measurements of the transport critical current density of both low and high temperature superconductors. By measuring J_c over a wide range of fields, temperatures and sample orientations new information on the pinning of the flux line lattice has been obtained. Some results cannot be explained by existing theories; others are inconclusive as to which theory describes them best. This final chapter summarizes the main conclusions of the thesis and offers some ideas for future work.

Previous probes for measuring the transport critical current have been limited to small temperature ranges and/or could only measure small values of the critical current. The $J_c(B,T)$ probe presented in chapter four is small enough to fit inside the bore of a high field magnet (a 15/17 Tesla system in Durham) and is capable of measuring critical currents accurately up to 500 Amps. The sample temperature can be varied from 2K to 150K and can be kept fixed to the following degrees of accuracy: $\pm$50mK at and below 4.2K; $\pm$70mK at 20K; $\pm$100mK at 80K and $\pm$200mK at 150K. Short sections of wires and tapes, thin films and bulk specimens can be measured. Because of the small sample size, above 4.2K, Joule heating can limit the maximum critical current that can be measured to below 500A. To keep within the temperature accuracy quoted above, for the samples in this thesis the critical current could be measured up to 30A at 20K and up to 50A at 80K.

Some commercial Nb(46.5wt%)Ti multifilamentary wire was measured in chapter five with the field perpendicular and parallel to the wire axis. The parallel orientation had a higher J_c and effective upper critical field (as measured by extrapolation of the $J_c(B)$ data to zero and also by a resistive transition). Existing theories of the Lorentz force free J_c could not explain the results. From scaling of the pinning force it was demonstrated for the first time that the orientation, field and temperature dependence of J_c was determined solely by the anisotropic effective upper critical field and not the Lorentz force. Possible reasons for the anisotropy in the upper critical field were discussed including variations in the microstructure and complicated flux cutting events

restricting the flux motion. These new findings highlight the incomplete understanding of flux line dynamics, even in materials that have been studied for 25 years and suggest caution when measuring upper critical fields.

In chapter six a $Bi_2Sr_2Ca_2Cu_3O_x$ silver-clad tape was investigated. Detailed measurements of J_c were taken for three orientations of the field with respect to the sample: perpendicular to the tape surface and therefore mostly parallel to the c-axis, labelled BPC; parallel to the tape surface (and the ab-planes) and perpendicular to the current, labelled BPAB; parallel to the tape surface and the current, giving a zero macroscopic Lorentz force and labelled LFF.

Below 10K a dramatic anomaly in J_c, at a field defined as $B_j(T)$, was observed for all three orientations. Such an anomaly has been observed once before by other authors but measurements had only been taken for the BPAB orientation and at 4.2K. The work in chapter six shows for the first time that the anomaly occurs at the same field for all three orientations and disappears at above 10K. It is suggested that the grain boundaries of the BICC tape contain some low T_c BSCCO phase material, possibly the 2201 or 2011 phase, which has a T_c of approximately 10.8K. The field $B_j(T)$ is the upper critical field of this phase. The anomaly marks a change from a regime where J_c is determined by strong S-S'-S Josephson coupling between grains to one where J_c is determined by intrinsic properties of BSCCO and a few remaining strong connections between grains. This result clearly demonstrates the importance of good inter-grain connectivity in obtaining higher values of J_c in BSCCO-2223 tapes.

Above 10K, $J_c(B,T)$ was explained by the following model: there are two types of intergrain connections in the tape, coupling via S-N-S Josephson junctions and ab-plane connections where the current can transfer between grains without leaving the crystal ab-planes. There are relatively few ab-plane connections and in fields less than 1T, the current is determined by a network of S-N-S Josephson junctions between the grains. As the field is increased these junctions become broken and J_c drops quickly. Above 1T, the ab-plane connections become the dominant intergrain connections with (initially)

a weaker field dependence. $J_c(B,T)$ is now determined by the intrinsic properties of BSCCO.

In fields above 1T, $J_c(B,T)$ can be described by an exponential field function or alternatively, by Kramer's pinning model. It was found that the exponential function $J_c(B,T)=\alpha_j(T)\exp\{-B/ß(T)\}$ best described the data over all temperatures and orientations above fields of 1T. The parameter $\alpha_j(T)$ is the zero field J_c if the grains were connected via the ab-plane connections only. The Lorentz force dependence of BSCCO tapes is rarely studied. Such data in chapter six supported the idea of intrinsic pinning of the flux by the ab-planes. Any reduction of J_c with an increase in the field is then due to the average field component parallel to the c-axis. The possible mechanisms by which $J_c(B,T)$ is reduced by a field perpendicular to the ab-plane with the exponential function dependence were discussed. It was suggested that a pinning mechanism was most likely and that the theory of collective pinning in layered structures provided the best framework for describing $J_c(B,T)$. The parameter ß(T) then describes the temperature dependence of the average pinning potential.

There was a sharp change in the temperature dependencies of $\alpha_j(T)$ and ß(T) at 55K. By plotting J_c against $(1-t^2)$ for fixed magnetic fields a field dependent line, $T_\alpha(B)$, was calculated that also marked a clear change in the temperature dependence of J_c. It was discussed that a change in the exponential parameters and the line $T_\alpha(B)$ should provide the same information. It was noted that a field dependent change in ß(T) would cause an unnoticeable change in the field dependence of J_c at the temperatures involved. The change in the parameters at 55K is related to T_α at $B=0$. The line T_α defines a low temperature to high temperature crossover in the B-T phase diagram of the tape. Above $T_\alpha(B)$, $J_c(B,T)$ has a stronger field and temperature dependence than it does below it. It was concluded that $T_\alpha(B)$ marked a pinning phase transition such as the 2D to 3D pinning transition predicted by collective pinning theory. To be able to prove conclusively what type of transition $T_\alpha(B)$ defines and what mechanism determines $J_c(B,T)$ in the tape, more information is required on the B,T and J dependencies of the average pinning potentials.

Finally, the behaviour of $J_c(B,T)$ as the irreversibility line is reached was found to be different for a field parallel and perpendicular to the tape surface. This characteristic has not been discussed before in the literature. For the BPAB and LFF orientations $J_c(B,T)$ was exponential with field down to the smallest measurable values. With the BPC orientation $J_c(B)$ departed from the exponential law at a field $B_d(T)$ and started to decrease rapidly before the irreversibility line was reached. The curve $B_d(T)$ probably corresponds to a FLL phase transition which reduces J_c to zero. Further work is required to ascertain what type of transition it is. When the field is parallel to the ab-plane J_c is reduced to zero by a thermal depinning mechanism.

From all these results on the tape, a complicated B-T phase diagram has been calculated. For applications at the higher temperatures it appears that the line $T_\alpha(B)$ needs to be raised, rather than just the irreversibility line.

The same description of S-N-S Josephson junction behaviour at low fields and a J_c determined by ab-plane connections in high fields could also explain $J_c(B,T)$ for three BSCCO-2212 wires in chapter seven. As with the 2223 tape, the high field data was analysed using Kramer's flux shear model and an exponential field function. Again, it was concluded that the exponential field function provided a more complete description of the data. Each wire filament has an untextured core but at the 2212-Ag interface the grains are highly aligned. The performance of the 19 and 37 filament wires was significantly better than that of the monocore wire and it was concluded that most of the ab-plane connections exist in the interface region of each filament. There was little difference in the performance of the 19 and 37 filament wires below 40K. Above this temperature the 19 filament wire had the better J_c in low fields whilst the 37 filament wire had a better J_c in high fields. Then at 40K in very high fields, J_c of the 37 filament wire started to drop below that of the 19 filament wire. It was suggested that the phase purity and density of the 19 filament wire was better but that it had less ab-plane connections (because of its fewer filaments). These results highlight again that a higher J_c corresponds to better texture and connectivity between BSCCO grains.

Because of the difference in texture between the wires and tape, comparison of the intrinsic properties of BSCCO-2223 and BSCCO-2212 was difficult. It was proposed that there may be a crossover in the field and temperature dependencies of $J_c(B,T)$ for the wires between 20K and 40K, though more data is required to show if this is correct.

The high field performance of the multifilamentary BSCCO-2212 wires offers potential for use in commercial applications at temperatures up to 20K. Higher values of J_c should be obtained by increasing the number of filaments, which improves the overall texture and connectivity, whilst maintaining the phase purity and density.

Many conclusions in the literature are drawn from $J_c(B,T)$ measurements of a limited data set. Lorentz force free orientations are rarely studied although they can supply extra information. Care must be taken when fitting the data to accepted models. The work in this thesis has shown that the data can often be closely fitted to more than one model. The different models point to quite different approaches to improve J_c and it must be decided which one best describes $J_c(B,T)$ over the whole B-T phase diagram. To investigate in more detail the flux line dynamics in BSCCO *comprehensive* measurements of the transport $J_c(B,T)$ are required on thin films and crystals. This means a wide range of temperatures, fields and orientations on the same sample. For wires and tapes a better idea of the microstructure of the particular sample being measured is essential. Variations in J_c could then be directly related to microstructural changes, especially those at the grain boundaries. The results summarised above show how important inter-grain connections are and more work needs to be done to ascertain whether the model of ab-plane connections described here is correct. Finally a better picture can be obtained if the transport J_c measurements are supplemented by magnetic measurements of J_c and other properties on the *same* sample. In addition there is still information to be gained from further measurements on low temperature superconductors, whose fundamental superconducting parameters are well known. In particular, more investigations on the force free J_c and artificially produced layered structures would be useful.

Flux line dynamics and pinning in the high temperature superconductors is a complex and confusing subject. There are many theories in the literature which compliment and contradict each other. It is certain that even in 25 years time the subject will not be fully understood. The greatest drive in the meantime should be towards understanding how high values of transport J_c are obtained in these materials. This thesis has shown that $J_c(B,T)$ in high temperature wires and tapes can be raised by better texturing, better connectivity and a higher density of pinning centres. Wires and tapes that are good enough to be used in real applications by engineers can then be produced.

Appendix 1: The $J_c(B)$ of some PbSn tapes at 4.2K

This appendix contains preliminary results of $J_c(B)$ measurements on PbSn tapes at 4.2K. The measurements were taken to compare to the low field behaviour of a BSCCO-2223 tape for different field orientations. The results are interesting but not sufficiently central to the work of this thesis to allow further investigation in the time available.

PbSn has a lower critical field of 45mT and an upper critical field of 110mT so any changes in J_c at the critical fields could be easily observed using the high field superconducting magnet. The fabrication procedure is described and $J_c(B)$ for three different sized samples in three orientations is presented. This is followed by a brief discussion of the data.

$Pb_{0.87}Sn_{0.13}$ ingots were made by mixing the correct ratio of Pn and Sn and heating to 600°C in an argon atmosphere for 4 hours, after which the mixture was allowed to cool slowly. The ingots were then rolled into tapes down to a thickness of 0.07 mm from which the rectangular samples were cut. The three samples measured were labelled A,B and C and had the following dimensions:
Sample A - 0.16 mm thick/1.10 mm wide;
Sample B - 0.07 mm thick/1.18 mm wide;
Sample C - 0.13 mm thick/1.16 mm wide;

Each sample was approximately 10 mm long.

The samples were soldered (with Indium) in parallel to a copper strip to prevent them melting during quenches. Both sides of the sample were covered in the solder. $J_c(B)$ was measured in liquid helium for each sample in three orientations labelled positions 1,2 and 3:
Position 1 - field parallel to tape surface and perpendicular to the current;
Position 2 - field perpendicular to both the tape surface and the current;
Position 3 - field parallel to both the tape surface and the current.

Figures app2.1a,b and c show the results for samples A,B, and C respectively. Common to each curve: J_c does not peak at zero field; the Lorentz force free orientation (position 3) has a double peak in low fields and a higher J_c than the other two orientations for most fields; the $J_c(B)$ curves are shifted to the right by 10-15 mT because of the presence of a remnant field. This remnant field has been calculated as the field at which J_c is a maximum for positions 1 and 2 and the field at which J_c reaches a minimum between the two small low field peaks for position 3.

The remnant fields for each curve have been subtracted and the data replotted on a log-log scale in figures app2.2a,b,c. The resulting set of curves are distinctly different for each sample. The magnitude of J_c for sample C is a factor of at least 4 higher than samples A and B. There appears to be no correlation between J_c and one of the samples dimensions. With each curve $J_c(B)$ is initially constant until some field when it starts to decrease. This decrease in J_c can be fitted to a power law for each curve. For sample C this power law holds down the limit at which J_c can be measured. For samples A and B the power law only fits the data for a limited field range. Each sample will be briefly discussed in turn:

Sample A

There is an anomaly in J_c for position 3 at B_{c2} and above this field a sizeable J_c is still measured. The J_c for position 1 is slightly higher than for position 2 at all fields. The data for all three orientations has been fitted to a power law between B_{c1} and B_{c2} and the following dependences were found:
for positions 1 and 2,

$$J_C \propto B^{-2.0} \qquad \text{app1}$$

and for position 3,

$$J_C \propto B^{-1.8} \qquad \text{app2}$$

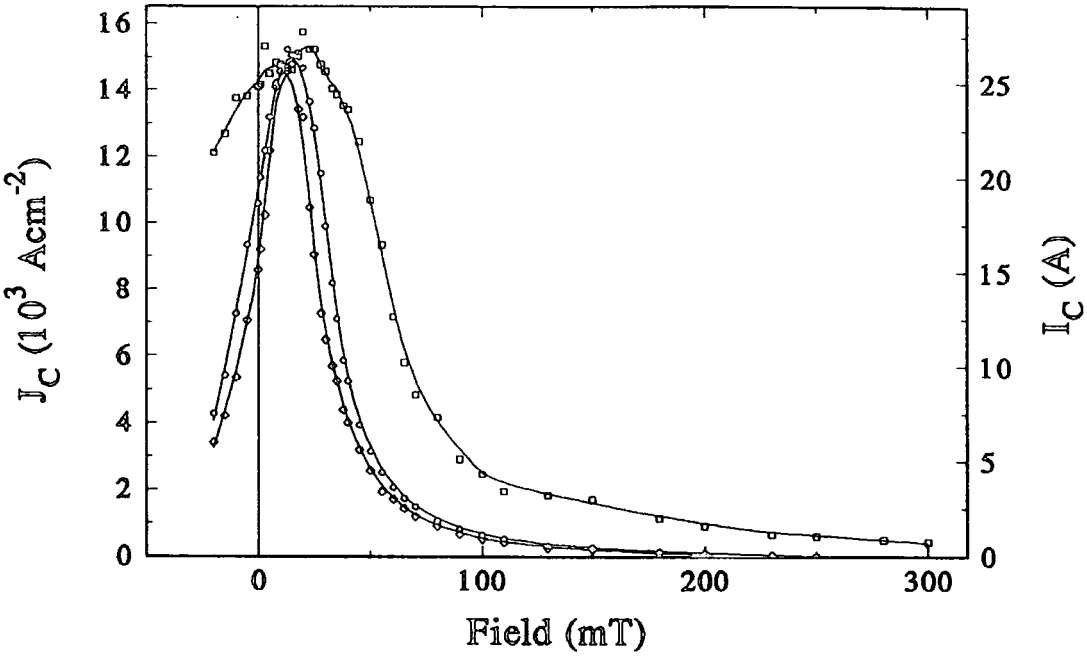

(a)

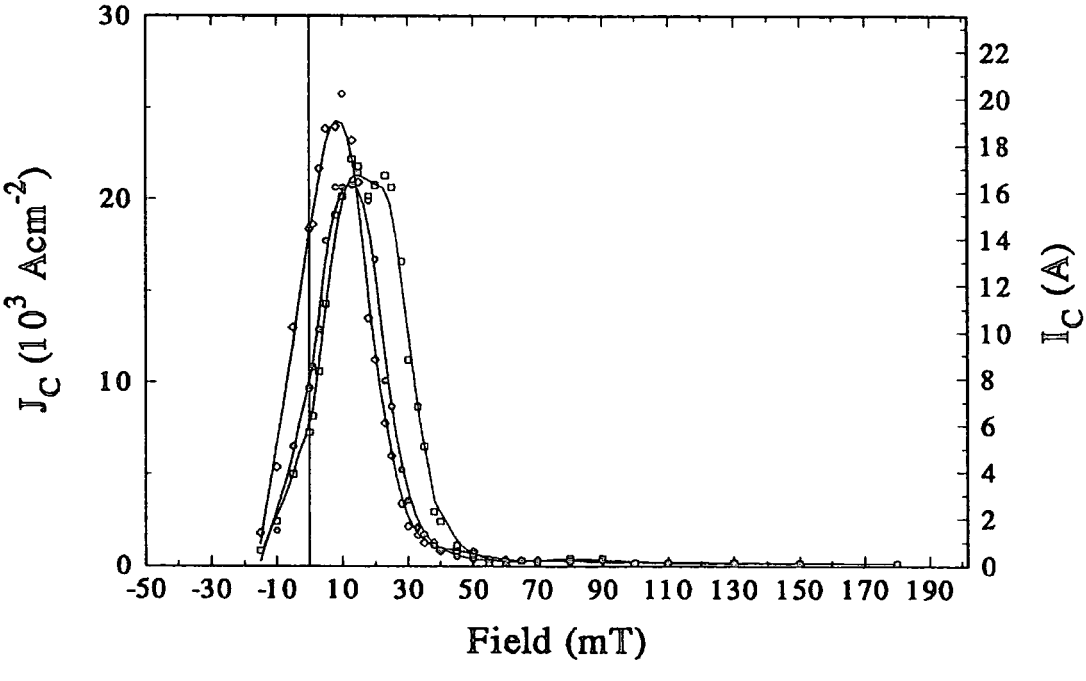

(b)

Figure app2.1: $J_C(B)$ of the $Pb_{0.87}Sn_{0.13}$ tapes where (a),(b) and (c)(on next page) correspond to samples A,B, and C. In each plot: ●, position 1; ◇, position 2 and □, position 3.

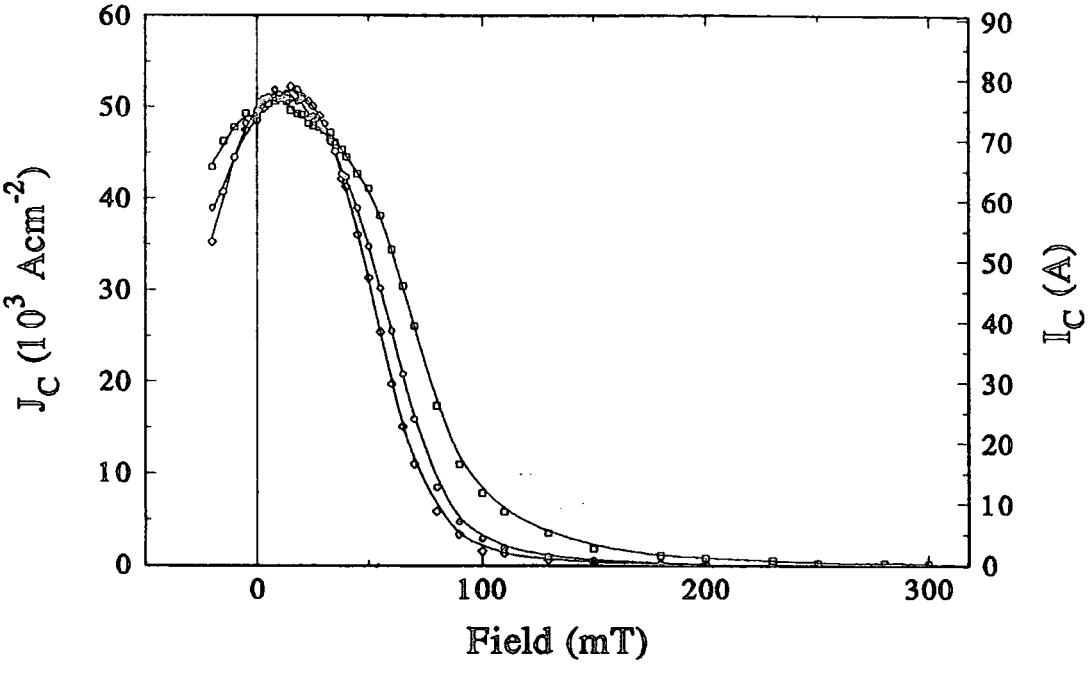

Figure app2.1(c): for description see previous page

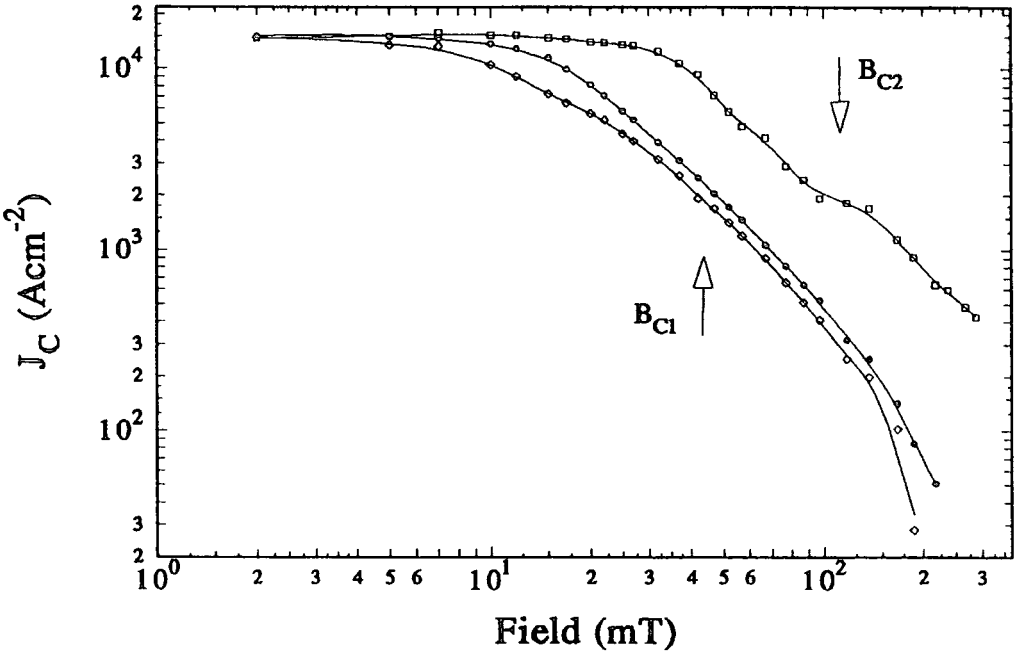

Figure app2.2(a): for description see the next page

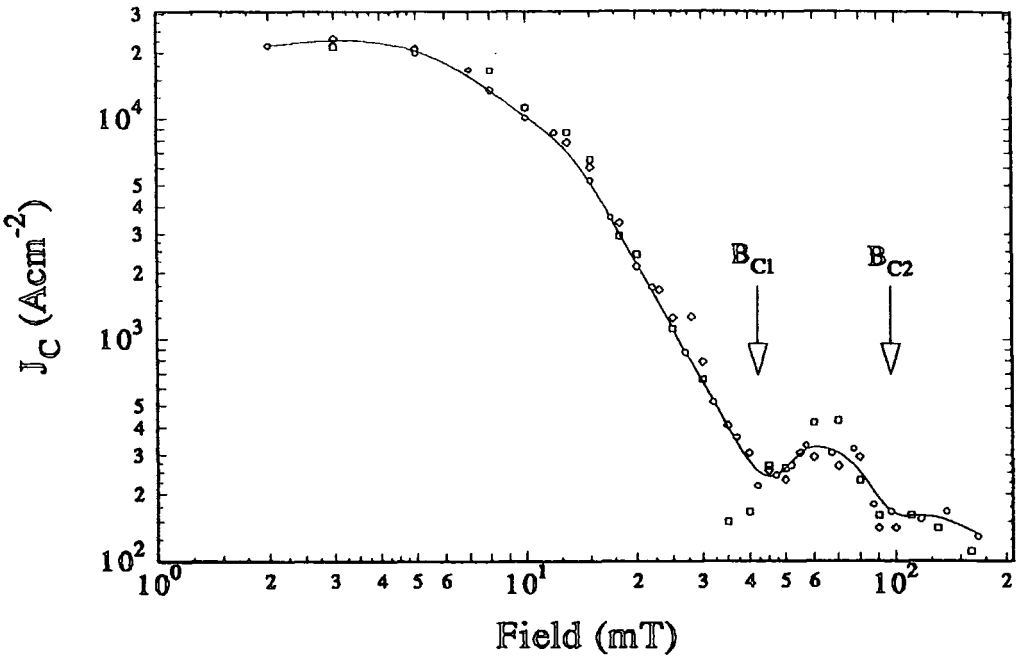

(b)

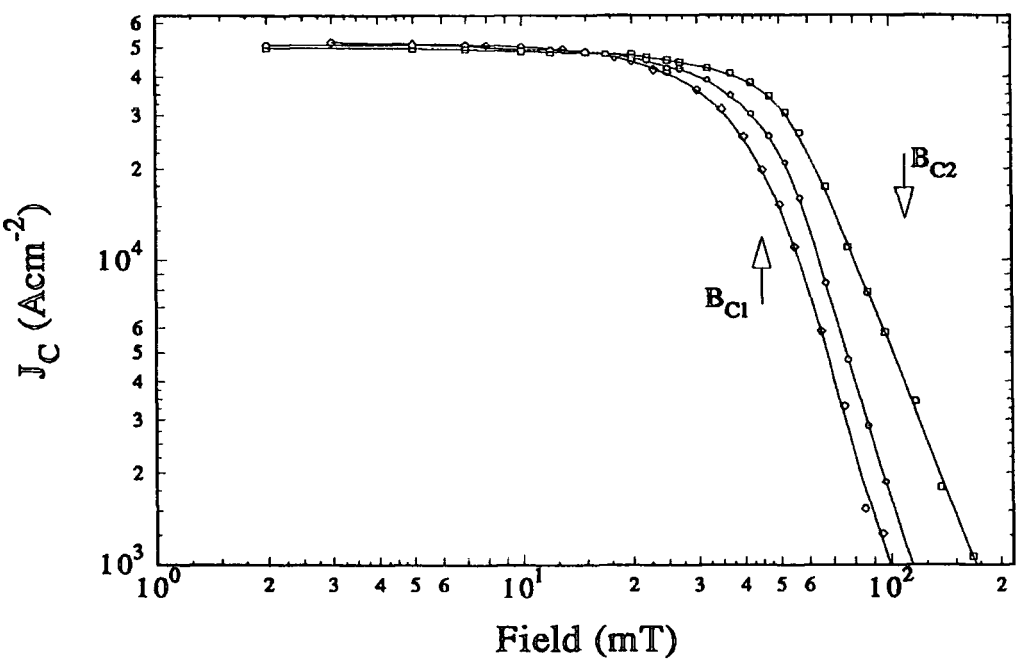

(c)

Figure app2.2: $J_c(B)$ of the $Pb_{0.87}Sn_{0.13}$ tapes on a log-log scale with adjusted field values to take account of the remnant field. The symbols are the same as for figure app2.1. (a), (b) and (c) correspond to sample A,B and C.

Sample B

All three orientations follow a similar curve. Sample B is the thinnest sample has a distinctly different behaviour than the other two samples. J_c decreases as the power law

$$J_C \propto B^{-3.0} \qquad \text{app3}$$

before B_{c1}. It reaches a minimum at B_{c1} then increases and peaks between B_{c1} and B_{c2} before decreasing towards zero at B_{c2}.

Sample C

J_c is the same for all three orientations up to a field just below B_{c1}. Above B_{c1}, J_c can be described by the power laws:

for positions 1 and 2,

$$J_C \propto B^{-4.0} \qquad \text{app4}$$

and for position 3,

$$J_C \propto B^{-3.5} \qquad \text{app5}$$

As for sample A, position 1 has a slightly higher J_c than position 2.

Because the samples were coated in indium solder on both sides, any surface currents when the field is parallel to the tape surface should be minimal. That position 1 has a higher J_c compared to position 2 in samples A and C suggests that there are some surface currents present. For the thinner sample B there are none. As for the NbTi wire in chapter 5 the Lorentz force free orientation (position 3) has the highest J_c and appears to have a higher effective upper critical field than 110 mT. This large difference is not apparent in sample B however, suggesting that it may be connected large surface currents.

These preliminary results are very interesting, in particular: the peak effect observed bewteen B_{c1} and B_{c2} in sample B; the kink in $J_c(B)$ at a similar position for position 3 of sample A; and the lack of correlation between J_c and a sample dimension, suggesting perhaps, that surface effects may be more important. Further investigation is warranted.

Appendix 2: List of Asyst Programs

This appendix list the software programs, written using Asyst (Keithley), that controlled the $J_c(B,T)$ measurement equipment. A brief description of each program is given. The programs were written by Chris Friend and Dr Luc Le Lay over a period of at least six months and ran on an IBM PS/2. All communication was via the IEEE protocol except for the magnet controller which used the RS232 protocol. All programs include real-time plotting of the measurements being performed.

Note on power supply used

There are two versions of most programs so that J_c can be measured using one of two power supplies. The character # in some of the following program names stands for the number 1 or 2. Programs which use the 100A Thor power supply have the number 1 at the end of their name and programs with the number 2 use the 500A power supply, built in-house.

Initialization program

The program SETUP.PRO contains the correct initialization procedures for all the measuring equipment. It is called by all programs at the start of running.

Measurement of V-I characteristics at a fixed field and temperature

The program VITRACE#.PRO measures the V-I trace of a sample at a field and temperature set manually by the user. It ramps the sample current which is measured with a voltmeter across a standard resistor and measures the voltage drop with the Keithley Nanovoltmeter. The V-I data are saved to a Lotus 1-2-3 file named by the user. The program variables are held in the Asyst file VITRACE#.VAR. An older less sophisticated version of the program is SINGLEIC.PRO.

Measurements of the V-I characteristics in a varying field

VIFIELD#.PRO and its associated variable file VIFIELD#.VAR, is similar to VITRACE#.PRO except that it includes control of the superconducting magnet. The user can input up to 50 different magnetic fields at which the measurements are to be taken. The temperature is fixed manually. The V-I data at each field are saved in the same Lotus file. An old version of the program is called FIELDIC2.PRO.

Measurement of V-I characteristics at varying fields and temperatures

The file JCBT#.PRO is the main control program for taking measurements of V-I traces at temperatures and fields which are fixed and controlled by the computer. This main block takes all the user input information such as file names, time of one trace, up to 20 different temperatures and up to 50 different fields for *each* temperature, etc. At the start of running it calls the following sub-programs:

FIELD#.PRO - this does a similar task to VIFIELD.PRO, it ramps the fields at each temperature and takes the V-I traces. The data for each temperature are saved in separate Lotus files such as name1.wk1, name2.wk1, name3.wk1 etc. where name is specified by the user;
LOWTEMP#.PRO - this program fixes and controls the temperature via the Lakeshore temperature controller. The temperatures are input by the user in the form of the corresponding RhFe thermometer resistances. At each temperature the field is ramped to zero and the capacitance thermometer is used to ramp and control the temperature of the sample chamber. The temperature is continuously monitored during ramping by reading the RhFe thermometer resistance;
OHMSKELV.PRO - this program converts the RhFe thermometer resistance (in Ohms) to a temperature in Kelvins;
JCBT#.VAR - contains all the variables used by the JCBT program.

Resistive measurement of the upper critical field

This measurement is controlled by the program BC2.PRO. The temperature is fixed manually. A constant current is supplied to the sample and whilst the magnetic field is ramped the voltage drop is measured by the Nanovoltmeter and converted to a resistance. All variables are contained within BC2.PRO.

Appendix 3: List of Publications

The following is a list of publications/submissions from work contained in this thesis as of September 1994:

1. *Transverse and longitudinal critical current densities in Nb46.5wt%Ti multifilamentary wire from 2K up to T_c in magnetic fields up to 15 Tesla*,
C.M. Friend and D.P. Hampshire, pg. 23 'Applied Superconductivity', Proceedings of EUCAS 1993, ed. H.C. Freyhardt (DGM, VERLAG 1993).

2. *Evidence that pair-breaking at the grain-boundaries of $Bi_2Sr_2Ca_2Cu_3O_x$ tapes determines the critical current density above 10K in high magnetic fields*,
L. Le Lay, C.M. Friend, T. Maruyama, K. Osamura and D.P. Hampshire, J. Phys: Condensed Matter **6**, 10053 (1994).

3. *A probe for the measurement of the transport critical current density of superconductors in high magnetic fields and at temperatures between 2 and 150K*,
C.M. Friend and D.P. Hampshire, Meas. Sci. & Technol. **6**(1), 98 (1995).

4. *Studies of $J_c(B,T)$ in Bi(2223) tapes*,
D.P. Hampshire, C.M. Friend, T. Maruyama, K. Osamura and L. Le Lay, to be published in ISTEC, Kyoto Japan, June 1994.

5. *Critical Current Density of $Bi_2Sr_2Ca_1Cu_2O_x$ monocore and multifilamentary wires from 4.2K up to T_c in high magnetic fields*,
C.M. Friend, J. Tenbrink and D.P. Hampshire, submitted to J. Appl. Phys., January 1995.

6. *Anomalous behaviour in the critical current density of a $Bi_2Sr_2Ca_2Cu_3O_x$ tape below 10K*,
C.M. Friend, D.P. Hampshire, to be submitted to App. Phys. Lett.

7. *A description of the field, temperature and orientation dependence of the critical current density for a $Bi_2Sr_2Ca_2Cu_3O_x$ tape in high fields up to 15 Tesla*, C.M. Friend, D.P. Hampshire, to be submitted to J. Appl. Phys.

8. *Evidence that the $J_C(B,T)$ of a $Bi_2Sr_2Ca_2Cu_3O_x$ tape is determined by S-N-S Josephson coupling in low magnetic fields at temperatures above 10K*, C.M. Friend, D.P. Hampshire, in progress.